

Design Principles and Synergistic Effects of Chlorination on a Conjugated Backbone for Efficient Organic Photovoltaics: A Critical Review


Gururaj P. Kini, Sung Jae Jeon, and Doo Kyung Moon*

The pursuit of low-cost, flexible, and lightweight renewable power resources has led to outstanding advancements in organic solar cells (OSCs). Among the successful design principles developed for synthesizing efficient conjugated electron donor (ED) or acceptor (EA) units for OSCs, chlorination has recently emerged as a reliable approach, despite being neglected over the years. In fact, several recent studies have indicated that chlorination is more potent for large-scale production than the highly studied fluorination in several aspects, such as easy and low-cost synthesis of materials, lowering energy levels, easy tuning of molecular orientation, and morphology, thus realizing impressive power conversion efficiencies in OSCs up to 17%. Herein, an up-to-date summary of the current progress in photovoltaic results realized by incorporating a chlorinated ED or EA into OSCs is presented to recognize the benefits and drawbacks of this interesting substituent in photoactive materials. Furthermore, other aspects of chlorinated materials for application in all-small-molecule, semitransparent, tandem, ternary, single-component, and indoor OSCs are also presented. Consequently, a concise outlook is provided for future design and development of chlorinated ED or EA units, which will facilitate utilization of this approach to achieve the goal of low-cost and large-area OSCs.

1. Introduction

Organic solar cells (OSCs) are blossoming among solar cell research communities due to their benefits such as low cost, lightweight, flexibility and large-scale roll-to-roll solution processing.^[1] Recent progress in OSC research has pushed the power conversion efficiencies (PCEs) of both single-junction and tandem structures up to 17%,^[1],2] which is considered as the starting point for commercial application, regardless of their limited area. This phenomenal accomplishment regarding the PCEs of OSCs is directly associated with the collaborative efforts on photoactive material design optimization (development of novel electron donor (ED) and electron acceptor (EA) units) and advanced device engineering.

Dr. G. P. Kini, Dr. S. J. Jeon, Prof. D. K. Moon
Nano and Information Materials (NIMs) Laboratory
Department of Chemical Engineering
Konkuk University
120 Neungdong-ro, Gwangjin-gu, Seoul 05029, Korea
E-mail: dkmoon@konkuk.ac.kr

 The ORCID identification number(s) for the author(s) of this article can be found under <https://doi.org/10.1002/adma.201906175>.

DOI: 10.1002/adma.201906175

Generally, the active layer of OSCs is mainly composed of two materials, that is, the ED and EA. Nanoscale phase separation between these materials aids efficient exciton dissociation via three-dimensional (3D) charge transfer pathways, which results in the swift transfer of electrons and holes to the respective electrodes to generate power.^[3] At present, the principal mechanisms governing the functioning of bulk heterojunction (BHJ) solar cells are well defined, providing a clear idea about the requirements for ideal high-efficiency photoactive materials.^[1c,4] As the properties of photovoltaic materials such as the molecular energy levels, absorption, distribution of π -electrons, and charge carrier properties greatly affect their photovoltaic performance, before design and synthesis of the conjugated ED and/or EA, a basic structure–property relationship study is necessary to obtain a clear understanding of impact of structural modification on the intrinsic properties of the photoactive

materials to meet the desired application requirements.^[1c,f,4a,5]

Over the years, various design strategies to modulate optoelectronic properties and charge transfer in conjugated materials have evolved to a great extent, which enables great augmentation of the PCEs of OSCs. These strategies include appropriate selection of D (donor) and/or A (acceptor) units,^[1c,4b,5a,6] side-chain engineering,^[7] atomic or functional group substitution,^[7i,8] addition of aromatic fused groups, etc.^[5b,9] Among the atomic substitution approach, fluorination is a highly studied and well-proven chemical modification for designing efficient EDs and EAs, which has delivered excellent PCEs over the years.^[2a,6a,7b,8a,10] Benefiting from its small size (van der Waals radius of F atom is 1.35 Å)^[11] and strongest electronegativity (3.98 for F on the Pauling scale),^[12] fluorine (F) can easily modulate the frontier energy levels and enhance the molecular absorption without negatively affecting the molecular packing.^[8a,10a] Moreover, a fluorinated conjugated backbone was proved to enhance the coplanarity, crystallinity, and charge carrier mobilities, resulting from the non-covalent intermolecular interactions of F...H, F...S, and so on.^[8a,10a,13] Despite their advantages, these fluorinated polymers exhibit intrinsic demerits, such as tedious synthesis, low yields during fluorination, a high cost of the fluorinated reagents, and severe aggregation tendencies, which limit their use as active materials

for large-scale synthesis.^[6a,12,14] Consequently, the development of an alternate cost-effective method remains necessary to meet the goal of large-scale roll-to-roll production.

Chlorine (Cl), despite being the second-most electronegative atom next to F (3.16 for Cl on the Pauling scale),^[11] has not been explored as much as F over the years, mainly because of its large size (van der Waals radius of Cl atom is 1.75 Å), which presumably disrupts the planarity of the conjugated backbone.^[12] However, recently, many research groups have devoted their attention to studying the effect of chlorination on the conjugated backbone because of its low cost, easy preparation, and higher yields compared to F counterparts.^[14b,15] These studies indicated various advantages of Cl insertion in the material design like: 1) the empty 3d orbitals of Cl atom could help π -electron delocalization more effectively, thereby further frontier lowering the energy levels over that of fluorination;^[8d,15b,16] 2) the higher dipole moment of C–Cl bond over C–F bond (1.46 versus 1.41 e.s. units $\times 10^{18}$)^[17] will benefit broadening of the absorption by the intramolecular charge transfer (ICT) effect;^[15c,16,18] 3) the planarity of conjugated backbone is increased through the heavy-atom effect of Cl-atom, resulting in higher crystallinity and charge mobility;^[15b,19] 4) chlorination can effectively improve the trade-off between open-circuit voltage (V_{OC}) and short-circuit current density (J_{SC}) in OSCs by minimizing non-radiative energy loss;^[2b] 5) and most importantly, synthesis of chlorinated photovoltaic materials (Cl-PVMs = polymer or small-molecule (SM) donor and nonfullerene acceptor (NFA)) is facile and economical compared to fluorinated counterparts, thus making these materials an ideal choice for large-area OSCs.^[14b,15] Finally, recently reported OSCs incorporating Cl-PVMs realized unprecedented record high PCEs of up to 17%,^[2b,h,7d,14b,15b,d,e,20] which further highlights the effectiveness of this strategy (Figure 1). Despite the aforementioned advantages of Cl incorporation, they also inherit few intrinsic limitations. For example, in few reports, it is observed that the large size of the Cl atom can negatively affect the planarity and intermolecular π - π stacking of the resulting polymers, thereby adversely affecting their BHJ morphology and photovoltaic performances.^[10b,15a,21] Consequently, the number of Cl substituents and their substitution position (backbone or side-chain) in the molecular design must be carefully considered before designing Cl-PVMs for OSCs.

Here, we systematically record the various design strategies and modifications involving incorporation of Cl substituents into the EDs or EAs for application in OSCs (reported up to August 2019). To get a clear understanding of chlorination design criteria, we have studied various aspects of chlorination, including the effects of Cl insertion into the “D” or “A” units of alternate “D–A”-type polymers, SMs and NFAs, and systematically related their structure–property characteristics to unveil the fundamental governing principles for future design of efficient active layer materials using chlorination. Moreover, the latest strides in chlorinated materials for application in all-small-molecule OSCs (ASMOSCs), semitransparent OSCs (STOSCs), tandem and ternary OSCs, single-component OSCs (SCOSCs), and indoor OSCs are also clearly discussed. We believe that this comprehensive review will provide a strong foundation for future innovation of chlorinated active layer



Gururaj P. Kini received his B.Sc. (2006) and M.Sc. (2008) degrees from the Karnatak University, Dharwad, Karnataka, India. After working at a pharmaceutical company as a research associate during 2008–2012, he began his Ph.D. study at the University of Science and Technology, KRICT, Daejeon, Korea. He completed his Ph.D. in 2017 and then worked as a postdoctoral fellow at the Konkuk University, Seoul, Korea (2017–2018). Now, he is an assistant professor at the Konkuk University, Seoul, Korea (2018–present). His research interests include design and synthesis of conjugated photoactive materials for organic electronics.



Sung Jae Jeon received his B.S. and Ph.D. degrees from the Department of Materials and Chemistry Engineering, Konkuk University, Republic of Korea, in 2013 and 2019. He is currently a postdoctoral researcher at the Nano & Information Materials Laboratory (NIMs), Department of Chemical Engineering, Konkuk University, Republic of Korea, working under the supervision of Prof. Doo Kyung Moon. His research focuses on designing and synthesizing conjugated materials for highly efficient organic electronics.



Doo Kyung Moon received his Ph.D. from the Tokyo Institute of Technology, Japan, in 1993, and had post-doc experience at the University of Arizona in USA (1993–1994) and the Korea Institute of Science and Technology (KIST, 1994–1995). Now, he is a professor at the Department of Chemical Engineering, Konkuk University, Republic of Korea. He was an adjunct professor of advanced industrial science and technology (AIST, 2009–2010). His research group works on the development of organic materials and organic electronic devices for organic solar cells, organic light emitting diodes, and piezoelectric nanogenerators. For details please see the lab website: <http://nanoscience.or.kr>.

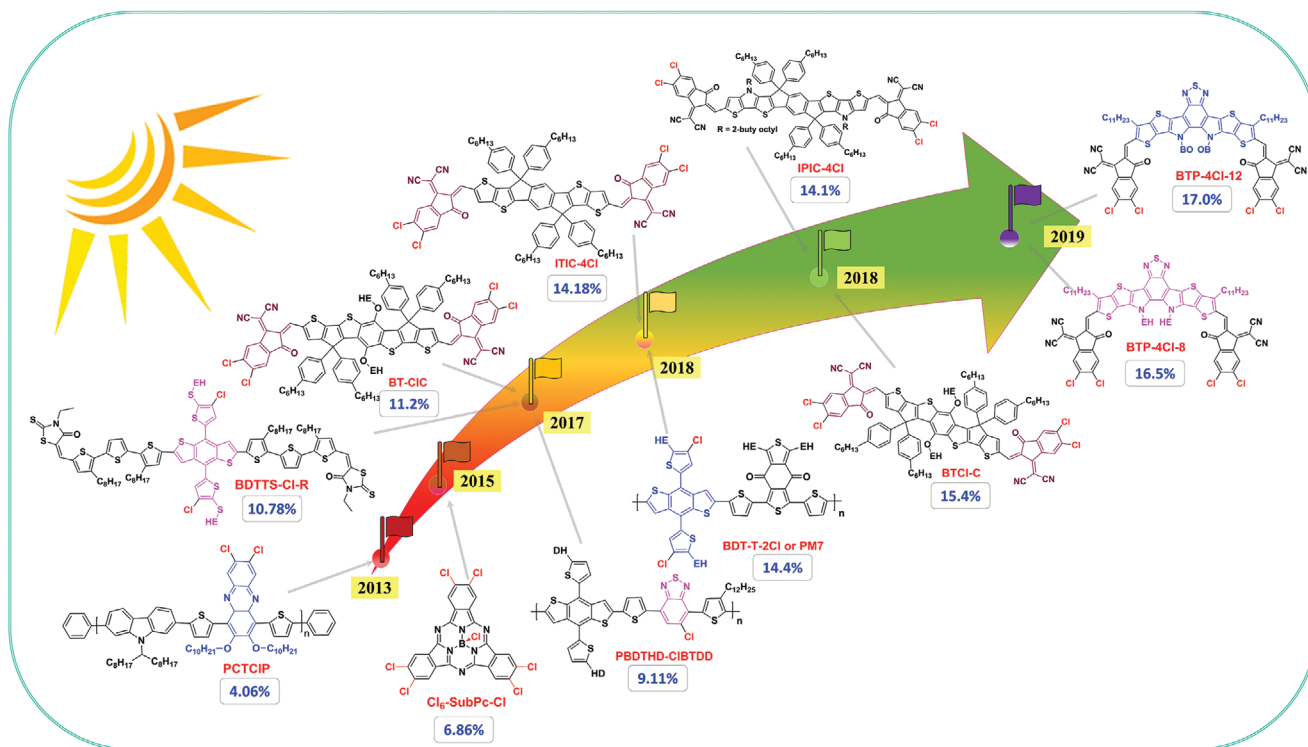


Figure 1. A brief timeline of the development of chlorinated photovoltaic materials for OSCs over the last 7 years (reported up to August 2019).

materials for OSCs and for moving toward the futuristic goal of low-cost and large-area organic photovoltaics.

2. Chlorination of Acceptor Units

Initially, mainstream chlorinated polymers for OSCs were designed based on alternate D–A cores wherein Cl substituents were introduced on electron-deficient “A” units owing to the strong electronegativity of the Cl atom. Therefore, we begin our discussion by studying a variety of such D–A polymers employing chlorinated acceptor units (Scheme 1), and the relevant photovoltaic characteristics are compiled in Table 1.

2.1. Chlorination of Phenazine

Phenazine is one of the earliest reported EA cores used for the synthesis of D–A polymers for OSCs.^[22] In 2013, Li et al. first introduced chlorination of phenazine as a means of tuning the frontier energy levels in a polymer, PCTCIP (P1, Scheme 1).^[23] As projected, P1 displayed a lower-lying HOMO and a lower optical bandgap (E_g^{opt}) than the non-Cl counterpart, which led to the higher PCE of 4.06% by enhancement of V_{OC} and J_{SC} .

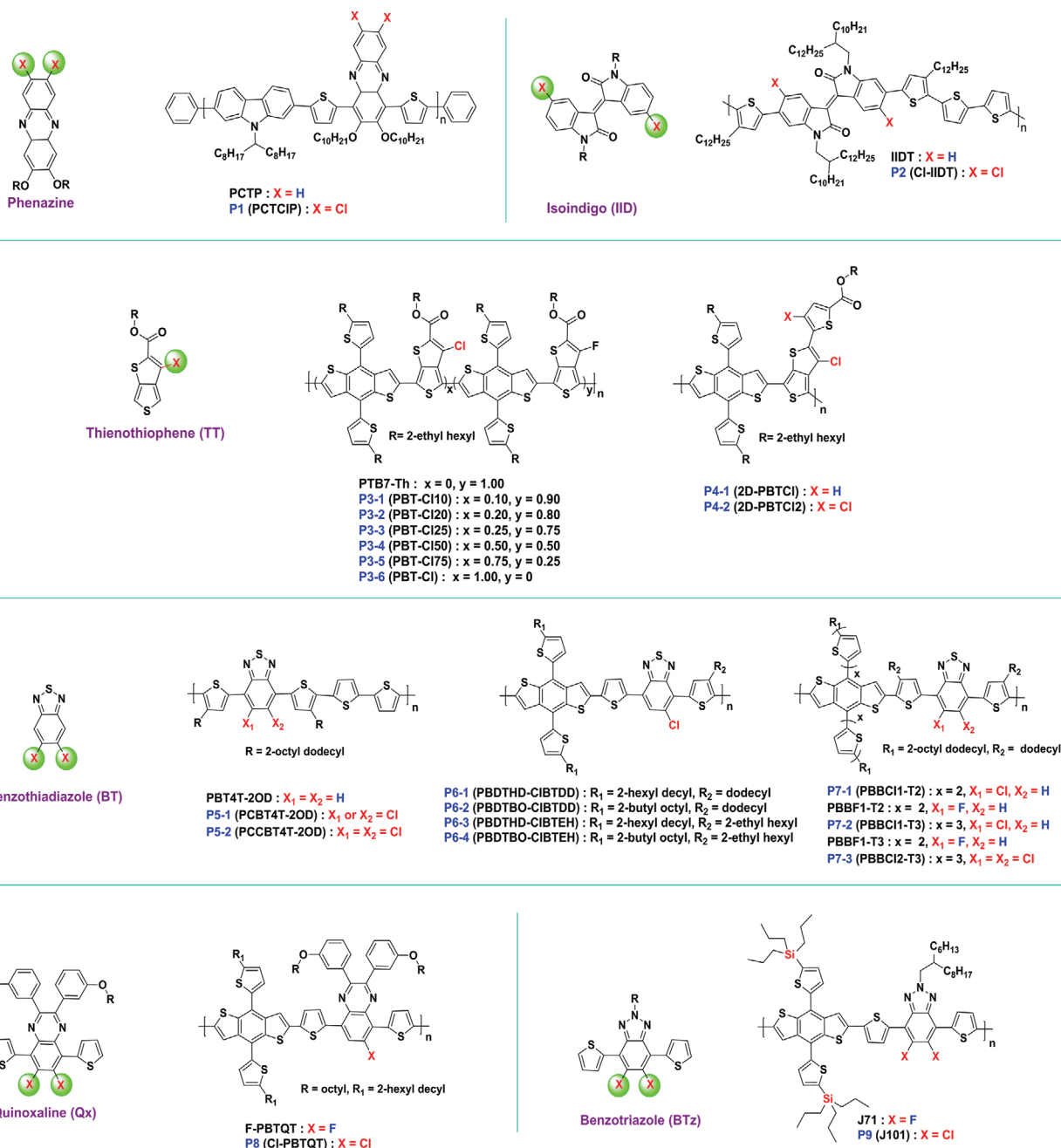
2.2. Chlorination of Isoindigo

Chlorinated isoindigo (Cl-IID) was first reported in 2013, and its various D–A polymers have been exclusively used in

ambipolar organic field-effect transistor (OFET) applications.^[24] Pei and co-workers first tested the Cl-IID-based polymer Cl-IIDT (P2, Scheme 1) for OSCs.^[25] They compared the performance of P2 with that of the without chlorination (IIDT) and fluorinated-IID (F-IIDT) analogs. In addition to the lower HOMO displayed by P2 than the analogs, the findings from grazing-incidence wide-angle X-ray scattering (GIWAXS) and atomic force microscopy (AFM) indicated that the steric hindrance caused by the large size of the Cl atom aided in overcoming the high crystallization tendency (by lowering the backbone planarity), thereby improving the miscibility and appropriate nanoscale phase separation in the P2:PC₇₁BM blend films. This phenomenon simultaneously improved the overall photovoltaic parameters (J_{SC} , V_{OC} , and fill factor [FF]), thereby resulting in an approximately fourfold increase in the PCE from 1.19% (F-IIDT) to 4.60% for P2. Thus, this was a first report, which clearly showed the various advantages of Cl insertion in the conjugated backbone other than decreasing the energy levels.

2.3. Chlorination of Thieno[3,4-*b*]thiophene

Thieno[3,4-*b*]thiophene (TT) is a widely used acceptor unit for synthesizing D–A copolymers for OSCs.^[1c,26] Chlorinated TT (Cl-TT) was first synthesized by He and co-workers to improve the PCE of PTB7-Th (having PCE of 7.64%, V_{OC} = 0.79 V) by increasing the V_{OC} .^[21a] They synthesized a series of terpolymers (P3-*n*, Scheme 1) with increasing ratio of Cl-TT (10, 20, 25, 50, 75, and 100%) along the well-known PTB7-Th polymer having alternate 4,8-bis(5-(2-ethylhexyl)thiophen-2-yl)benzo[1,2-*b*:4,5-*b'*]dithiophene (2D-BDT) as “D” and fluorinated TT (F-TT)



Scheme 1. Chemical structures of D–A-type polymers containing chlorinated acceptor units: phenazine; isoindigo (IID); thienothiophene (TT); benzothiadiazole (BT); quinoxaline (Qx), and benzotriazole (BTz).

as “A” units. The authors reported noticeable changes in the photoelectrochemical properties of these polymers, such as blueshifted absorption, an increase in the bandgap from 1.56 to 1.72 eV, and deepening HOMO energy levels from -5.29 to -5.73 eV, as the Cl-TT content was increased from 0% to 100% in PTB7-Th (Figure 2). These changes were mainly caused by the insertion of the Cl-TT unit, which resulted in a diminishing of planarity and conjugation in the polymers. After careful optimization of the Cl-TT content, the authors achieved a precise balance between energy levels, crystallinity, and morphology, which ensured the enhancement of overall PCE up to 8.31%

with a high V_{OC} of 0.82 V in PBTCl25 (P3-3) having 25% Cl-TT. Interestingly, this PCE was even higher than that of the reference polymer PTB7-Th (7.91%, V_{OC} = 0.79 V), which was tested parallelly. Moreover, as the content of Cl-TT increased from PTB7-Th (Cl = 0%) to PBTCl (P3-6, Cl = 100%), V_{OC} was noticeably improved from 0.79 to 0.92 V, emphasizing that the low V_{OC} problem of the PTB family polymers can be overcome by adding Cl-TT.^[27]

In addition to the fullerene system, the same group also evaluated the performance of P3-6 in the NF system by using the ITIC acceptor.^[28] The authors observed a higher PCE for

Table 1. Summary of optoelectronic properties and OSC parameters of various D–A-type copolymers containing different chlorinated acceptor units.

Material	Original name	HOMO [eV]	LUMO [eV]	E_g^{opt} [eV] ^{a)}	Acceptor	V_{OC} [V]	J_{SC} [mA cm ²]	FF [%]	PCE [%]	Hole mobility [cm ² V ⁻¹ s ⁻¹]	Ref.
P1	PCTCIP	−5.41 ^{a)}	−3.71 ^{b)}	1.70	PC ₇₁ BM	0.87	8.06	58.0	4.06	–	[23]
P2	Cl-IIDT	−5.53 ^{a)}	−3.85 ^{a)}	1.50	PC ₇₁ BM	0.75	10.00	61.0	4.60	1.06 × 10 ^{−5} d)	[25]
P3-1	PBTCI10	−5.35 ^{a)}	−3.73 ^{a)}	1.61	PC ₇₁ BM	0.80	14.07	69.28	7.79	1.6 × 10 ^{−4} d)	[21a]
P3-2	PBTCI20	−5.35 ^{a)}	−3.72 ^{a)}	1.56	PC ₇₁ BM	0.81	13.94	66.00	7.47	3.2 × 10 ^{−4} d)	[21a]
P3-3	PBTCI25	−5.36 ^{a)}	−3.71 ^{a)}	1.57	PC ₇₁ BM	0.82	15.31	66.19	8.31	6.1 × 10 ^{−4} d)	[21a]
P3-4	PBTCI50	−5.36 ^{a)}	−3.71 ^{a)}	1.58	PC ₇₁ BM	0.85	13.02	61.03	6.79	1.1 × 10 ^{−4} d)	[21a]
P3-5	PBTCI75	−5.50 ^{a)}	−3.70 ^{a)}	1.63	PC ₇₁ BM	0.89	11.55	57.86	5.90	9.7 × 10 ^{−5} d)	[21a]
P3-6	PBTCI	−5.73 ^{a)}	−3.69 ^{a)}	1.72	PC ₇₁ BM	0.92	10.24	50.23	4.75	5.5 × 10 ^{−5} d)	[21a]
	PBTCI	−5.43 ^{a)}	−3.55 ^{a)}	1.71	ITIC	0.91	14.53	58.00	7.57	1.3 × 10 ^{−4} e)	[28]
P4-1	2D-PBTCI	−5.45 ^{a)}	−3.60 ^{a)}	1.72	ITIC	0.91	15.79	61.32	8.81	4.9 × 10 ^{−4} e)	[21b]
P4-2	2D-PBTCI2	−5.43 ^{a)}	−3.63 ^{a)}	1.66	ITIC	0.87	14.52	58.43	7.38	1.1 × 10 ^{−4} e)	[21b]
P5-1	PCBT4T-2OD	−5.26 ^{a)}	−3.59 ^{a)}	1.59	PC ₇₁ BM	0.73	16.18	68.97	8.21	5.1 × 10 ^{−4} d)	[21c]
P5-2	PCCBT4T-2OD	−5.32 ^{a)}	−3.62 ^{a)}	1.61	PC ₇₁ BM	0.85	11.93	60.14	6.12	2.2 × 10 ^{−4} d)	[21c]
P6-1	PBDTHD-CIBTDD	−5.53 ^{a)}	−3.71 ^{a)}	1.68	PC ₇₁ BM	0.76	16.79	71.69	9.11	9.3 × 10 ^{−4} e)	[15a]
P6-2	PBDTBO-CIBTDD	−5.47 ^{a)}	−3.70 ^{a)}	1.70	PC ₇₁ BM	0.68	11.69	62.30	4.95	2.6 × 10 ^{−5} e)	[15a]
P6-3	PBDTHD-CIBTEH	−5.53 ^{a)}	−3.71 ^{a)}	1.71	PC ₇₁ BM	0.79	13.33	63.12	6.88	1.3 × 10 ^{−4} e)	[15a]
P6-4	PBDTBO-CIBTEH	−5.50 ^{a)}	−3.73 ^{a)}	1.69	PC ₇₁ BM	0.78	10.94	64.36	5.46	3.9 × 10 ^{−4} e)	[15a]
P7-1	PBBCI1-T2	−5.49 ^{a)}	−3.22 ^{a)}	1.60	PC ₇₁ BM	0.87	8.44	49.49	3.64	2.7 × 10 ^{−6} e)	[30]
P7-2	PBBCI1-T3	−5.44 ^{a)}	−3.38 ^{a)}	1.56	PC ₇₁ BM	0.73	13.75	68.59	6.87	2.5 × 10 ^{−4} e)	[30]
P7-3	PBBCI2-T3	−5.50 ^{a)}	−3.21 ^{a)}	1.59	PC ₇₁ BM	0.84	9.90	63.94	5.33	3.6 × 10 ^{−5} e)	[30]
P8	Cl-PBTQT	−5.33 ^{a)}	−3.56 ^{a)}	1.66	PC ₇₁ BM	0.95	14.08	61.00	8.16	5.5 × 10 ^{−5} d)	[31]
P9	J101	−5.30 ^{a)}	−3.50 ^{a)}	1.97	ZITI	0.93	21.25	72.48	14.43	2.18 × 10 ^{−4} e)	[12]

^{a)} Measured by cyclic voltammetry; ^{b)} Calculated by $E_{\text{LUMO}} = E_{\text{HOMO}} + E_g$; ^{c)} Calculated from the absorption edge of the polymer in a thin film state ($E_g^{\text{opt}} = 1240/\lambda_{\text{onset}}$ eV);

^{d)} Estimated from pristine polymer films using the SCLC method; ^{e)} Estimated from active layer blend using the SCLC method.

P3-6 (7.57%) than for PTB7-Th (6.62%). In addition to lowering the HOMO energy level, Cl-TT favored more complementary absorption with ITIC and optimal morphology, thereby boosting J_{SC} , V_{OC} , and the overall charge transport in the corresponding OSC devices.

Generally, the addition of 2D-extended conjugated heterocyclic side-chains to the TT unit is used to strengthen intermolecular π – π interactions and enhance the absorption in higher wavelength region, thereby resulting in a distinct enhancement of PCEs.^[29] Using the same strategy, Chao et al. further optimized the structural design of Cl-TT by adding an extended conjugated thiophene unit without and with Cl substitution to form the polymers 2D-PBTCI (P4-1) and 2D-PBTCI2 (P4-2), respectively (Scheme 1).^[21b] Though P4-2 showed a slightly lower bandgap than P4-1 due to the enhanced planarity ascribed to the Cl–S interactions between the thiophene and TT units; however, both polymers showed distinct blueshifted absorption relative to parent PTB7-Th. In OSCs, P4-1:ITIC blend demonstrated more complementary absorption, good miscibility, and optimum nanoscale morphology with an appropriate feature size compared to P4-2:ITIC blend. Consequently, P4-1:ITIC achieved higher hole mobility (μ_h), J_{SC} , and FF values, thus boosting the overall PCE up to 8.81%. These findings indicate that Cl substitution position has a marked effect on the polymer properties and PCEs along with a number of Cl substituents.

2.4. Chlorination of Benzothiadiazole

Benzothiadiazole (BT) is a highly studied “A” unit used for constructing D–A copolymers and SMs for OSCs.^[32] Despite the tremendous success of fluorinated BT (F-BT) in OSCs,^[6a,7b,i,13b] and OTFTs,^[33] chlorinated BT (Cl-BT)-based polymers have not been explored till 2017. This is because of steric hindrance caused by the large size of the Cl atom, which is expected to induce a distorted molecular arrangement.

To explore the relationship between the degree of chlorination and photovoltaic performances in OSCs, Hu et al. synthesized the polymers PCBT4T-2OD (P5-1) and PCCBT4T-2OD (P5-2) based on monochlorinated BT (1Cl-BT) and dichlorinated BT (2Cl-BT), respectively. For comparison, parent unsubstituted BT polymer (PBT4T-2OD) (Scheme 1 and Figure 3) was also synthesized.^[21c] P5-1 could exhibit a higher population of “face-on” molecular confirmation with a larger crystallite size compared to P5-2 and a favorable morphology with reasonably small domain sizes when blended with PC₇₁BM. Combining these benefits with lower HOMO, corresponding P5-1:PC₇₁BM delivers a superior PCE of 8.21% with the right balance between photovoltaic parameters (the observed PCEs for PBT4T-2OD and P5-2 were 4.89 and 6.12%, respectively). Although P5-2 devices displayed the highest V_{OC} of 0.85 V due to the increase in the Cl-content, they also showed a dramatic drop in the J_{SC} and FF because of the decreased intermolecular

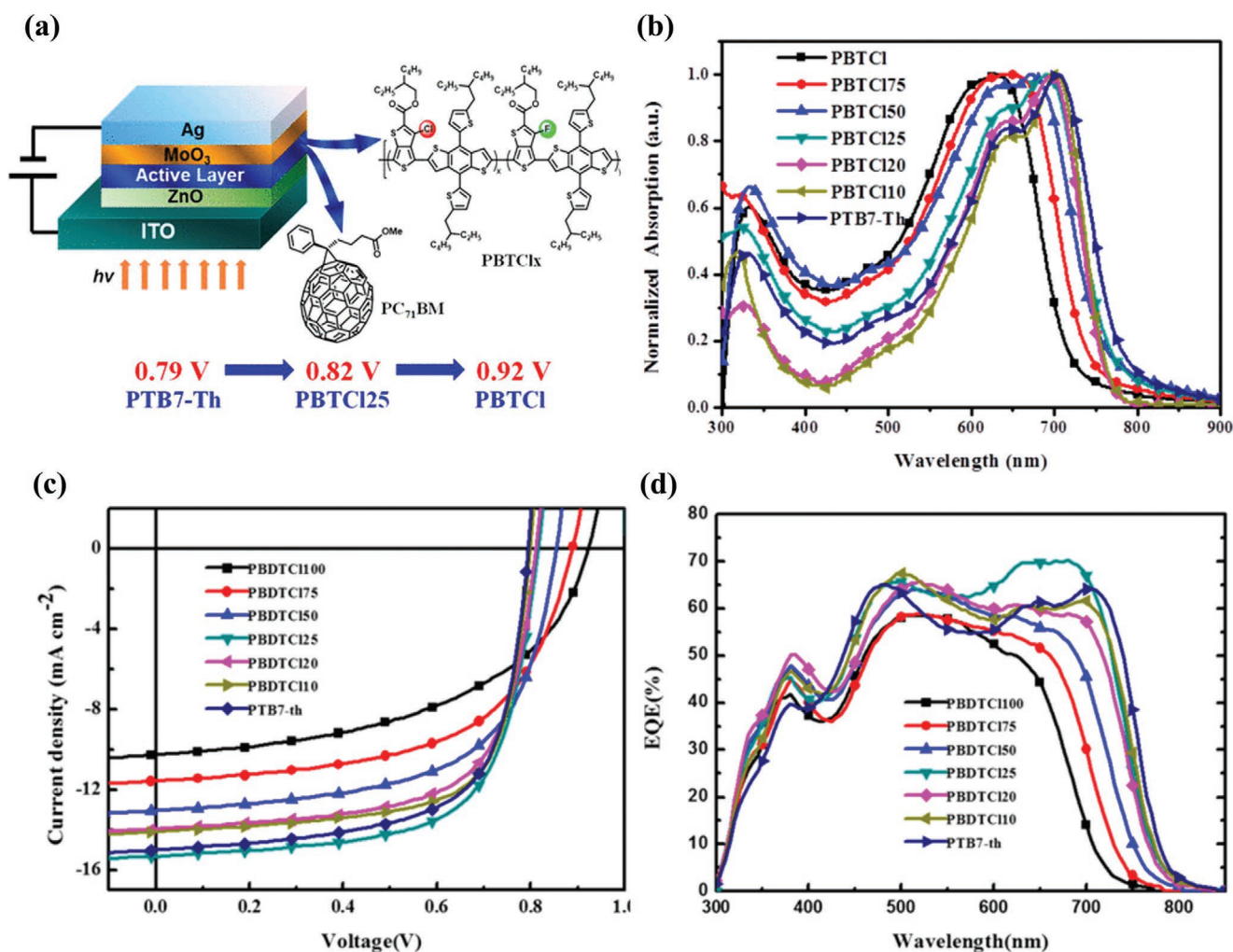


Figure 2. Influence of chlorination for the PBTC1x (P3-n) series: a) schematic diagram; b) normalized UV-vis absorption spectra of PBTC1, PBTC175, PBTC150, PBTC125, PBTC120, PBTC110, and PTB7-Th in the film state; c) *J*-*V* curves and d) EQE profiles of the optimized devices. a-d) Reproduced with permission.^[21a] Copyright 2017, American Chemical Society.

interaction and inferior morphology. These results indicate that 1Cl-BT is beneficial to enhance photovoltaic performances over 2Cl-BT.

Later, Mo et al. synthesized another series of D-A copolymers (P6-n, Scheme 1) based on alternate Cl-BT and 2D-BDT units considering the concise and low-cost synthesis of Cl-BT (Scheme 1).^[15a] They optimized the polymer design by varying the alkyl chains in the conjugated backbone, which had a marked effect on the polymer solubility, as well as on the aggregation and molecular orientations of the blend films. Attributed to the Cl substitution, all P6-n polymers showed lower HOMO energy levels, which resulted in a higher *V*_{OC} in OSC devices. By employing an optimized PBDTHD-ClBTDD (P6-1):PC₇₁BM blend film with a thickness of ≈250 nm, the authors achieved the best PCE of 9.11%, with high *J*_{SC} (16.79 mA cm⁻²), *V*_{OC} (0.76 V) and FF (71.69%), and an impressive *μ*_h of 9.3 × 10⁻⁴ cm² V⁻¹ s⁻¹. This was the highest PCE value achieved using chlorinated polymer donors during that time. Additionally, P6-1:PC₇₁BM blend also possesses excellent thickness tolerance, with overall PCEs over 8.3% for active layer thicknesses

ranging from 180 to 320 nm, emphasizing they could be further useful in roll-to-roll printing processes.

To compare the synergistic effects of chlorination and fluorination on the performance of OSCs, Yang et al. prepared the new polymers PBBCl1-T2 (P7-1) and PBBCl1-T3 (P7-2) based on alternate 1Cl-BT and modified 2D-BDT cores and simultaneously compared them with the corresponding fluorinated counterparts (Scheme 1).^[30] In addition to the lower HOMO achieved by incorporating Cl atom into P7-1 and P7-2, authors minimized the steric effect caused by the Cl atom in the conjugated backbone by grafting longer *π*-conjugated side-chains onto BDT. The BHJ morphology measurements using AFM and transmission electron microscopy (TEM) revealed that the chlorination also greatly influenced the morphology of blends by facilitating the fibrillar nanostructures with the optimum fiber width. Consequently, these factors led to higher PCEs of 3.64% and 6.87% for P7-1 and P7-2, respectively, than for their respective fluorine counterparts. Furthermore, PBBCl2-T3 (P7-3), the dichloro-counterpart of P7-2 was also synthesized, but it showed the poor performance of 5.33% because of the distorted backbone

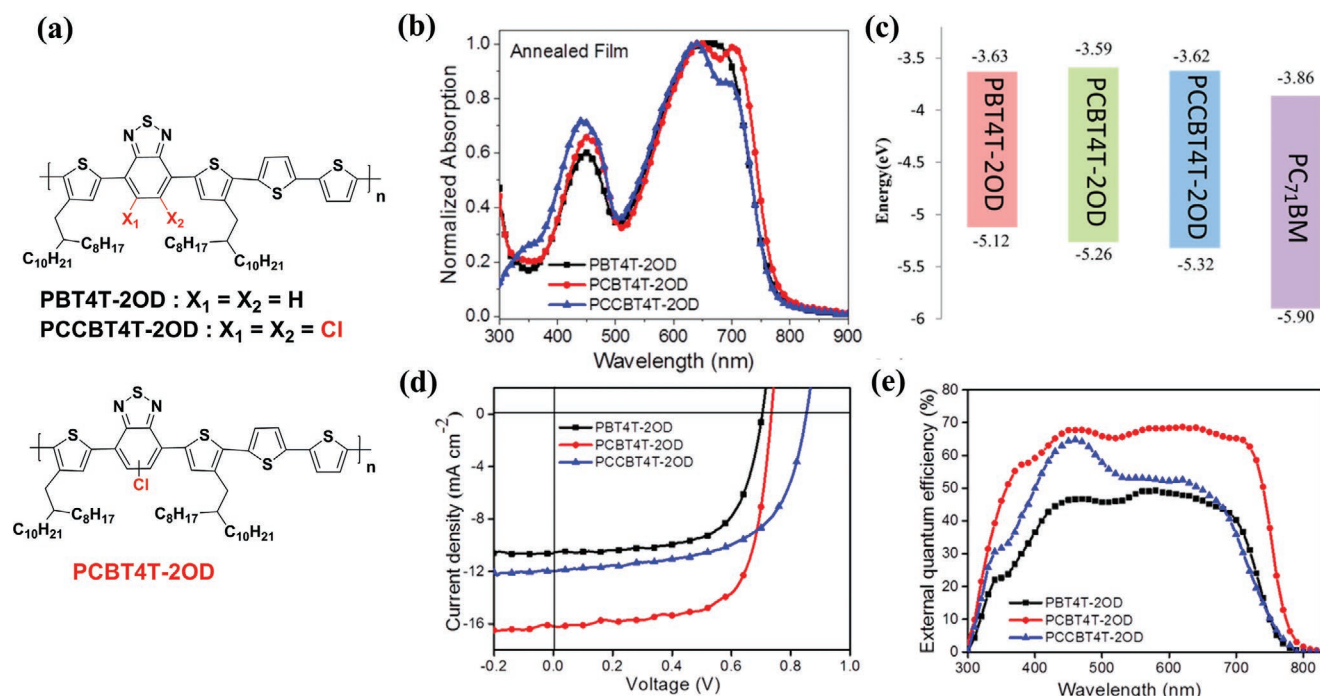


Figure 3. a) Chemical structures of PBT4T-2OD, PCBT4T-2OD, and PCCBT4T-2OD (**P5-n**) polymers; b) UV-vis absorption spectra of the polymers in an annealed film state; c) energy level diagrams for the polymers and PC₇₁BM; d) *J*-*V* curves and e) EQE profiles of the optimized devices. a-e) Reproduced with permission.^[21c] Copyright 2017, American Chemical Society.

caused by two Cl atoms present in the polymer backbone. Thus, these observations further substantiated that 1Cl-BT is more appropriate for enhancing the PCEs in OSCs.

2.5. Chlorination of Quinoxaline

Motivated by the successful strategy of monochlorination of BT acceptor unit, Zhang et al. synthesized the polymer Cl-PBTQT (**P8**) with alternate monochlorinated quinoxaline (Cl-Qx) and 2D-BDT (having 2-hexyl decyl alkyl chains) (Scheme 1).^[31] For comparison, the fluorinated analog of **P8**, F-PBTQT, was also synthesized. Like other chlorination studies, the introduction of Cl in helped to realize the lower HOMO, a precise balance between ordered packing and ideal domain sizes in the **P8**:PC₇₁BM blend by decreasing the aggregation. These factors synergistically enhanced the charge separation and photovoltaic performances up to 8.16% in the **P8**-based OSCs, which is approximately 33% higher than that for F-PBTQT (6.12%).

2.6. Chlorination of Benzotriazole

It is well known that 2-alkyl-benzo[*d*][1,2,3]triazole (BTz) and difluorinated BTz (2FBTz) are very popular acceptor cores used for synthesizing efficient wide-bandgap polymer donors for OSCs.^[7d,8a,34] Recently, Wang et al. introduced dichlorinated BTz as an acceptor core for preparing wide-bandgap D-A copolymer J101 (**P9**, Scheme 1) for NF-OSCs.^[12] **P9** displayed a deeper HOMO energy level, higher oscillator strength, and absorption

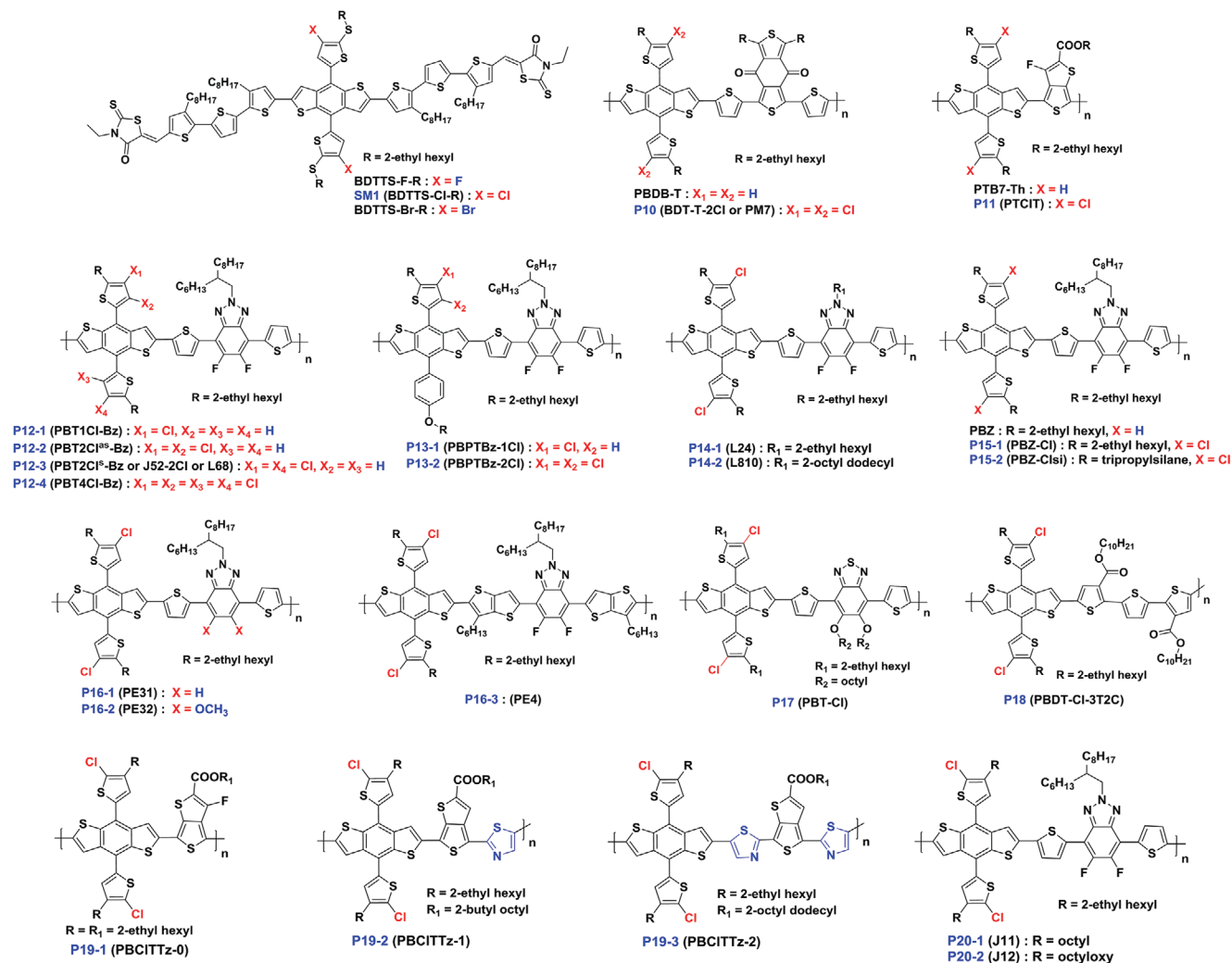
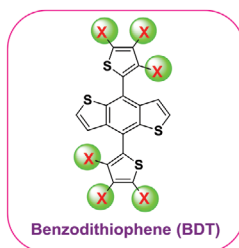
coefficient than corresponding 2FBTz analog J71, despite their higher torsional angle and reduced planarity. Interestingly, by pairing **P9** with appropriate indenoindene-based new NFA named ZITI, **P9**:ZITI blend films featured a superior BHJ morphology and efficient charge transport properties with lower charge recombination. As a result, drastic changes in the photovoltaic parameters and jump of PCE from 12.82% (for J71:ZITI blend) to 14.43% were observed in the case of **P9**:ZITI.

In short, chlorination on acceptor units is an ideal choice for enhancing a *V*_{oc} by lowering the frontier energy levels. However, the incorporation of higher Cl content in the acceptor backbone can adversely affect their device efficiency due to the decreased planarity and crystallinity caused by the large size of the Cl atom. Consequently, this strategy can be majorly preferred in D-A-type polymer design having high aggregation tendencies, thereby improving effective charge separation and transport by decreasing aggregation and improving the nanoscale morphology. Further, future innovations by varying the number and position of Cl-substituents on the side-chains of the acceptor units such as quinoxaline,^[35] 2D extended TT^[21b] might also need to be explored more precisely, as chlorination side-chains will not affect backbone planarity and aggregations in the film state.

3. Chlorine Substitution on Donor Units

3.1. Chlorination of Benzodithiophene Units

Benzo[1,2-*b*:4,5-*b'*]-dithiophene (BDT) is the most popular and widely used donor material for synthesizing D-A copolymers



Scheme 2. Chemical structures of D–A-type polymers containing chlorinated benzodithiophene (BDT) donor unit.

and SMs for OSCs.^[6b,36] One unique advantage of using BDT as the donor unit is the ease of introducing various functional groups onto the side-chains.^[6b,36,37] Recently, many studies have also focused on elucidating the effect of chlorination on the thienyl side-chains of BDT to realize the impressive photovoltaic performances (**Scheme 2**). The corresponding detailed characteristics, including the OSC parameters of these polymers, are summarized in **Table 2**.

Peng and co-workers first reported the synthesis of chlorinated alkylthiophenyl-substituted BDT (2Cl-SBDT), **Scheme 2**, which has symmetrically substituted Cl atoms in the

2D-alkylthiophenyl side-chains of the BDT unit and tested the applicability of this material to efficient SM solar cells.^[38] They synthesized a series of SM donors, BDTTS-F-R, BDTTS-Cl-R (**SM1**, **Scheme 2**), and BDTTS-Br-R based on the central BDT donor core with different halogen atoms on the alkylthiophenyl side-chains (X-SBDT, where X = F, Cl, and Br) and terminal 3-ethyl-rhodanine acceptors (A–D–A-type) to study the effects of halogens on properties of the SMs. The density functional theory (DFT) study revealed that the dihedral angle along the main chain or between main and side-chain was increased according to the halogen size (order of BDTTS-Br-R (12.9/54.1°)

Table 2. Summary of optoelectronic properties and OSC parameters of various D–A-type copolymers containing different chlorinated donor units.

Material	Original name	HOMO [eV]	LUMO [eV]	E_g^{opt} [eV] ^{c)}	Acceptor	V_{oc} [V]	J_{sc} [mA cm ⁻²]	FF [%]	PCE [%]	Hole mobility [cm ² V ⁻¹ s ⁻¹]	Ref.
SM1	BDTTS-Cl-R	-5.35 ^{a)}	-2.84 ^{a)}	1.77	PC ₇₁ BM	0.96	14.92	75.3	10.78	$2.79 \times 10^{-4\text{e}}$	[38]
	PBDB-T-2Cl	-5.51 ^{a)}	-3.72 ^{b)}	1.79	IT-4F	0.86	21.80	77.00	14.4	$2.13 \times 10^{-4\text{d}}$	[14b]
	PM7	-5.52 ^{a)}	-3.57 ^{a)}	1.79	IT-4F	0.88	20.90	71.1	13.1 ^{f)}	$6.67 \times 10^{-4\text{d}}$	[15b]
P10	PBDBT2Cl	–	–	–	IT-4F	0.85	20.67	74.81	13.14	$3.4 \times 10^{-4\text{e}}$	[39a]
	PBDB-TCl	–	–	–	IT-4F	0.88	20.4	74.8	13.5	$8.6 \times 10^{-5\text{e}}$	[39b]
	PM7	-5.52 ^{a)}	-3.57 ^{a)}	1.79	IDT6CN-M	1.05	16.4	77.5	13.3	$5.86 \times 10^{-5\text{e}}$	[40]
P11	PBCIT	-5.47 ^{a)}	-3.61 ^{a)}	1.64	ITIC	1.01	13.95	60.05	8.46	$2.45 \times 10^{-4\text{e}}$	[21d]
P12-1	PBT1Cl-Bz	-5.39 ^{a)}	-3.57 ^{a)}	1.93	IT-4F	0.71	16.85	63.48	7.60	$1.5 \times 10^{-4\text{e}}$	[15c]
P12-2	PBT2Cl ^{as} -Bz	-5.48 ^{a)}	-3.56 ^{a)}	1.97	IT-4F	0.79	13.43	41.75	4.43	$4.9 \times 10^{-5\text{e}}$	[15c]
P12-3	PBT2Cl ^s -Bz	-5.47 ^{a)}	-3.58 ^{a)}	1.96	IT-4F	0.77	15.55	65.21	7.80	$2.2 \times 10^{-4\text{e}}$	[15c]
P12-4	PBT4Cl-Bz	-5.64 ^{a)}	-3.57 ^{a)}	2.01	IT-4F	0.96	16.42	58.69	9.25	$3.4 \times 10^{-4\text{e}}$	[15c]
	J52-2Cl	-5.53 ^{a)}	-3.59 ^{b)}	1.94	ITIC	0.95	17.17	70.2	11.53	$9.5 \times 10^{-4\text{e}}$	[20a]
	J52-2Cl	-5.39 ^{a)}	-3.45 ^{b)}	1.94	BTA3	1.24	13.16	66.62	10.50	$3.26 \times 10^{-4\text{e}}$	[41]
P12-3	J52-Cl	-5.39 ^{a)}	-3.45 ^{a)}	1.94	Y6	0.84	23.77	61.44	12.31	$3.57 \times 10^{-4\text{e}}$	[42]
	L68	-5.51 ^{a)}	-3.56 ^{b)}	1.95	IT-4F	0.75	19.50	63.2	9.30	$8.0 \times 10^{-4\text{e}}$	[7d]
P13-1	PBPTBz-1Cl	-5.32 ^{a)}	-3.55 ^{a)}	1.97	IT-M	0.87	14.78	50.20	6.46	$1.6 \times 10^{-4\text{e}}$	[43]
P13-2	PBPTBz-2Cl	-5.41 ^{a)}	-3.54 ^{a)}	1.98	IT-M	0.99	14.92	48.61	7.18	$1.3 \times 10^{-4\text{e}}$	[43]
P14-1	L24	-5.43 ^{a)}	-3.48 ^{b)}	1.95	IT-4F	0.495	7.41	36.3	1.33	$3.65 \times 10^{-4\text{e}}$	[7d]
P14-2	L810	-5.57 ^{a)}	-3.58 ^{b)}	1.99	IT-4F	0.79	20.76	73.5	12.1	$8.98 \times 10^{-4\text{e}}$	[7d]
P15-1	PBZ-Cl	-5.39 ^{a)}	-3.41 ^{a)}	1.94	IT-4F	0.80	17.7	68.3	9.7	$8.06 \times 10^{-4\text{d}}$	[7e]
P15-2	PBZ-ClSi	-5.56 ^{a)}	-3.50 ^{a)}	1.94	IT-4F	0.93	19.2	71.5	12.8 ^{f)}	$1.02 \times 10^{-3\text{d}}$	[7e]
P16-1	PE31	-5.24 ^{a)}	-3.35 ^{b)}	1.89	Y6	0.80	20.45	46.86	7.62	$0.51 \times 10^{-4\text{e}}$	[42]
P16-2	PE32	-5.20 ^{a)}	-3.28 ^{b)}	1.92	Y6	0.75	18.44	53.03	7.31	$1.97 \times 10^{-4\text{e}}$	[42]
P16-3	PE4	-5.42 ^{a)}	-3.49 ^{b)}	1.93	Y6	0.84	22.21	75.43	14.02	$8.04 \times 10^{-4\text{e}}$	[42]
P17	PBT-Cl	-5.51 ^{a)}	-3.60 ^{a)}	1.78	IT-4F	0.78	21.03	70.0	11.6	$5.92 \times 10^{-4\text{e}}$	[44]
P18	PBDT-Cl-3T2C	-5.56 ^{a)}	-3.58 ^{a)}	1.98	IT-4F	0.87	18.63	62.80	10.18	$3.5 \times 10^{-5\text{e}}$	[45]
P19-1	PBCITtz-0	-5.55 ^{a)}	-3.87 ^{b)}	1.68	PC ₇₁ BM	0.94	12.77	56.98	6.85	$8.58 \times 10^{-5\text{e}}$	[46]
P19-2	PBCITtz-1	-5.57 ^{a)}	-3.87 ^{b)}	1.70	PC ₇₁ BM	0.94	14.09	63.57	8.42	$9.45 \times 10^{-5\text{e}}$	[46]
P19-3	PBCITtz-2	-5.63 ^{a)}	-3.88 ^{b)}	1.75	PC ₇₁ BM	1.01	9.93	62.17	6.26	$1.26 \times 10^{-6\text{e}}$	[46]
P20-1	J11	-5.48 ^{a)}	-3.23 ^{a)}	1.96	m-ITIC	0.935	18.05	73.0	12.32	$1.06 \times 10^{-4\text{e}}$	[47]
P20-2	J12	-5.51 ^{a)}	-3.26 ^{a)}	1.94	m-ITIC	0.943	16.64	55.7	8.74	$0.22 \times 10^{-4\text{e}}$	[47]
P21-1	PDBT(E)BTz-p	-5.65 ^{a)}	-3.65 ^{a)}	2.02	IT-4F	0.98	14.38	48.2	6.96	$7.3 \times 10^{-5\text{d}}$	[48]
P21-2	PDBT(E)BTz-d	-5.60 ^{a)}	-3.68 ^{a)}	2.00	IT-4F	0.95	14.68	54.5	7.81	$1.6 \times 10^{-5\text{d}}$	[48]
P22-1	PDBT-Cl	-5.41 ^{a)}	-3.56 ^{a)}	1.83	IT-4F	0.82	22.3	69.0	12.6	$2.03 \times 10^{-3\text{e}}$	[49]
P22-2	PDBT-2Cl	-5.49 ^{a)}	-3.59 ^{a)}	1.92	IT-4F	0.99	15.1	42.0	6.2	$3.16 \times 10^{-4\text{e}}$	[49]
P23	PBT4T-Cl	-5.33 ^{a)}	-3.64 ^{a)}	1.67	PC ₇₁ BM	0.80	18.71	74.60	11.18	$2.6 \times 10^{-3\text{e}}$	[15f]
P24	PBT3TClSe	-5.32 ^{a)}	-3.62 ^{a)}	1.70	PC ₇₁ BM	0.77	18.93	67.83	9.89	$7.4 \times 10^{-4\text{e}}$	[8h]
P25-1	PDCBT-Cl	-5.34 ^{a)}	-3.01 ^{a)}	1.91	ITIC-Th1	0.94	18.50	71.2	12.38	$0.84 \times 10^{-4\text{d}}$	[50]
P25-2	PDCBT-2Cl	-5.44 ^{a)}	-3.00 ^{a)}	1.95	ITIC-Th1	0.99	13.54	51.8	6.94	$0.49 \times 10^{-4\text{d}}$	[50]
P26-1	PCI(3)BDB-T	-5.54 ^{a)}	-3.27 ^{a)}	2.11	IT-4F	0.88	0.88	23.74	0.18	–	[20b]
P26-2	PCI(4)BDB-T	-5.48 ^{a)}	-3.47 ^{a)}	1.78	IT-4F	0.84	20.60	71.09	12.33	$2.57 \times 10^{-5\text{d}}$	[20b]
P27	P(Cl)	-5.47 ^{a)}	-3.50 ^{b)}	1.97	ITIC-Th	0.89	18.6	68.1	11.4	$3.41 \times 10^{-4\text{e}}$	[51]
P28-1	P(F–Cl)	-5.64 ^{a)}	-3.66 ^{b)}	1.99	IT-4F	0.879	20.3	66.0	11.8	$1.05 \times 10^{-4\text{e}}$	[52]
P28-2	P(Cl–Cl)	-5.70 ^{a)}	-3.68 ^{b)}	2.02	IT-4F	0.899	20.3	56.1	10.2	$2.85 \times 10^{-5\text{e}}$	[52]
P28-3	P(F–Cl)(BDD = 0.2)	-5.62 ^{a)}	-3.74 ^{b)}	1.88	IT-4F	0.838	21.3	71.0	12.7	$4.91 \times 10^{-4\text{e}}$	[52]
P28-4	P(Cl–Cl)(BDD = 0.2)	-5.67 ^{a)}	-3.77 ^{b)}	1.90	IT-4F	0.899	20.9	71.7	13.5 ^{f)}	$6.76 \times 10^{-4\text{e}}$	[52]

^{a)} Measured by cyclic voltammetry; ^{b)} Calculated by $E_{\text{LUMO}} = E_{\text{HOMO}} + E_g$; ^{c)} Calculated from the absorption edge of the polymer in a thin film state ($E_g^{\text{opt}} = 1240/\lambda_{\text{onset}}$ eV);

^{d)} Estimated from pristine polymer films using the SCLC method; ^{e)} Estimated from active layer blend using the SCLC method; ^{f)} Processed by eco-friendly solvents.

> SM1 (12.7/53.6°) > BDTTS-F-R (12.5/52.8°)), thereby affecting molecular packing of the SMs in the film state. Thus, authors overcome the excessive aggregation and phase separated morphology exhibited by OSCs devices of BDTTS-F-R by adding large-sized Cl or Br atoms in the molecular structure of SM. Also, SM1-based OSCs showed deep HOMO, a right balance between the crystallinity and nanoscale morphology when blended with PC₇₁BM. Thus, OSCs based on SM1 showed enhanced PCEs up to 10.78%, which is one of the highest efficiencies for single-junction OSCs using SM and PC₇₁BM as the active layer combination.

Employing the same concept, Hou and co-workers reported a case study of Cl incorporation in the popular PBDB-T-SF polymer design,^[10a] which previously showed a record high PCE of 13.1% when blended with IT-4F acceptor unit. They synthesized the new chlorinated polymer PBDB-T-2Cl (**P10**) by replacing fluorinated 2D-BDT (2F-BDT) in PBDB-T-SF with chlorinated 2D-BDT (2Cl-BDT) and analyzed changes in the properties caused by the inclusion of Cl atoms (Scheme 2 and Figure 4).^[14b] The main motive behind this strategy was to utilize the more straightforward and cost-effective synthesis of 2Cl-BDT, which could be beneficial for lowering the cost of the polymer donor (Figure 4a–c). The DFT measurements showed that the Cl substitution on the side-chains did not significantly impact the conformation of the conjugated backbone, but it slightly lowered the HOMO energy levels and significantly increased the dipole moment (Figure 4d). These trends were substantiated by the lower HOMO energy levels displayed by **P10** compared to its fluorinated analog in cyclic voltammetry measurements, which resulted in the improvement of V_{OC} from 0.84 (for PBDB-T-2F) to 0.86 V (for **P10**) in optimized OSCs with IT-4F. Moreover, the **P10**:IT-4F blend also exhibited higher J_{SC} of 21.80 mA cm⁻² and an excellent FF of 77%, resulting from the higher EQE and superior morphology, thereby enhancing the overall PCE from 13% (PBDB-T-SF) to 14.4% (which was certified as 13.9% by the National Institute of Metrology [NIM] in China). This study was the first major breakthrough in the history of single-junction OSCs, where an efficiency beyond 14% was achieved. Further, the authors also tested the stability of these OSCs under maximum output conditions, where **P10** demonstrated superior stability than PBDB-T-2F, with retention of nearly 75% of the initial PCE after 1000 h of testing. Alongside, Zhang et al. also independently reported **P10** (named PM7) and tested its viability for processing with nonhalogenated solvents.^[15b] They fabricated **P10**:IT-4F-based OSC devices using toluene as a green solvent, achieving an impressive PCE of 13.1%. These outcomes further signify that **P10** can be used for large-area OSCs. Recently, few groups also evaluated the in-depth effect of different solvent additives on the carrier dynamics and morphology of the **P10** (named PBDBT2Cl or PBDB-TCl):IT-4F system.^[39] However, no further improvement in PCEs was observed. Later, Li and co-workers fabricated OSCs based on **P10** and an asymmetrical NFA, IDT6CN-M.^[40] In addition to the good miscibility of **P10**:IDT6CN-M blend favoring optimal morphology and efficient charge transfer, the lower HOMO energy of **P10** helped to achieve the highest V_{OC} of 1.05 V in OSCs. Consequently, **P10**:IDT6CN-M-based optimized solar cells showed an excellent PCE of 13.3%, with a low energy loss ($E_{loss} = E_g^{opt} - eV_{OC}$)

of 0.55 eV. Thus, compared to Cl substitution in the conjugated backbone, its substitution in the side-chain will help to overcome the steric hindrance caused by its large size, and thereby positively affecting the properties of polymers. Finally, these reports clearly showed the importance of chlorination in side-chains strategy for designing efficient polymers for OSCs, since such polymers have a simple synthesis, higher yields, a low cost, impressive efficiency, and good stability over their F-counterparts.

With the significant breakthrough in efficiency achieved using **P10**, many groups synthesized various D–A-type polymers using 2Cl-BDT donor unit (Scheme 2). He and co-workers designed and synthesized a new chlorinated polymer named PBClT (**P11**, Scheme 2) based on alternate 2Cl-BDT and F-TT.^[21d] By using 2Cl-BDT, the HOMO energy levels in **P11** were dramatically reduced (–5.47 eV) compared to F-counterpart PTB7-Th (–5.27 eV), which in turn synergistically enhanced the V_{OC} in the corresponding OSC devices up to 1.01 V. Moreover, chlorination also led to good miscibility, higher degrees of “face-on” molecular orientation, and optimal nanoscale morphology in the **P11**:ITIC blend films, thus facilitating efficient dissociation of photo-excitons by minimizing charge recombination. As a result, a high PCE of 8.46% was achieved with **P11**, which is approximately 22% higher than that with the PTB7-Th tested parallelly.

Inspired by the success of 2Cl-BDT, the same group further studied the effects of the number of Cl substituents and their substitution positions on the side-chains of 2D-BDT by developing a series of polymers with difluorinated benzotriazole (FTAZ) as acceptor block (**P12n**, Scheme 2).^[15c] Although an increase in the Cl-content resulted in a deeper HOMO in the polymers, their substitution positions also had a marked effect on the opto-electrochemical properties (Figure 5). Among the polymers, PBT4Cl-Bz (**P12-4**) with 4-Cl substituents showed the remarkable lowest HOMO level (–5.64 eV) and stronger aggregation behavior resulting in high absorption coefficients ($1.66 \times 10^5 \text{ M}^{-1} \text{ cm}^{-1}$). Furthermore, a single-crystal X-ray diffraction study showed that the tetra-Cl-substituted BDT analog exhibits compact molecular packing and smaller dihedral angles than the two-Cl analog (Figure 5e), signifying the higher number of Cl atoms on side-chains will not negatively impact intermolecular packing. Thus, the OSC based on **P12-4**:IT-4F showed the highest PCE of 9.25%, with excellent nanoscale morphology and good trade-off between the V_{OC} of 0.96 V and J_{SC} of 16.42 mA cm⁻² and a substantially low E_{loss} of 0.54 eV (the PCEs of PBT1Cl-Bz [**P12-1**], PBT2Cl^{as}-Bz [**P12-2**], and PBT2Cl^s-Bz [**P12-3**] were 7.60, 4.43, and 7.8%, respectively). Thus, these results clearly emphasize that the number of Cl substituents and their substitution position must be carefully tuned to realize the best efficiency. Recently, Liu et al. achieved a remarkable PCE of 11.53% with **P12-3** (named J52-2Cl) using a more appropriate NFA, that is, ITIC.^[20a] They observed that the **P12-3**:ITIC blend film could yield optimal phase-separated morphology with a higher domain purity, an excitation diffusion probability $\approx 98\%$, and weak charge recombination compared to J52:ITIC, a without-Cl analog. All these factors translated into a remarkable enhancement of PCE values with improved photovoltaic parameters and high charge mobility. In another case study, Tang et al. tested the performances of **P12-3** with the new NFA unit BTA3,

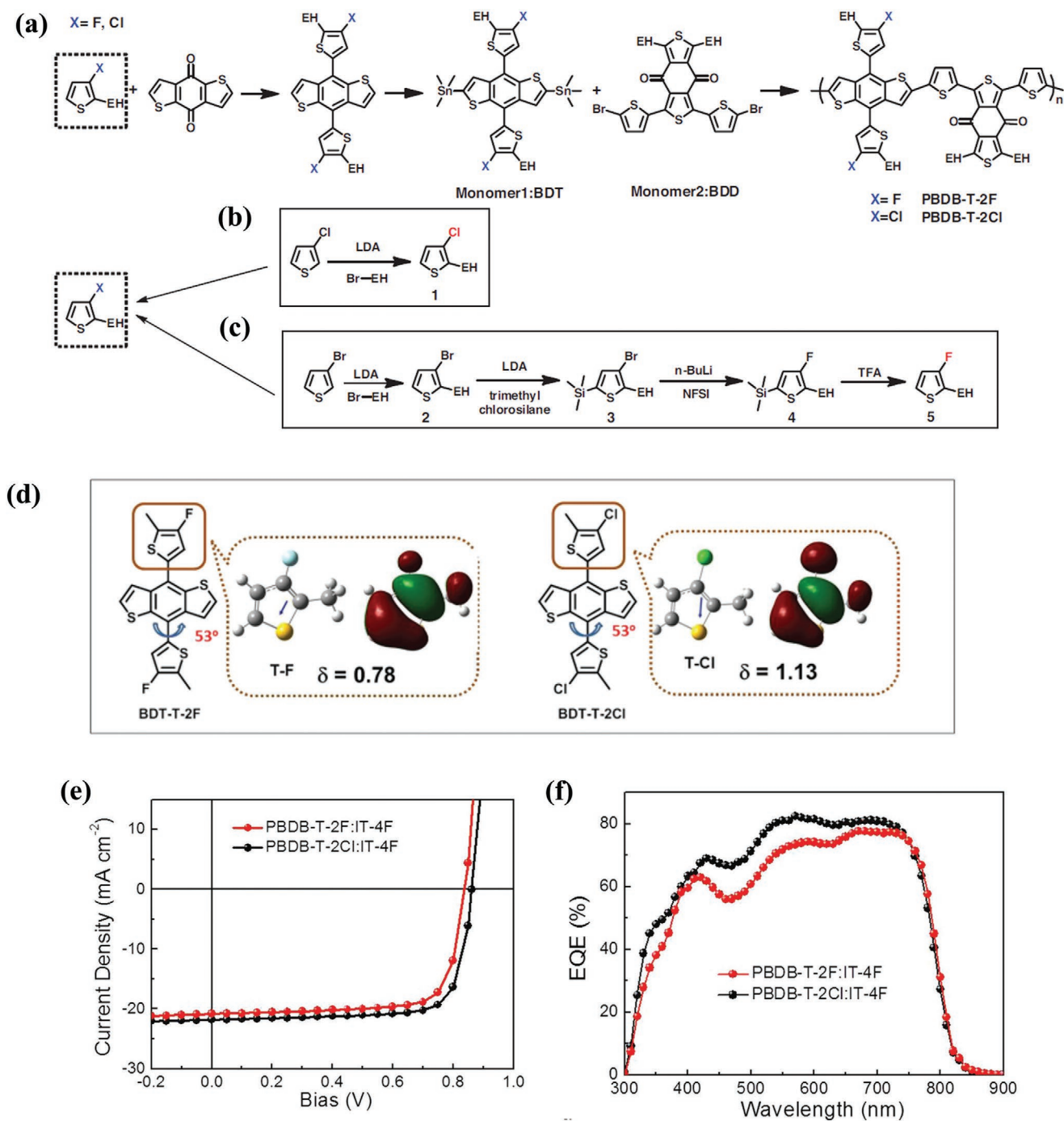


Figure 4. a) Chemical structures and synthetic route of the PBDB-T-2F and PBDB-T-2Cl (P10) polymers; b,c) synthetic routes for: b) the chlorinated monomer (1 step) and c) the fluorinated monomer (4 steps); d) twisting effects in the two BDT units, showing the dipole moments and HOMO surfaces in the thiophene side groups; e) J - V curves and f) EQE profiles of optimized devices. a-f) Reproduced with permission.^[14b] Copyright 2018, Wiley-VCH.

which was synthesized by using “Same-A-Strategy” (SAS).^[41] Benefitting from the favorable molecular orientation, high crystallinity, optimal morphology, and balanced carrier mobilities of the P12-3:BTa3 blend films, they achieved a PCE as high as 10.50% with breakthrough V_{OC} of 1.24 V reported to date for OSCs. The Fourier transform photocurrent spectroscopy (FTPS), external quantum efficiency and electroluminescence

(EL) study indicated that the P12-3:BTa3 possessed low bimolecular charge recombination, an E_{loss} of 0.52 eV, and low non-radiative recombination loss, which resulted in this outstanding V_{OC} .

He and co-workers further evaluated the effect of chlorination in asymmetric BDT-based polymers by preparing two new polymers, PBPTBz-1Cl (P13-1) and PBPTBz-2Cl (P13-2), having

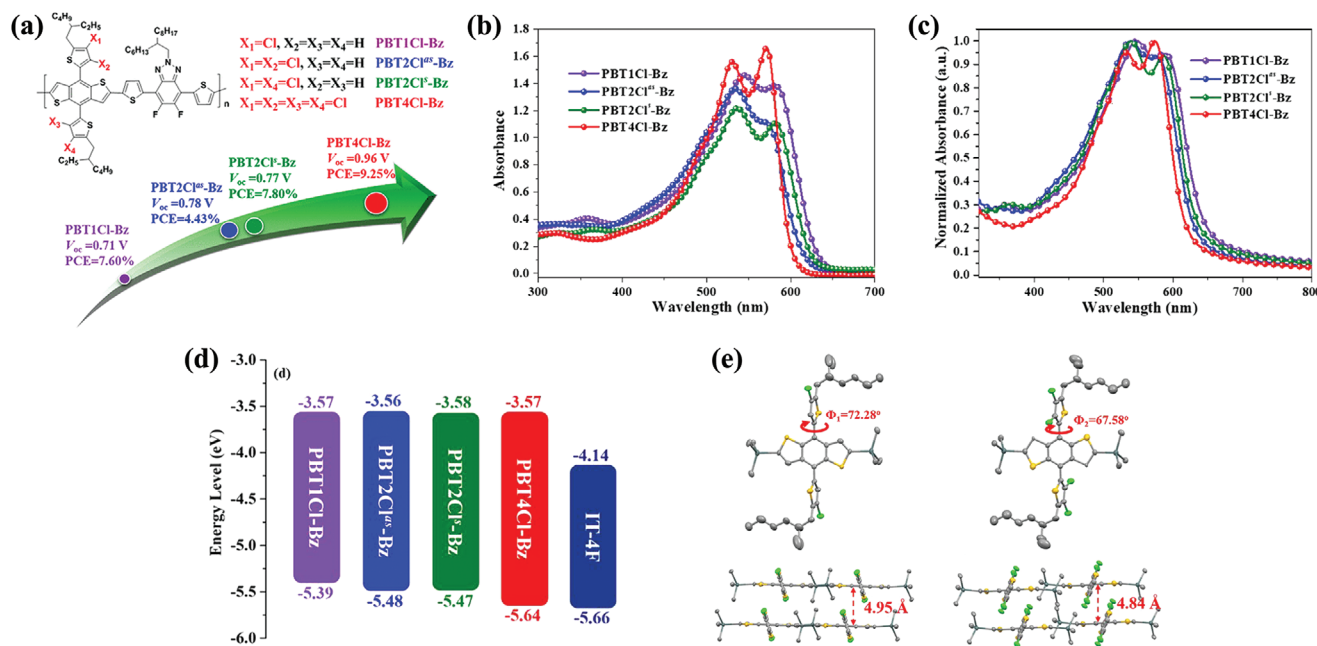


Figure 5. Effects of number of Cl substituents and their substitution positions in the PBTnCl-Bz (P12-n) series: a) chemical structures of the polymers; b) absorption spectra of four polymers in diluted chlorobenzene (CB) solution at 20 °C; c) normalized UV-vis absorption spectra of thin films; d) energy level diagrams of the corresponding donor polymers and IT-4F acceptor; and e) crystal structures and packing profiles of the monomers with two and four Cl substituents. a–e) Reproduced with permission.^[15c] Copyright 2018, American Chemical Society.

BDT unit incorporated with Cl-substituted thienyl and alkoxy phenyl units (Scheme 2).^[43] However, no further enhancement seen in the PCEs compared to the symmetrical counterparts P12-3 and P12-4, respectively (the PCEs of P13-1 and P13-2 were 6.46 and 7.18%, respectively).

Fine-tuning of the size and type of alkyl chain is a commonly used strategy for controlling the aggregation and solubility of conjugated polymers.^[1c,7a] As shown in Scheme 2, Chen and co-workers studied the effect of alkyl chain variation in the P12-3 (named L68) structure by preparing two new polymers, L24 (P14-1) and L810 (P14-2), with different alkyl chains on 2F-BTz.^[7d] The DFT calculations showed that the incorporation of 2Cl-BDT into the polymer backbone did not cause much distortion along the polymer backbone; interestingly, it resulted in a smaller dihedral angle than the corresponding fluorinated analog. Thus, chlorination helped to increase the molecular weight, π - π interactions, and formation of effective pathways for charge transport in the polymers, which in turn resulted in higher charge carrier mobility and photovoltaic parameters in the OSCs. By carefully optimizing the alkyl chains, the authors realized one of the highest efficiencies for FTAZ-based copolymers, that is, a PCE of 12.1%, with a high V_{OC} of 0.79 V, a high J_{SC} of 20.76 mA cm⁻², and a high FF of 73.5%, for P14-2:IT-4F having 2-octyl dodecyl alkyl chain.

The advantageous effect of alkyl chain tailoring can also be seen in the recent study by Su et al.^[7e] They introduced tripropylsilyl alkyl chains along with a Cl atom into the thienyl side-chains of BDT and evaluated their combined effects (Scheme 2 and Figure 6). Though all the polymers possessed similar bandgaps (≈ 1.94 eV), the polymers from PBZ (without Cl) to PBZ-Cl (P15-1, with Cl) and then PBZ-ClSi (P15-2, with Cl

and tripropylsilyl) exhibited a significantly lower HOMO, an enhanced absorption coefficient, and higher crystallinity originating from the combined effects of Cl and tripropylsilyl substituents. Additionally, P15-2 also displayed high and balanced charge mobility ($\mu_e/\mu_h = 2.57/2.11 \times 10^{-4}$ cm² V⁻¹ s⁻¹), appropriate phase separation with decreased charge recombination, and lower E_{loss} in the blend films with IT-4F. Consequently, optimized OSCs based on P15-2:IT-4F yielded the highest PCE of 12.8% for OSCs processed with a non-halogen solvent (1% 1-phenylnaphthalene (PN) in toluene). Further, P15-2:IT-4F-based OSCs displayed good thickness tolerance, with PCEs over 11% for 210 nm thick films, signifying that P15-2 could also be useful for fabricating large-area devices (Figure 6e).

To evaluate the effects of introducing different “A” units and π -bridging units in P12-3 polymer backbone, Tang et al. reported series of new chlorinated polymers, PE31 (P16-1), PE32 (P16-1), and PE4 (P16-3) based on alternate 2Cl-BDT as “D” unit and 2OR-BT, BTz, and hexylthieno[3,2-*b*]thiophene-bridged 2F-BTz, respectively as “A” units (Scheme 2).^[42] The DFT calculations result reflected significant changes in the backbone conformation of the polymers depending on the type of “A” or “ π -bridging units,” thereby affecting the optoelectronic properties and OSCs performances. So, resulting from the non-covalent interactions of F atoms in 2F-BTz, P12-3 and P16-3 demonstrated higher planarity and interchain interactions, thus, offering the enhanced J_{SC} and charge transport over other polymers. Furthermore, the introduction of hexylthieno[3,2-*b*]thiophene spacer in P16-3 led to a drastic change in the molecular orientation from zigzag (P12-3) to linear, which further conduce a well-ordered compact molecular packing and favorable morphology with smaller domain phases in the blend

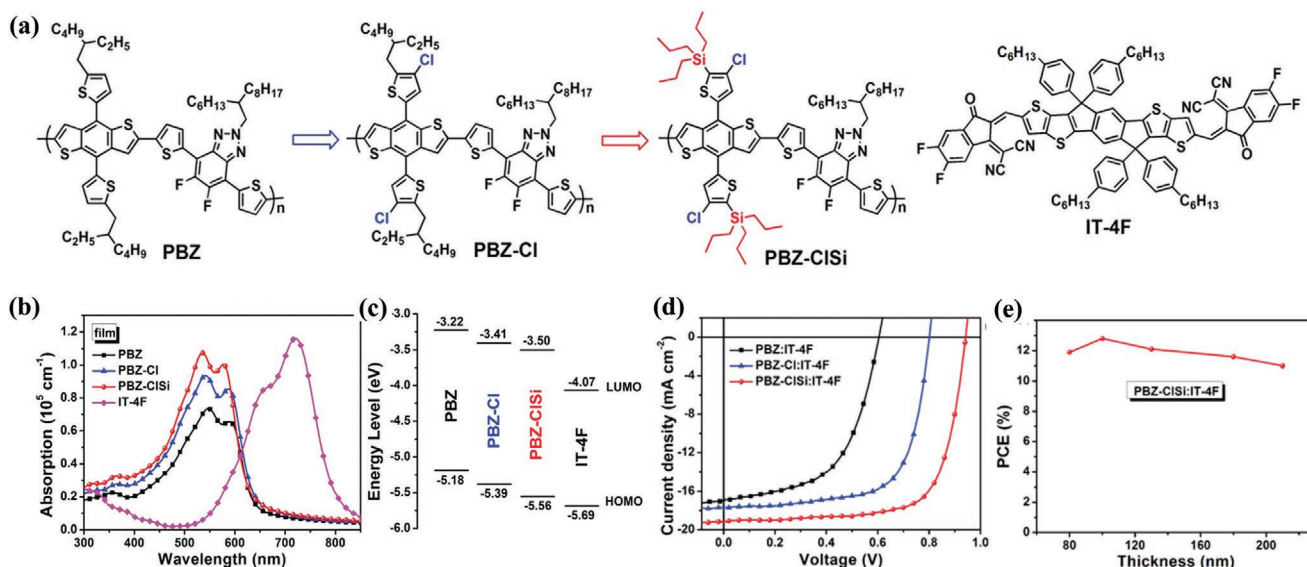


Figure 6. a) Chemical structures of PBZ, PBZ-Cl, PBZ-CISi (**P15-n**), and the IT-4F acceptor; b) molecular absorption coefficient of corresponding polymer donors in the thin film state; c) energy level diagrams of the polymer donors and IT-4F acceptor; d) J - V curves of the optimized OSC devices; and e) PCEs versus active layer thicknesses of the PBZ-CISi:IT-4F-based OSCs. a-d) Reproduced with permission.^[7e] Copyright 2019, The Royal Society of Chemistry.

films with Y6. Thus, OSCs based on **P16-3**:Y6 demonstrated the highest efficiency of 14.02% with a very high FF of 75.43% over other polymers in the series (PCE of **P16-1**, **P16-2**, and **P12-3** found to be 7.62, 7.31, and 12.31, respectively). These findings indicate that along with the chlorination, robust optimization of each molecular structure is also necessary for achieving appropriate morphology and high efficiency.

Inspired by the advantages of incorporating 2Cl-BDT as a donor unit in D-A copolymer design, Li and co-workers synthesized the new polymer PBT-Cl (**P17**, Scheme 2) with alternate 2Cl-BDT as the “D” unit and dialkoxy-substituted BT (2OR-BT) as the “A” unit.^[44] Similar to other chlorinated polymers, **P17** also showed lower HOMO, higher and balanced charge carrier mobility, and superior morphology, owing to the incorporation of 2Cl-BDT. Therefore, these factors boosting the efficiency of **P17**:IT-4F up to 11.60% in OSC devices fabricated with both CB and *m*-xylene solvent systems with slight differences in photovoltaic parameters.

A direct comparison of the effects of F and Cl incorporation was carried out by Huang et al. by synthesizing D-A copolymers based on alternate carboxylate-substituted polythiophene acceptors and 2F-BDT (PBDT-F-3T2C) or 2Cl-BDT (PBDT-Cl-3T2C, **P18**) donor (Scheme 2).^[45] **P18** demonstrated a low-lying frontier energy level due to the empty 3d orbitals of the Cl atom, whereas PBDT-F-3T2C exhibited higher crystallinity, attributed to stronger intermolecular interactions of the F atoms. When mixed with the IT-4F acceptor, PBDT-F-3T2C had a higher absorption coefficient, favorable morphology, and higher charge mobility, thus, slightly outperforming the Cl-counterpart **P18** (10.18%) with a PCE of 11.67%.

Yang and co-workers changed the position of Cl-atom in thienyl side-chains of 2Cl-BDT and simultaneously studied the effect of different numbers of thiazole (Tz) spacers by preparing a series of new polymers PBClITz-0 (**P19-1**), PBClITz-1 (**P19-2**), and PBClITz-2 (**P19-3**).^[46] As expected, the simultaneous effects

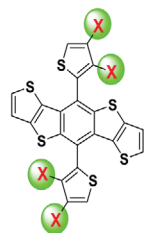
of chlorination and an increasing number of Tz units resulted in a higher V_{OC} of 1.01 eV in the OSCs based on **P19-3**. However, optimized blend films of **P19-2**:PC₇₁BM displayed superior morphology, lower charge recombination, and higher μ_h among the new polymers, thereby ensuring the best PCE of 8.42%.

Qui et al. reported two new chlorinated donor polymers based on alternate BDT and 2F-BTz units, J11 (**P20-1**) and J12 (**P20-2**), having Cl substituents (α -position) and flexible alkyl or alkoxy chains (β -position), respectively, at the thienyl side-chain of the BDT core (Scheme 2).^[47] Though, the presence of alkyl or alkoxy chains did not considerably affect absorption profiles of the polymers, **P20-2** displayed lower HOMO energy levels due to the stronger inductive effect of meta alkoxy chain, decreased aggregation, and enhanced miscibility with NFA m-ITTC. As a result, **P20-1**:m-ITTC-based OSCs showed higher charge carrier mobilities and superior morphology with smaller phase-separated domains than **P20-2**:m-ITTC blend (PCE of 8.74%), thereby resulting in a superior PCE of 12.32%.

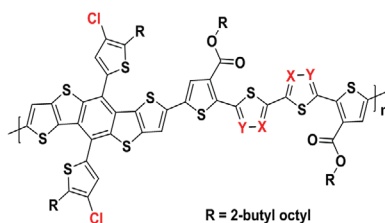
3.2. Chlorination of Dithienobenzodithiophene Units

Liu et al. reported two regioisomeric wide-bandgap polymers, PDBT(E)BTz-p (**P21-1**) and PDBT(E)BTz-d (**P21-2**), based on alternate chlorinated dithieno[2,3-*d*:2',3'-*d'*]benzo[1,2-*b*:4,5-*b'*]dithiophene (DTBDT) and dicarboxylate substituted 2,2'-bithiazole or 5,5'-bithiazole as the “D” and “A” units, respectively (Scheme 3).^[48] In addition to the chlorination effect, the authors also studied the structure-property relationship for different nitrogen topologies on the polymeric backbone. After mixing **P21-1** and **P21-2** with IT-4F acceptor, the authors achieved moderate PCEs of 6.96% and 7.81%, respectively, because of random molecular orientation and poor morphology of the blend films.

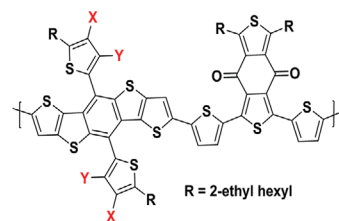
Further, Huang et al. studied the effect of halogenation on thienyl side-chains of DTBDT by synthesizing series of



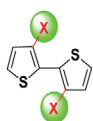
Dithieno-benzodithiophene (DTBDT)



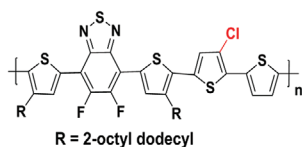
P21-1 (PDBT(E)BTz-p) : X = N, Y = H
P21-2 (PDBT(E)BTz-d) : X = H, Y = N



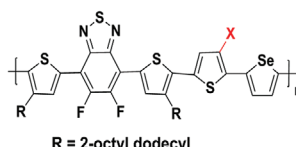
PDBT-F : X = F, Y = H
PDBT-2F : X = F, Y = F
P22-1 (PDBT-Cl) : X = Cl, Y = H
P22-2 (PDBT-2Cl) : X = Y = Cl



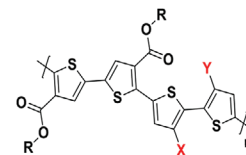
Bithiophene



P23 (PBT4T-Cl)



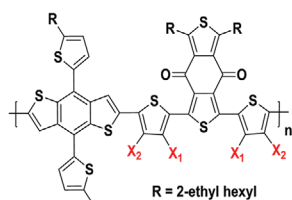
PBT3TSe : X = H
P24 (PBT3TClSe) : X = Cl



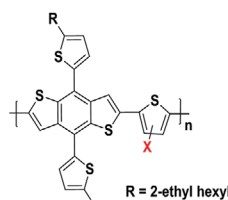
PDCBT : X = Y = H
PDCBT-F : X = H, Y = F (or X = F, Y = H)
PDCBT-2F : X = Y = F
P25-1 (PDCBT-Cl) : X = H, Y = Cl (or X = Cl, Y = H)
P25-2 (PDCBT-2Cl) : X = Y = Cl



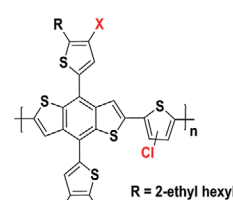
Thiophene



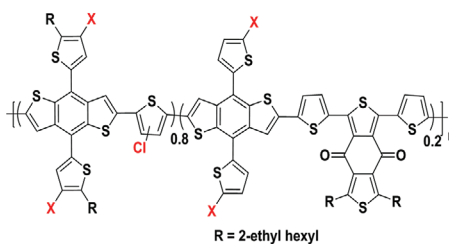
P26-1 (PCl(3)BDB-T) : X₁ = Cl, X₂ = H
P26-2 (PCl(4)BDB-T) : X₁ = H, X₂ = Cl



P(Th) : X = H
P27 (P(Cl)) : X = Cl



P28-1 (P(F-Cl)) : X = F
P28-2 (P(Cl-Cl)) : X = Cl



P28-3 P(F-Cl)(BDD = 0.2) : X = F
P28-4 P(Cl-Cl)(BDD = 0.2) : X = Cl

Scheme 3. Chemical structures of D–A-type polymers containing different chlorinated donor units: dithienobenzodithiophene (DTBDT), bithiophene, and thiophene.

PDBT-X-based polymers (X = F, Cl [PDBT-Cl, **P22-1**], 2F, and 2Cl [PDBT-2Cl, **P22-2**]), having different halogen content (Scheme 3).^[49] By controlling the number and position of F or Cl substituents, authors could control HOMO energy levels (from -5.39 to -5.49 eV), absorption profiles, and molecular orderings in the resulted polymers. In OSCs, **P22-1**:IT-4F revealed the “face-on” molecular orientation and superior nanoscale morphology, thereby realizing excellent charge transport properties with lower bimolecular charge recombination. Thus, OSCs based on **P22-1**:IT-4F outperform other polymers in the series with notable PCE of 12.6%. However, further chlorination of **P22-1** into **P22-2** harmed molecular packing

and morphology due to the larger steric hindrance. Therefore, **P22-2** demonstrated poor PCE of 6.2% despite its high V_{OC} of 0.99 V originating from its higher Cl-content.

3.3. Chlorination of Bithiophene

Over the years, simple structured 2,2'-bithiophene (BTh) has emerged as a prominent and efficient donor unit for developing high-performing polymer donors for OSCs.^[6a,7b] In 2018, He and co-workers demonstrated the effects of incorporating Cl atoms into BTh by synthesizing the corresponding polymer

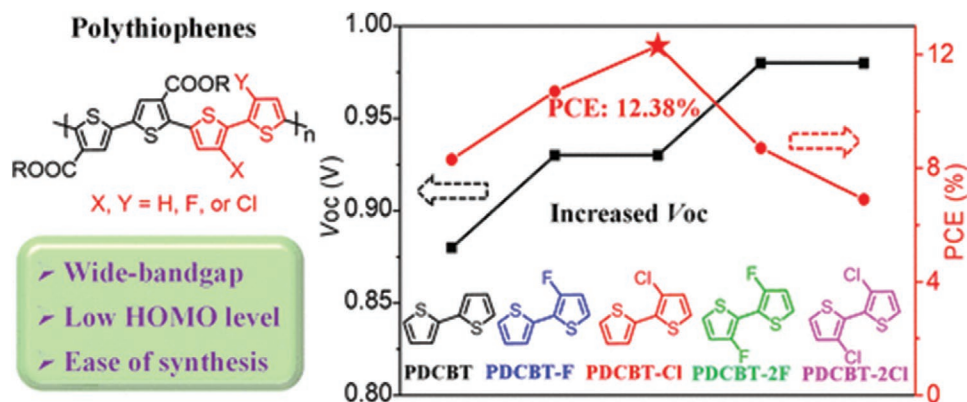


Figure 7. Effects of different numbers of halogen substituents in PCDBT-X (P25-n)-based polymer donors. Reproduced with permission.^[50] Copyright 2019, American Chemical Society.

PBT4T-Cl (**P23**, Scheme 3).^[15f] This polymer design is inspired by the previously reported PffBT4T-2OD class of polymer, which yielded a world record efficiency of 11.7% when blended with PC₇₁BM.^[7b] The authors specifically introduced only one Cl atom in the BTh unit to maintain minimum planarity in **P23**. The GIWAXS, AFM, and TEM measurements revealed the marked improvement in molecular packing, morphology, and charge dynamics in the OSC devices based on **P23**:PC₇₁BM blend caused by incorporating 3-chloro-2,2'-bithiophene (Cl-BTh). As a result, optimized OSCs based on **P23**:PC₇₁BM showed superior PCEs of up to 11.18% with a high J_{SC} (18.71 mA cm⁻²), V_{OC} (0.80 V), and FF (74.60%). Importantly, this is the highest efficiency achieved by chlorinated polymer donors and fullerene-based acceptors reported to date. Additionally, **P23** devices also showed superior stability by retaining a PCE of 8.16% after 50 days under a glovebox without encapsulation, resulting from the enhanced intermolecular interactions from Cl atoms as revealed by time-dependent absorption spectra analysis. In summary, **P23** has a simple synthesis, a low cost, high efficiency, and reasonable stability, which will be eventually beneficial for commercialization.

Over the years, replacing thiophene with selenophene (Se) is evolved as an effective way to tune the energy levels and enhance the crystallinity in conjugated polymers.^[1c,53] Zhong et al. optimized the **P23** polymer design by replacing Cl-BTh with 2-(selenophen-2-yl)thiophene or 3-chloro-2-(selenophen-2-yl)thiophene as “D” units to form two polymers, PBT3TSe and PBT3TClSe (**P24**, Scheme 3), respectively.^[8h] They studied the effect of Se-incorporation together with chlorination in OSCs. Though incorporation of Se with metalloid properties helped to achieve a lower bandgap and stronger interchain π - π aggregations in the polymers, they upshifted the HOMO energy levels due to the strong electron-donating nature of Se. Thus, optimized **P24**:PC₇₁BM demonstrated a PCE of 9.89% with a slightly higher J_{SC} of 18.93 mA cm⁻² and a lower V_{OC} of 0.77 V than **P23**.

Together with Cl-BTh, Wang et al. also tested the effects of insertion of 3,3'-dichloro-2,2'-bithiophene (2Cl-BTh) unit in the polymer backbone by polymerizing both the donor units with carboxylate-substituted polythiophene acceptors to form new polymers, PDCBT-Cl (**P25-1**) and PDCBT-2Cl (**P25-2**), respectively (Scheme 3 and Figure 7).^[50] Parallely, without halogen (PDCBT), monofluorinated (PDCBT-F), and difluorinated

(PDCBT-2F) analogs were also prepared to evaluate the impact of different halogen atoms. Indeed, the incorporation of halogens (Cl or F atoms) effectively downshifted the molecular energy levels, resulting in the enhancement of the V_{OC} in OSCs. The DFT results indicated that the planarity of the polymer backbone improved from PDCBT to PDCBT-F and then PDCBT-2F (the torsion angles between two thiophene rings were 12°, 1.7°, and 0.6°, respectively), due to the smaller size F atom over H atom. In contrast, this angle was increased to 15.2° and then 42.8° in the cases of **P25-1** and **P25-2**, respectively, due to the large size of the Cl atom. As a result, all these polymers exhibited distinct molecular packing and optoelectronic properties based on the type and number of halogen substituents. In OSCs, **P25-1**:ITIC-Th1 blend films displayed superior morphology with favorable molecular packing and miscibility compared to the other blends. Therefore, a noticeable PCE of 12.38% was achieved using **P25-1**:ITIC-Th1-based OSC devices. In contrast, **P25-2** displayed the lowest PCE of 6.94% due to the blueshifted absorption, poor molecular stacking, and inferior morphology attributed to the distorted polymer backbone. Thus, these outcomes further substantiating multi-chlorination in the polymer backbone is not always a favorable strategy for improving the PCEs, as the large size of Cl atom will significantly hamper polymer aggregation and morphology.

3.4. Chlorination of Thiophene

One unique advantage of introducing a thiophene linker into the conjugated polymer backbone is the ease of grafting various functional groups, thereby tailoring the frontier energy levels and molecular orientation in the resulted polymers.^[7a,j,54] Based on this principle, Wu et al. synthesized the polymers PCl(3)BDB-T (**P26-1**) and PCl(4)BDB-T (**P26-2**) with the same backbone but different Cl orientations on the linker thiophene (Scheme 3).^[20b] They emphasized that a minor variation in the Cl orientation dramatically affected the opto-electrochemical properties, planarity, and charge carrier properties of these polymers. Thus, the **P26-1**:IT-4F-based device showed a very poor PCE of 0.18%, whereas the **P26-2**:IT-4F-based device showed an outstanding PCE of 12.33% with good coplanarity, balanced mobilities, and optimal morphology. Through a very

detailed structure–property relationship study, the authors found that the primary reason for the poor PCE of **P26-1** was its distorted backbone and poor morphology, which completely hampered the intramolecular and intermolecular charge transport in OSCs.

Very recently, our group achieved a significant breakthrough by synthesizing the easily scalable and low-cost chlorinated polymer donor P(Cl) (**P27**, Scheme 3). **P27** consists of alternate electron-rich 2D-BDT and simple 3-chlorothiophene (Cl-Th) as the “D” and “A” units, respectively.^[51] We designed **P27** by adopting the low synthetic complexity (SC) approach indicated by Po et al.^[55] Obviously, Cl incorporation in **P27** ensured a higher molecular weight, an excellent absorption coefficient of $70617 \text{ M}^{-1} \text{ cm}^{-1}$ at 530 nm, a wide bandgap (1.97 eV), and a low-lying HOMO energy level (−5.47 eV). Moreover, **P27** also showed complementary absorption and excellent energy levels matching with ITIC-Th. In the inverted OSC, optimized **P27**:ITIC-Th blend films exhibited favorable aggregation with a smaller π – π stacking distance and optimal morphology, thus affording superior PCEs of up to 11.4% in OSCs with excellent stability (certified PCE by the Nano Convergence Practical Application Center in the Republic of Korea [NCPAC] was 12.14%). Notably, this PCE is approximately ≈ 4.66 times higher than that of the unchlorinated counterpart synthesized in parallel.

Importantly, we also assessed the SC and cost-effectiveness of **P27** by comparing with well-known commercialized donor polymers such as P3HT, PTB7, PTB7-Th, and PBDB-T, among which **P27** had the lowest SC of 36.7%. In summary, **P27** was found to be inexpensive and has a facile synthesis with a higher yield, superior photovoltaic performance, and excellent stability, and thus has enormous potential in module fabrication.

In the continuation work, we further tried to optimize the **P27** design by replacing the 2D-BDT donor with 2F-BDT or 2Cl-BDT to form new polymers P(F–Cl) (**P28-1**) and P(Cl–Cl) (**P28-2**), respectively (Scheme 3 and Figure 8).^[52] In addition to deeper HOMO energy levels owing to the presence of F or Cl units on BDT, both the polymers displayed higher aggregation tendencies resulting in lower molecular weight due to decreased solubility. Thus, optimized OSCs with **P28-1**:IT-4F and **P28-2**:IT-4F blend films showed PCEs of 11.8% and 10.2%, respectively. Later, by adding a small amount of 1,3-bis(5-bromothiophen-2-yl)-5,7-bis(2-ethylhexyl)benzo[1,2-*c*:4,5-*c'*]dithiophene-4,8-dione (BDD) as a third component in the polymer backbone of **P28-1** and **P28-2**, we tried to improve their solubilities and molecular weights by lowering their aggregation. Thus, two new terpolymers P(F–Cl)(BDD = 0.2) (**P28-3**) and P(Cl–Cl)(BDD = 0.2) (**P28-4**) were prepared based on the D1–A1–D1–A2 approach. As anticipated, **P28-3** and **P28-4**

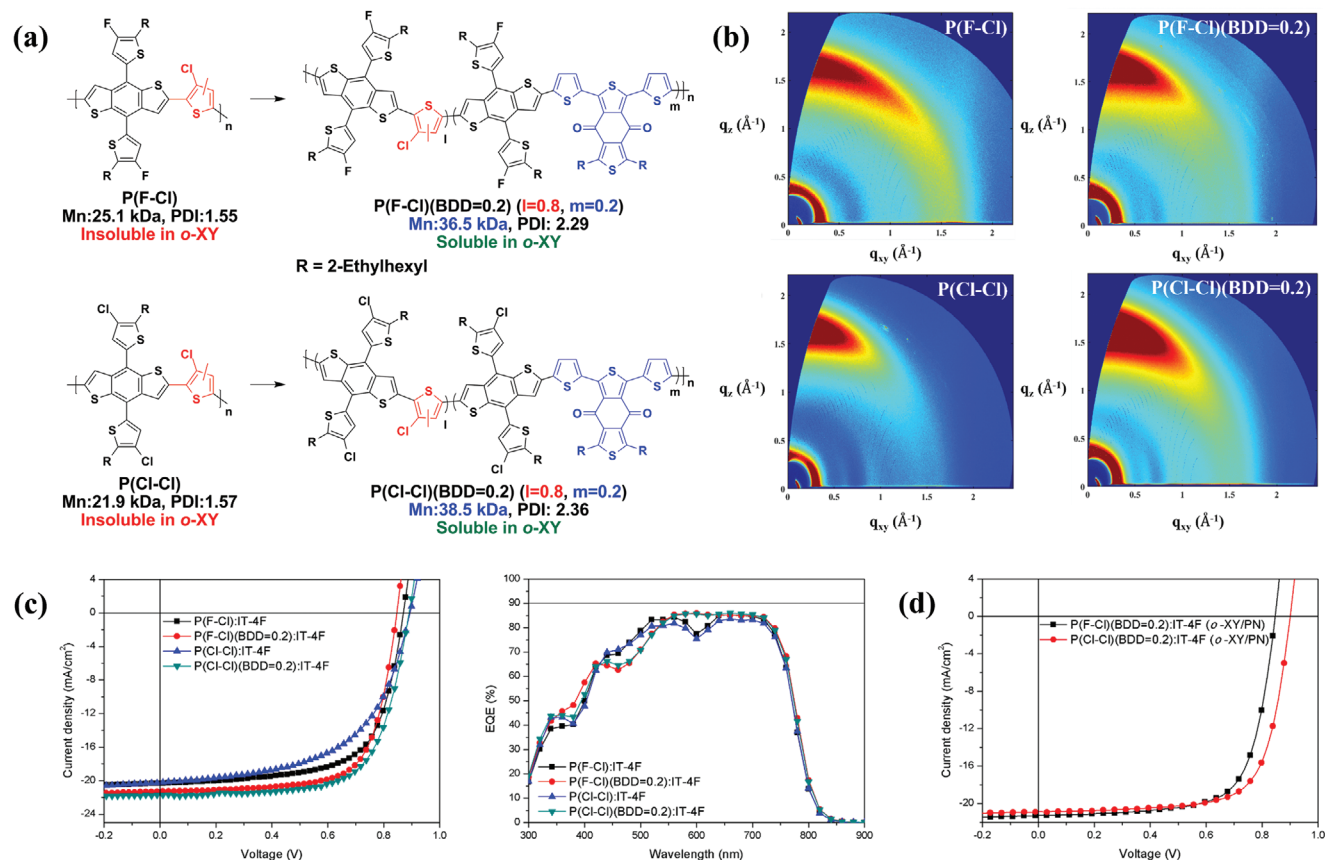


Figure 8. a) Chemical structures of P(F–Cl), P(Cl–Cl), P(F–Cl)(BDD = 0.2), and P(Cl–Cl)(BDD = 0.2) (**P28-n**); b) corresponding 2D-GIWAXS profiles of pristine polymers; c) J–V curves and EQE profiles of optimized OSC devices based on polymer:IT-4F; and d) J–V curves of P(F–Cl)(BDD = 0.2) and P(Cl–Cl)(BDD = 0.2) devices processed with eco-friendly o-xylene:1-phenylnaphthalene (99.5:0.5, v/v %) solvent system. a–d) Reproduced with permission.^[52] Copyright 2019, Wiley-VCH.

displayed higher molecular weights and solubility than their parent D–A polymers because of the decreased aggregation tendencies caused by the insertion of BDD as the third component. Furthermore, by mixing with IT-4F, both these blend films displayed good miscibility and superior morphology, resulting in efficient exciton diffusion and charge transfer. Consequently, corresponding OSCs **P28-3** and **P28-4** showed remarkable PCEs of 12.7% and 13.2%, respectively, with improvement in the overall photovoltaic parameters. Due to the good solubility of these polymers in eco-friendly *o*-xylene, we also fabricated OSCs using *o*-xylene:PN as processing solvent (99.5:0.5, v/v%). Remarkably, both these polymers yielded impressive PCEs of 12.2% and 13.5%, respectively, due to an excellent balance between molecular weight and solubility (NCPAC certified PCEs were 12.70% and 13.97% for **P28-3** and **P28-4**, respectively). To sum up, our in-depth study indicates that chlorination strategy could be the most reliable method for constructing low-cost, high-performance, and eco-friendly OSCs.

Undoubtedly, chlorination on the donor units offers vast opportunities to tailor the optoelectronic properties compared to its insertion on the acceptor units. From the above-discussed examples, several important points can be taken away. The impact of chlorination on the molecular packing and crystallinity of the materials is mainly reliant on their substitution position. One can overcome the inherent twisting of the backbone caused by the large-sized Cl atom by introducing them in the side-chains. Additionally, chlorination in the side-chains can simultaneously improve the J_{SC} , V_{OC} , and charge carrier mobilities by lowering frontier HOMO energy levels, enhancing the absorption and crystallinity. Thus, it remains one of the most reliable approaches in recent years for designing efficient D–A polymers or small-molecule donors, delivering PCE over 14%. In the meantime, it is essential to note that chlorination on the donor backbone and excess of chlorination on the side-chains have similar negative effects on the aggregation and nanoscale morphology, as observed in the case of chlorinated acceptor units. Consequently, realizing the high efficiency through chlorination on the donor backbone or multi chlorination on the side-chains is far from simple, and hence, careful optimization of each molecular structure is essential to achieve an optimal trade-off between crystallinity and morphology. Among the side-chain modifications of BDT and DTBDT, most of these reports follow only one approach, that is, chlorination on the thienyl side-chains of 2D-BDT. Therefore, elucidation of Cl incorporation on the other heterocyclic side-chains (e.g., benzyl or naphthyl)^[56] on BDT or DTBDT will be an interesting research topic. Besides, molecular design strategy with low synthetic complexity and processing using non-halogen solvent must also be focused during the future designing of the chlorinated donor molecules, as they are more suitable for commercial application.

4. Chlorination on Nonfullerene Acceptor Units

Although fullerene-based acceptors dominated as the ideal choice of EAs for OSCs for over two decades,^[6a,57] their intrinsic limitations, such as complex synthesis, high cost, and poor

stability, paved the way for the development of their replacements, the so-called NFAs.^[58] Since 2015, rapid progress has been realized in the development of NFAs, which not only outperformed the fullerene OSCs in terms of efficiency, but they also favored easier tuning of the optoelectronic properties and morphology and better stability.^[2b,f,5b,58,59] Currently, many research groups have already incorporated Cl atoms onto the many popular NFAs to examine whether their incorporation can improve their photoelectrochemical properties and performances in OSCs. (**Schemes 4** and **5**).

4.1. Earlier Developments of Chlorinated NFAs

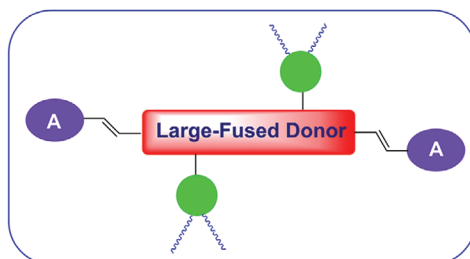
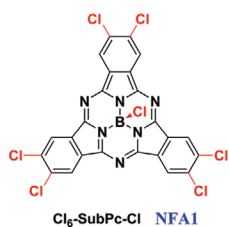
Subphthalocyanines (SubPCs) were considered to be one of the early reported NFAs and are composed of central boron atoms surrounded by fully conjugated diiminoisindole moieties forming an aromatic macrocyclic structure.^[60] These NFAs exhibited some beneficial properties, such as higher chemical and thermal stability, favorable energy levels, and strong absorption coefficients, thus delivering initial success to the OSCs.^[60] In 2015, Cnops et al. synthesized a series of subphthalocyanine-based SMs with different electron-withdrawing substituents as NFAs, among which the chlorinated NFA named Cl6-SubPc-Cl (**NFA1**, Scheme 4) showed the best performance of 6.86% with a SubNc donor.^[61] However, the fabrication of OSCs with **NFA1** involves expensive vacuum thermal processing due to which these types of acceptors have not been further explored extensively.

4.2. A–D–A-Type Chlorinated NFAs

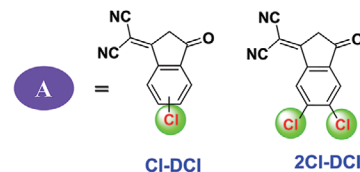
Among various design strategies used for developing NFAs, an “A–D–A”- or “A–(π -spacer)–D–(π -spacer)–A”-type fused-ring electron acceptor (FREA) has proved to be one of the most successful designs to date.^[5b,58,62] In addition to the easy tailoring of optoelectronic properties and bandgap of these FREAs by judicious selection of molecular units, such as varying the core “D” and/or “A” units, alkyl chains, and spacer, this molecular design also allows easy control of the molecular orientation and optimal morphology.^[5b,58,59] Thus, molecular engineering in this design strategy delivers a wide variety of new NFAs with high performance in OSC devices. Recently, many research groups incorporated different chlorinated units, such as 2-(5 or 6-chloro-3-oxo-2,3-dihydro-1H-inden-1-ylidene)malononitrile (Cl-DCI), 2-(5,6-dichloro-3-oxo-2,3-dihydro-1H-inden-1-ylidene)malononitrile (2Cl-DCI), 2-(1-chloro-6-oxo-5,6-dihydro-4H-cyclopenta[*c*]thiophen-4-ylidene)malononitrile (CPTCN-Cl), and 2-(2-chloro-6-oxo-5,6-dihydro-4H-cyclopenta[*b*]thiophen-4-ylidene)-malononitrile (TIC-Cl) as terminal “A” units to synthesize various new Cl-NFAs as shown in Schemes 4 and 5 and their detailed optoelectronic and OSC device characteristics are summarized in **Table 3**.

Since the discovery of ITIC by Lin et al. in 2015,^[63] ITIC has been evolved as an excellent EA core for high-performance NF-OSCs due to its unique characteristics, such as broad absorption, suitable FMO energy levels, high electron mobility, and superior PCEs with various D–A polymers.^[5b,8e,g,i,34c,58,59] Yang et al. were the first to report a series of X-ITIC-based

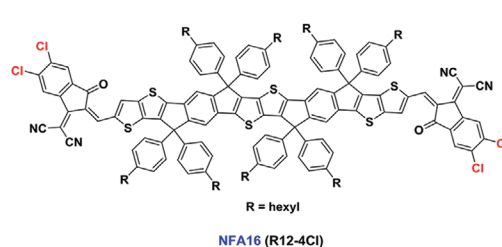
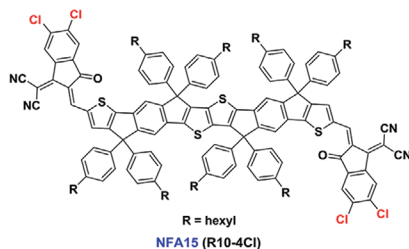
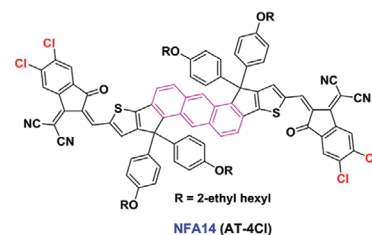
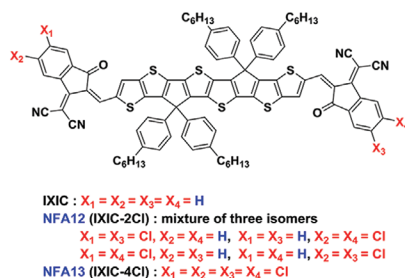
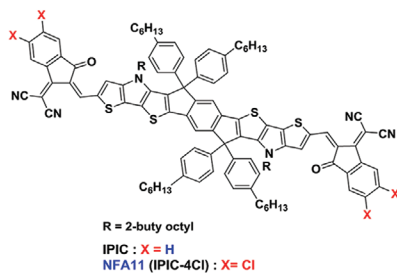
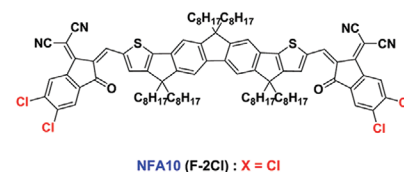
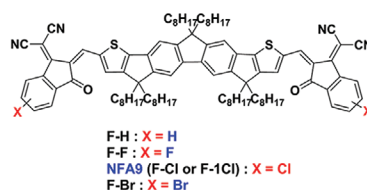
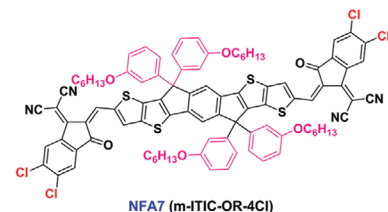
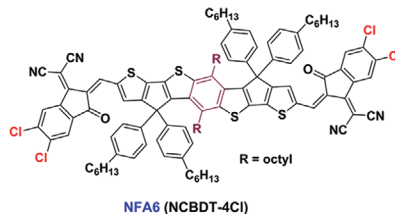
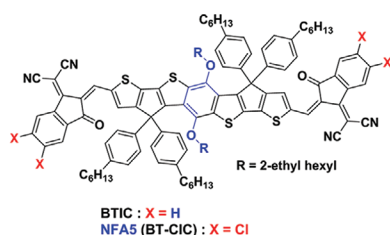
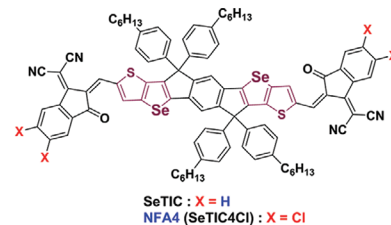
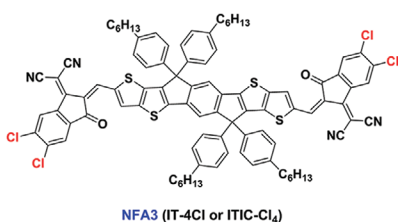
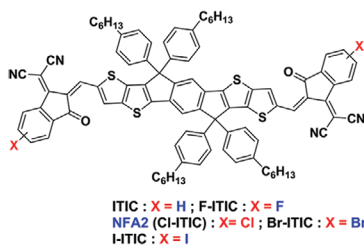
A–D–A type NFAs



Chlorination on dicyanovinylindanone (DCI)

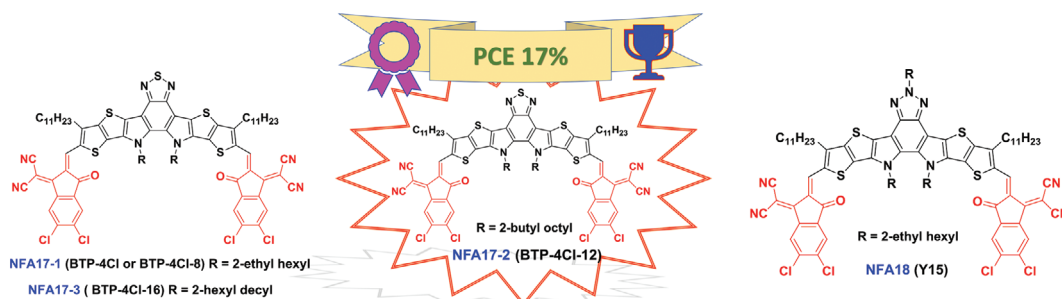


Chlorinated dicyanovinylindanone-based NFAs :

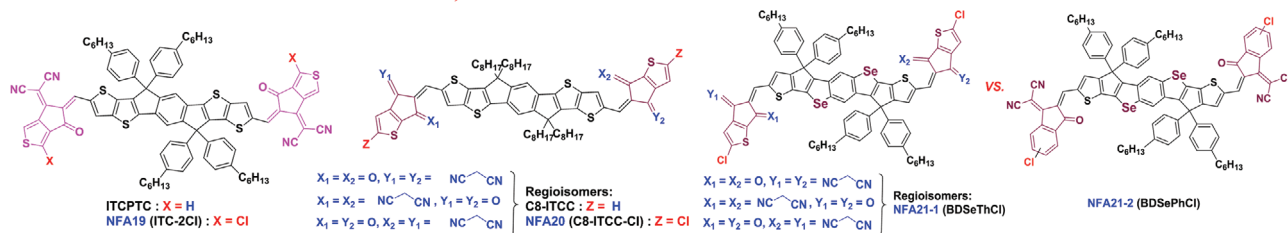


Scheme 4. Chemical structures of various “A–D–A”-type chlorinated nonfullerene acceptor units having chlorinated DCI-Cl as terminal “A” units.

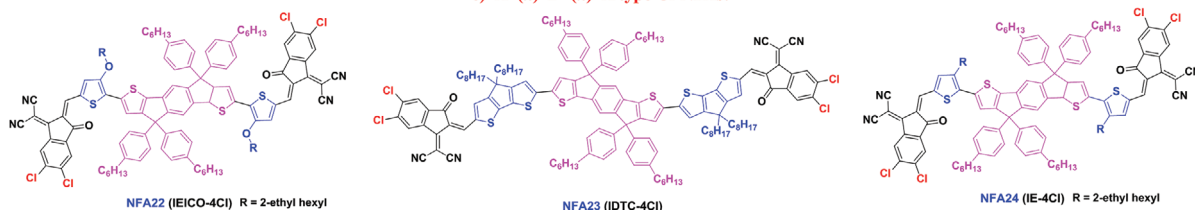
a) Fused benzothiadiazole and benzotriazole based CI-NFAs:



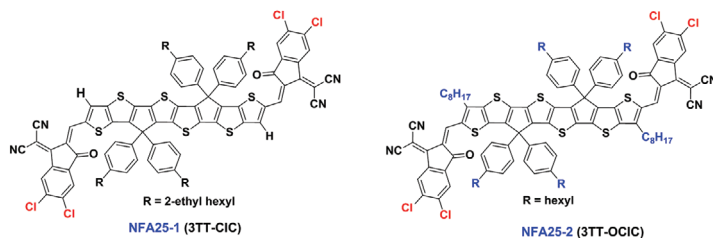
b) CPTCN-Cl and TIC-Cl based CI-NFAs:



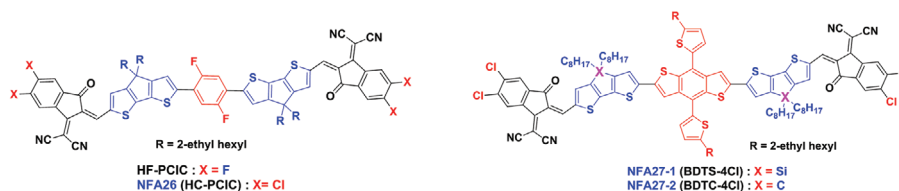
c) A-(π)-D-(π)-A type CI-NFAs:



d) Effect of alkyl chains:



e) CI-NFAs based on Non-fused architecture:
(A-D'-D'-A type)



Scheme 5. a–c) Chemical structures of: a) fused benzothiadiazole and benzotriazole based CI-NFAs; b) “A–D–A”-type CI-NFAs unit with chlorinated CPTCN-Cl or TIC-Cl as terminal “A” units; c) “A–(π -spacer)–D–(π -spacer)–A”-type CI-NFAs units; d) effect of alkyl chains; and e) CI-NFAs based on non-fused architecture.

NFAs (X = F, Cl (NFA2), Br, and I) by incorporating different halogenated 1,1-dicyanomethylene-3-indanone (DCI)^[64] “A” units in ITIC (Scheme 4).^[19] Their aim of this study was to estimate the effects of various halogens (F, Cl, Br, and I) on the energy levels, absorption, and charge transport properties of

these newly prepared NFAs. In fact, the introduction of halogens led to lower HOMO/LUMO energy levels and higher crystallinity in the new acceptors owing to the strong electronegativity and “heavy atom effect” of the halogens. Additionally, by substituting them at the terminal positions of DCI units, they

Table 3. Summary of optoelectronic properties and OSC parameters of various chlorinated nonfullerene acceptor units.

NFA	Original name	HOMO [eV]	LUMO [eV]	E_g^{opt} [eV] ^{c)}	Donor	V_{oc} [V]	J_{sc} [mA cm ⁻²]	FF [%]	PCE [%]	Electron mobility [cm ² V ⁻¹ s ⁻¹]	Ref.
NFA1	Cl6-SubPc-Cl	–	–3.61 ^{a)}	–	Sub Nc	1.04	10.1	66.6	6.86	–	[61]
NFA2	Cl-ITIC	–5.70 ^{a)}	–4.14 ^{b)}	1.56	PTPDBDT	0.94	15.6	65.0	9.5	$1.9 \times 10^{-4\text{d}}$	[19]
	IT-2Cl	–5.68 ^{a)}	–3.99 ^{a)}	1.55	PBDB-T-2F	0.92	19.08	74.8	13.16		[15d]
	IT-4Cl	–5.75 ^{a)}	–4.09 ^{a)}	1.48	PBDB-T-2F	0.79	22.67	75.2	13.45		[15d]
	IT-4Cl	–5.75 ^{a)}	–4.09 ^{a)}	1.48	PBDB-T-2F	0.78	22.25	73.0	12.67		[16]
NFA3					PBDB-T-2Cl	0.81	22.01	74.0	13.37		[16]
	ITIC-Cl ₄	–5.5 ^{a)}	–3.9 ^{a)}	1.45	PBDB-T	0.74	21.50	57.0	9.6	–	[65]
	IT-4Cl	–5.75 ^{a)}	–4.06 ^{a)}	1.48	PBFTT	0.76	19.7	73.9	11.1	$3.38 \times 10^{-4\text{e}}$	[66]
NFA4	SeTIC4Cl	–5.65 ^{a)}	–4.08 ^{a)}	1.44	PM6	0.78	22.92	75.0	13.32	$1.6 \times 10^{-4\text{e}}$	[15e]
NFA5	BT-CIC	–5.49 ^{a)}	–4.08 ^{a)}	1.33	PCE-10	0.70	22.50	71.0	11.2	$2.1 \times 10^{-4\text{e}}$	[18a]
NFA6	NCBDT-4Cl	–5.60 ^{a)}	–4.02 ^{a)}	1.40	PBDB-T-SF	0.85	22.35	74.3	14.1	$1.85 \times 10^{-4\text{e}}$	[68]
NFA7	m-ITIC-OR-4Cl	–5.78 ^{a)}	–4.05 ^{a)}	1.52	BO2FC8	0.83	20.2	63.3	11.0	$2.5 \times 10^{-3\text{e}}$	[69]
NFA8	ID-4Cl	–5.81 ^{a)}	–4.01 ^{a)}	1.51	PM6	0.767	17.87	74.76	10.25	$4.32 \times 10^{-5\text{e}}$	[71]
NFA9	F-Cl	–5.62 ^{a)}	–4.04 ^{a)}	1.58	PBDB-T	0.87	17.61	75.0	11.47	$1.15 \times 10^{-4\text{e}}$	[72]
NFA11	IPIC-4Cl	–5.51 ^{a)}	–3.95 ^{a)}	1.32	PBDB-T	0.81	22.2	74.0	13.4	$1.0 \times 10^{-4\text{e}}$	[73]
NFA12	IXIC-2Cl	–5.20 ^{a)}	–3.90 ^{a)}	1.30	PBDB-T	0.73	23.6	70.9	12.2	$1.02 \times 10^{-3\text{d}}$	[74]
NFA13	IXIC-4Cl	–5.20 ^{a)}	–3.95 ^{a)}	1.25	PBDB-T	0.69	22.9	71.2	11.2	$1.10 \times 10^{-3\text{d}}$	[74]
NFA14	AT-4Cl	–5.71 ^{a)}	–3.89 ^{a)}	1.60	PBDB-T	0.90	19.52	75.5	13.27	$1.85 \times 10^{-4\text{e}}$	[75]
NFA15	R10-4Cl	–5.35 ^{a)}	–3.91 ^{a)}	1.43	PBDB-T	0.85	18.9	66.6	10.7	$2.3 \times 10^{-5\text{e}}$	[76]
NFA16	R12-4Cl	–5.26 ^{a)}	–3.95 ^{a)}	1.35	PBDB-T	0.75	18.5	66.9	9.3	$2.1 \times 10^{-5\text{e}}$	[76]
NFA17-1	BTP-4Cl	–5.68 ^{a)}	–4.12 ^{a)}	1.40	PBDB-TF	0.867	25.4	75.0	16.5	–	[2b]
	BTP-4Cl-8	–5.67 ^{a)}	–4.11 ^{a)}	1.40	PBDB-TF	0.872	25.2	74.3	16.3		[2h]
NFA17-2	BTP-4Cl-12	–5.66 ^{a)}	–4.09 ^{a)}	1.39	PBDB-TF	0.858	25.6	77.6	17.0		[2h]
NFA17-3	BTP-4Cl-16	–5.68 ^{a)}	–4.09 ^{a)}	1.39	PBDB-TF	0.862	24.2	74.8	15.6		[2h]
NFA18	Y15	–5.56 ^{a)}	–3.93 ^{a)}	1.30	PM6	0.867	23.79	68.49	14.13	$5.22 \times 10^{-4\text{e}}$	[77]
NFA19	ITC-2Cl	–5.58 ^{a)}	–4.01 ^{a)}	1.58	PM6	0.91	20.1	74.1	13.6	$7.78 \times 10^{-4\text{d}}$	[78]
NFA20	C8-ITCC-Cl	–5.50 ^{a)}	–3.93 ^{a)}	1.58	PBDB-TF	0.95	17.9	73.0	12.4	$6.6 \times 10^{-4\text{e}}$	[79]
NFA21-1	BDSeThCl	–5.58 ^{a)}	–3.82 ^{a)}	1.55	PM7	0.97	17.85	68.8	11.91	$3.99 \times 10^{-4\text{e}}$	[80]
NFA21-2	BDSePhCl	–5.61 ^{a)}	–3.96 ^{a)}	1.41	PM7	0.92	20.35	73.1	13.68	$5.07 \times 10^{-4\text{e}}$	[80]
					J52	0.70	23.8	60.7	10.1	–	[18b]
NFA22	IEICO-4Cl	–5.56 ^{a)}	–4.23 ^{a)}	1.23	PBDB-T	0.744	20.8	62.5	9.67	–	[18b]
					PTB7-Th	0.727	22.8	62.0	10.3	–	[18b]
NFA23	IDTC-4Cl	–5.50 ^{a)}	–3.79 ^{a)}	1.35	PBDB-T	0.822	19.19	60.2	9.50	$2.84 \times 10^{-4\text{d}}$	[81]
NFA24	IE-4Cl	–5.54	–4.11	1.43	PBDB-T	0.86	21.49	60.0	11.1	$3.7 \times 10^{-4\text{e}}$	[82]
NFA25-1	3TT-CIC	–5.24 ^{a)}	–3.95 ^{a)}	1.23	PCE-10	0.65	26.67	69.0	11.96	$1.18 \times 10^{-4\text{e}}$	[83]
NFA25-2	3TT-OCIC	–5.22 ^{a)}	–3.91 ^{a)}	1.29	PCE-10	0.68	26.49	69.0	12.43	$1.36 \times 10^{-4\text{e}}$	[83]
NFA26	HC-PCIC	–5.54 ^{a)}	–3.87 ^{a)}	1.67	PBDB-TF	0.88	17.54	72.69	11.48	$2.24 \times 10^{-4\text{e}}$	[84]
NFA27-1	BDTS-4Cl	–5.45 ^{a)}	–3.82 ^{a)}	1.46	PBDB-T	0.83	9.80	45.9	3.73	$2.61 \times 10^{-4\text{e}}$	[85]
NFA27-2	BDTC-4Cl	–5.35 ^{a)}	–3.75 ^{a)}	1.42	PBDB-T	0.864	18.56	59.5	9.54	$1.51 \times 10^{-4\text{e}}$	[85]
All-small-molecule organic solar cells (ASMOSCs)											
NFA9	F-1Cl	–5.46 ^{a)}	–3.75 ^{a)}	1.58	DRCN5T	0.975	13.07	63.7	8.12	$1.62 \times 10^{-4\text{e}}$	[86]
					DRCN5T	0.906	15.97	68.4	9.89	$2.22 \times 10^{-4\text{e}}$	[86]
NFA10	F-2Cl	–5.50 ^{a)}	–3.86 ^{a)}	1.54	DRTB-T SM	0.969	17.24	64.4	10.76	–	[86]

^{a)} Measured by cyclic voltammetry; ^{b)} Calculated by $E_{\text{LUMO}} = E_{\text{HOMO}} + E_g$; ^{c)} Calculated from the absorption edge of NFA in a thin film state ($E_g^{\text{opt}} = 1240/\lambda_{\text{onset}}$ eV); ^{d)} Estimated from pristine NFA using the SCLC method; ^{e)} Estimated from active layer blend using the SCLC method.

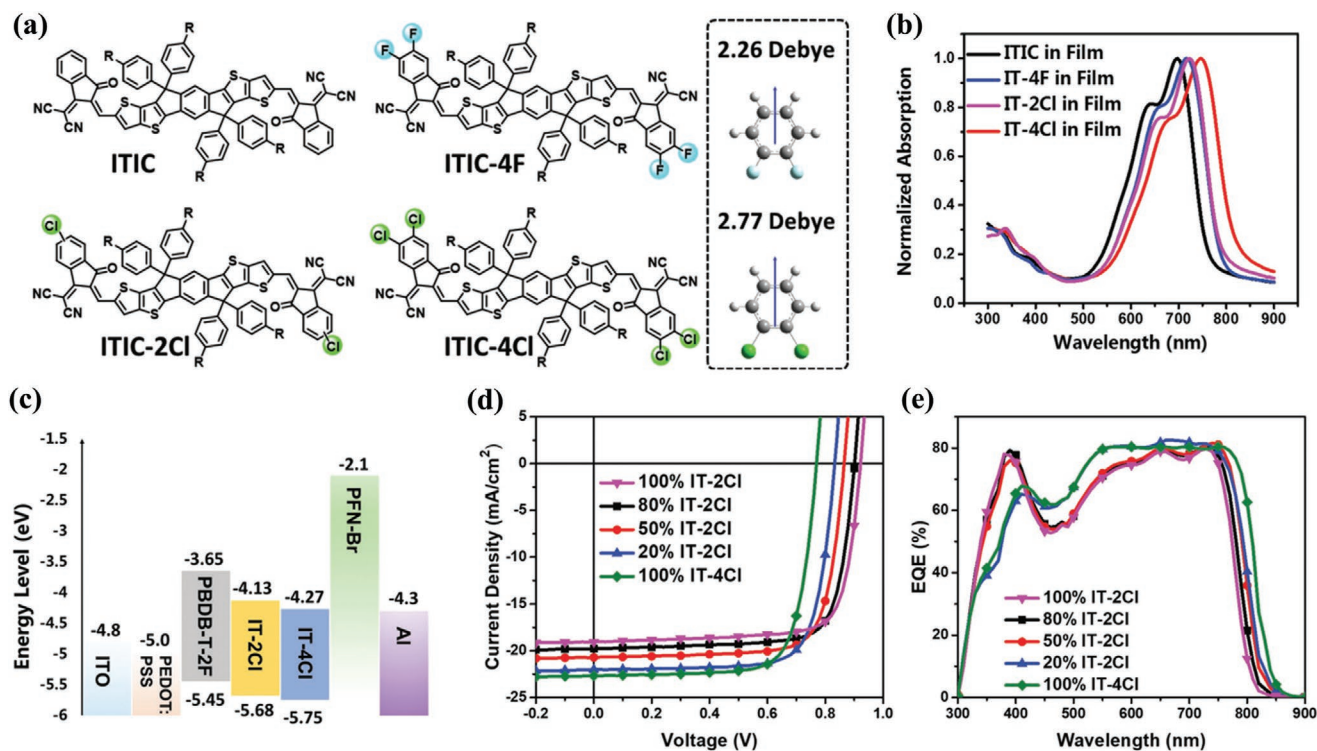


Figure 9. Typical A–D–A-type, ITIC, IT-4F, IT-2Cl, and IT-4Cl (NFA2 and NFA3) nonfullerene acceptors: a) chemical structures; b) absorption spectra in the film state; c) molecular energy level diagrams of EDs and EAs; and d) *J*–*V* characterizations and e) EQE plots of optimized binary and ternary OSC devices. a–e) Reproduced with permission.^[15d] Copyright 2018, Wiley-VCH.

could overcome the steric hindrance caused by the larger size of the halogens (Cl, Br, and I), thereby achieving a narrow bandgap than ITIC owing to the stronger ICT effect of halogens. Further, blending new NFAs with the PTPDBDT donor having complementary absorption and well-aligned energy levels, OSCs based on NFA2 achieved the highest PCE of 9.5%, with an impressive V_{OC} of 0.94 V and excellent trade-off between the photovoltaic parameters than other NFAs. This report was one of the early reports that emphasized that the chlorination strategy can also be used to modulate the optoelectronic properties of NFAs, without negatively affecting the backbone planarity.

By replacing the DCI “A” units of ITIC with 2Cl-DCI groups, Hou and co-workers designed a novel chlorinated acceptor unit named IT-4Cl (NFA3, Scheme 4) and further explored the effects of a number of Cl substituents on DCI by comparison with NFA2 (named IT-2Cl).^[15d] Notably, this design was based on the well-known IT-4F acceptor, which previously demonstrated a remarkable PCE of 13% (Figure 9).^[10a] The motive of these modifications was to utilize the advantages of chlorination, such as the low-cost and facile synthesis, deep energy levels, and redshifted absorption, thus designing efficient and cost-effective alternatives to IT-4F. The authors observed these desired effects in new NFAs; that is, NFA3 showed a HOMO that was 0.07 and 0.09 eV lower than that of NFA2 (2Cl) and IT-4F, respectively. Similarly, NFA3 showed a strong redshifted absorption compared to those of NFA2 and IT-4F (E_g^{opt} of NFA3, NFA2 and IT-4F were found to be 1.48, 1.55 and 1.55 eV, respectively), attributed to the stronger ICT effect and higher dipole moment of the C–Cl bond. When blended with the

PBDB-T-2F donor, both the OSC devices based on NFA2 or NFA3 exhibited broader absorption, optimal BHJ fibrillar morphology, and excellent charge transport properties compared to PBDB-T-2F:IT-4F blend, thereby affording superior PCEs of 13.16 and 13.45%, respectively. In comparison with PBDB-T-2F:NFA2, PBDB-T-2F:NFA3 devices exhibited a slightly lower V_{OC} of 0.79, which is attributed to ultralow-lying LUMO energy levels of NFA3. On the other hand, they displayed higher J_{SC} because of the higher photo-response of NFA3. Moreover, NFA3-based OSCs showed EQE values over 80% for wavelengths ranging from 550 to 780 nm, which has rarely been seen in OSCs (Figure 9e). Importantly, this report unlocked the possibility of synthesizing a variety of efficient FREAs by employing the 2Cl-DCI end group as an “A” unit in A–D–A-type NFAs. Later, the same group evaluated the influence of fluorination and chlorination on the properties of different ED (PBDB-T-2F or P10) and NFA (IT-4F or NFA3) combinations.^[16] Their outcomes indicated that although all the OSCs with various ED:EA mixtures produced good PCEs ranging from 13% to 14%, chlorination was found to be more advantageous over fluorination in large-scale applications because of its facile synthesis and lower cost.

Laventure et al. also independently reported NFA3 (named ITIC-Cl₄) and achieved PCEs of up to 9.1% by combining it with a different polymer donor called PBDB-T.^[65] The lower PCE, in this case, might be due to the higher-lying FMOs of donor PBDB-T, thereby lacking well-aligned energy level matching, as observed in the case of PBDB-T-2F:NFA3 blend. Recently, Su et al. achieved a PCE of 11.1% using a PBFTT:NFA3 blend

owing to the well-matched energy levels, broad absorption, high crystallinity, and good blend morphology.^[66] Thus, along with the structural optimization of both the donor and acceptor designs, the selection of appropriate D–A combinations will also play a crucial role in achieving the best PCE.

Hou and co-workers synthesized a Se analog of ITIC, in which the central indacene core was fused with two selenopheno[3,2-*b*]thiophene units to afford a new seven-membered heterocyclic core (SeT) and the corresponding NFAs SeTIC and SeTIC4Cl (NFA4, Scheme 4), formed by end-capping the SeT core with DCI and 2Cl-DCI units, respectively.^[15e] Compared with ITIC, NFA4 showed near-infrared (NIR) absorption with a reduced bandgap of 1.44 eV owing to the enhanced ICT effect of chlorination and stronger electron donation ability of SeT.^[1c,53] Additionally, incorporation of two 2Cl-DCI units further decreased the FMO energy levels, increased crystallinity, and favored the optimal morphology with suppressed germinate charge recombination in PM6:NFA4 blend films. Consequently, an excellent PCE of 13.32% along with high J_{SC} (22.92 mA cm⁻²) and FF (75%) were realized from NFA4:PM6-based devices, which was ≈ 1.8 times higher than that for non-chlorinated PM6:SeTIC counterpart (PCE of 7.46%). Additionally, NFA4:PM6 devices showed remarkable thickness tolerance (showing PCE of 11.3% at 300 nm thickness), suggesting that NFA4 might also be beneficial for the fabrication of large-area devices.

Inspired by the chlorination strategy, Forrest and co-workers incorporated 2Cl-DCI units into their previously synthesized BT-IC^[67] acceptor to form a new NFA, BT-ClC (NFA5, Scheme 4).^[18a] Indeed, NFA5 exhibited significantly superior performance in OSC devices when using PCE-10 as the donor, realizing a maximum PCE of 11.2%, in comparison to 8.3% when BT-IC was employed. Again, the differences in the PCEs manifested from the remarkable J_{SC} of 22.5 mA cm⁻² and a high FF of 71% demonstrated by using chlorinated NFA5 as the “EA” unit. Thus, the insertion of chlorinated 2Cl-DCI units favored NIR absorption ($E_g^{opt} = 1.33$ eV), ordered molecular packing in the solid-state, higher electron mobilities (2.1×10^{-4} cm²V⁻¹ s⁻¹), and excellent BHJ morphology.

Chen and collaborators further modified the structure of NFA5 by replacing the alkoxy chains of the central BDT donor with an octyl chain to form new NFA, NCBTD-4Cl (NFA6, Scheme 4).^[68] Compared to NFA5, the insertion of an alkyl chain with less electron-donating nature led to downshifting of the HOMO/LUMO energy levels in NFA6, which in turn resulted in a slightly enhanced bandgap (E_g^{opt} of 1.40 eV). In OSCs, the optimized PBDB-T-SF:NFA6 blend exhibited increased effective absorption range (from 300 to 850 nm), superior morphology, and efficient charge transport, leading to a high PCE of 13.1% without any post-treatment. Moreover, the addition of solvent additive 1,8-diiodooctane (DIO) and thermal treatment further helped to achieve a record PCE of 14.1%, with a remarkably low E_{loss} of 0.55 eV. Although the V_{OC} of the device slightly decreased because of the addition of DIO, the J_{SC} and FF were significantly elevated due to the improved BHJ morphology with well-segregated crystalline phases.

Recently, Lin et al. synthesized a new NFA named m-ITIC-OR-4Cl (NFA7, Scheme 4) by introducing meta-alkoxy chains into NFA3 core with the aim of improving the solubility and

molecular orientation.^[69] The authors tested their performance with two donor polymer BO2FC8 and BO2FEH, having different alkyl chains in their molecular structure. In-depth quantitative analysis of BO2FC8:NFA7 and BO2FEH:NFA7 blend films using 2D-GIWAXS and 2D-grazing-incidence small-angle X-ray scattering (GISAXS) revealed that the minor alkyl chain change in donor polymer structures dramatically affected shape and size of aggregated domains and molecular orientation of the blend components, thereby influencing their performance. Thus, relative to BO2FEH:NFA7 blend (PCE of 6.4%), introduction of BO2FC8 having linear alkyl chain favored the formation of smaller disc-shaped domains of NFA7 and appropriate phase separation in BO2FC8:NFA7 blend, thereby leading to the best PCE of 11% via formation of well-developed charge carrier pathways.

Zhan and collaborators optimized the molecular structure of the five-membered 2,2'-(4,4,9,9-tetrahexyl-4,9-dihydro-s-indaceno[1,2-*b*:5,6-*b'*]dithiophene-2,7-diyl)bis[methylidyne(3-oxo-1H-indene-2,1(3H)-diylidene)]bis-propanedinitrile (IDIC)^[6d,70] acceptor core by replacing terminal DCI “A” units with 2Cl-DCI to form a new NFA, ID-4Cl (NFA8, Scheme 4).^[71] As expected, NFA8 displayed strong absorption in the NIR region with a smaller E_g^{opt} of 1.51 eV, an excellent absorption coefficient (3×10^5 M⁻¹ cm⁻¹ at 690 nm), improved molecular packing, and higher crystallinity in OSCs owing to the incorporation of the 2Cl-DCI units. In conventional OSCs, PCEs as high as 10.25% was reported with PM6:NFA8 blend.

In another halogenation case study, Chen and co-workers reported a new class of FDICTF-based^[87] NFAs, that is, F-H, F-F, F-Cl (NFA9), and F-Br, by introducing different halogen atoms on the DCI end groups to study their structure-property relationship in OSCs (Scheme 4).^[72] Like other halogenated studies, all new halogenated-NFAs showed redshifted absorption, enhanced crystallinities, and higher charge-carrier mobilities relative to F-H. In OSCs, devices based on PBDB-T:NFA9 and PBDB-T:F-Br blends showed lowest π - π packing distance with “face-on” molecular orientation and superior morphology with bicontinuous fibrillar interpenetrating networks compared to the other blends, thereby resulting in higher charge transport, J_{SC} , FF, and PCEs up to 11.47% and 12.05%, respectively. Later, F-2Cl (NFA10, Scheme 4), a tetra-Cl analog of F-H, was also synthesized by substituting two 2Cl-DCI groups and was used in ASMOSCs (discussed below).^[86]

Geng et al. synthesized a new narrow bandgap NFA named IPIC-4Cl (NFA11, Scheme 4), which is composed of a central indacenobis-(dithieno[3,2-*b*:2',3'-*d*]pyrrol) (INP) core^[88] and a peripheral 2Cl-DCI end group.^[73] They analyzed the impact of chlorination in NFA11 by comparison with IPIC (without halogen) and IPIC-4F (with F) counterparts. As a result of the stronger ICT effect and higher dipole moment of C–Cl bond, NFA11 demonstrated a narrow bandgap (1.32 eV) and a high extinction coefficient of 2.90×10^5 M⁻¹ cm⁻¹ relative to IPIC and IPIC-4F. A GIWAXS study revealed that even though both halogenated acceptors favored the “face-on” molecular orientation in their pristine film state, NFA11 displayed a stronger intermolecular aggregation with compact π - π stacking distance of 3.45 Å. By mixing NFA11 with the complementary absorbing polymer donor PBDB-T, the authors achieved superior PCEs of up to 13.4%, with the right balance between $J_{SC} = 22.2$ mA cm⁻²,

$V_{OC} = 0.81$ V, and $FF = 74\%$, balanced charge mobilities ($\mu_h/\mu_e = 1.26$), and an extremely low energy loss of 0.51 eV. Resonant soft X-ray scattering (R-SoXS) and morphology studies further indicated that PBDB-T:NFA11 possesses an improved morphology with smaller domains, which effectively facilitating efficient charge transport with minimized charge recombination, leading to high efficiency.

In another case, the Yan group end capped the central fused terthieno[3,2-*b*]thiophene (3TT)^[89] central “D” core with DCI, Cl-DCI, and 2Cl-DCI “A” units to form the three new NFAs, that is, IXIC, IXIC-2Cl (NFA12), and IXIC-4Cl (NFA13), respectively (Scheme 4).^[74] The primary intent behind this strategy was to enhance the J_{SC} and efficiency in OSCs by increasing the absorption profiles of the SMs. As projected, these three NFAs showed absorption beyond 900 nm, attributed to the extended π -conjugation length and strong electron-donating capability of the central 3TT core. Additionally, the insertion of chlorinated Cl-IC and 2Cl-IC end groups further extended absorption up to 990 nm (the E_g^{opt} of IXIC, NFA12, and NFA13 was 1.35, 1.30, and 1.25 eV, respectively), lowered the energy levels, and enhanced the crystallinity. In OSC devices, blend films of PBDB-T:NFA12 showed optimal nanoscale morphology, higher charge carrier mobilities, and efficient charge generation and dissociation with lower charge recombination quenching compared to PBDB-T:NFA13 blend, which results in a higher PCE of 12.2% (11.2% for PBDB-T:NFA13) with a remarkable J_{SC} of 23.6 mA cm⁻² and FF of 70.9%.

Feng et al. also synthesized a new A–D–A-type Cl-NFA, AT-4Cl (NFA14, Scheme 4), formed by a central heptacyclic “D” unit composed of π -extended anthracene fused with a thiophene unit and end-capped by two 2Cl-DCI groups.^[75] Because of the combined benefits rendered by the insertion of anthracene donor core and 2Cl-IC end groups, NFA14 possesses strong absorption ranging from 600 to 770 nm, a lower HOMO/LUMO (–5.71/–3.89 eV), and a narrow bandgap of 1.60 eV. Moreover, when NFA14 was mixed with PBDB-TF donor, the authors achieved the appropriate molecular packing, good miscibility, and desired phase separation with lower bimolecular charge recombination required for efficient charge transfer in OSCs. Consequently, optimized PBDB-TF:NFA14 afforded an outstanding PCE of 13.27%, with enhanced $J_{SC} = 19.52$ mA cm⁻², $V_{OC} = 0.90$ V, and $FF = 75.5\%$.

He and co-workers synthesized two new NFAs, R10-4Cl (NFA15), and R12-4Cl (NFA16), with 10-ring and 12-ring-fused cores as central “D” units and 2Cl-DCI as terminal “A” units (Scheme 4), respectively.^[76] Though, NFA15 and NFA16 demonstrated broader absorption (600–900 nm) range with an E_g^{opt} of 1.43 and 1.35 eV, respectively, owing to the increased fused core, but no considerable change was observed in the absorption profiles compared to the NFAs having central six- or eight-membered heterocyclic core.^[5b] Single-crystal X-ray crystallographic results revealed that the NFA15 possess two distinct types of molecular packing, that is, one between the end groups of the adjacent molecules with a π – π stacking distance of 3.32 Å and the other between the two molecules with an angle of approximately 64.7° due to the close contact of S···O with a distance of 3.15 Å; hence, these resulted in an interpenetrated network for rapid charge transfer. In inverted OSCs using the PBDB-T donor, NFA15 showed “face-on”

molecular orientation, higher crystallinity, and favorable BHJ morphology with smaller domain phases, resulting in a higher PCE of 10.7% than the NFA16 counterpart (9.3%). Thus, these outcomes signify that enhancing the number of rings in the acceptor core cannot always guarantee a higher efficiency.

Recently, Hou and co-workers produced record efficiencies of 16.5% and 15.3% for single-junction solar cells with 0.09 and 1 cm² active areas, respectively, using a new fused benzothiadiazole-based Cl-NFA named BTP-4Cl (NFA17-1, Scheme 5 and Figure 10).^[2b] This NFA was produced by replacing the difluorinated DCI (2F-DCI) units of Y6 (newly named BTP-4F) with 2Cl-DCI units, which previously demonstrated remarkable PCE over 15%.^[2a] As established by the chlorination design strategy, the optimized PBDB-TF:NFA17-1 blend in OSCs displayed a high J_{SC} of 25.4 mA cm⁻² and a high FF of 75%, attributed to the low bandgap of NFA17-1 ($E_g^{opt} = 1.4$ eV) and optimized BHJ morphology of blend film. More interestingly, because of the excellent electroluminescence quantum efficiency (EQE_{EL} of 3.47×10^{-4}) and lower reduced non-radiative energy loss ($E_{loss,nr} = 0.206$ eV), PBDB-TF:NFA17-1 blend films also unexpectedly realized higher V_{OC} (0.867 V) than its fluorinated counterpart PBDB-TF:BTP-4F ($V_{OC} = 0.834$ V, EQE_{EL} of 1.40×10^{-4} , and $E_{loss,nr} = 0.230$ eV) despite of the lower LUMO energy levels of NFA17-1. In summary, these results demonstrate that the non-radiative energy loss in OCSs can be overcome by fine-tuning of the molecular structure using chlorination.

Further, the same group recently optimized the molecular structure of NFA17-1 to utilize acceptor for larger-area production technologies.^[2h] Two new Cl-SMs, that is, BTP-4Cl-12 (NFA17-2) and BTP-4Cl-16 (NFA17-3) were prepared by replacing branched 2-ethyl hexyl alkyl chains of NFA17-1 (renamed as BTP-4Cl-8) with 2-butyl octyl and 2-hexyl decyl alkyl chains, respectively, as shown in Scheme 5. Though variation of alkyl chains did not significantly affect the absorption profiles and energy levels of all the Cl-NFAs; however, NFA17-2 and NFA17-3 showed higher absorption co-efficient than NFA17-1, which suggested the enhanced intermolecular packing favored by the longer alkyl chains. Moreover, by blending with PBDB-TF donor unit, OSCs on PBDB-TF:NFA17-2 blend realized the crucial balance between crystallinity and processability, thereby, leading to optimal BHJ morphology and effective charge transport with suppressed charge recombination. Thus, PBDB-TF:NFA17-2 blend showed good compatibility with both spin-coating and blade-coating processing techniques and providing outstanding world-record performances for single-junction solar cells, that is, PCEs of 17% (with a high $J_{SC} = 25.6$ mA cm⁻², $V_{OC} = 0.858$ V, and $FF = 77.6\%$ and which was certified as 16.7% by NIM, China) and 15.5%, respectively, for active areas 0.09 and 1.07 cm² thereby outperforming their counterparts. Besides, PBDB-TF:NFA17-2 devices also showed excellent thickness tolerance and good stability signifying it might be suitable for the fabrication of large-area OSCs.

Later, Luo et al. also prepared new Cl-NFA named Y15 (NFA18) based on benzo[*d*][1,2,3] triazole with two 3-undecylthieno[2',3':4,5] thieno[3,2-*b*] pyrrole fused -7-heterocyclic ring as a central “D” unit and two 2Cl-DCI units as terminal “A” units (Scheme 5).^[77] As expected, NFA18 showed lower HOMO energy levels (–5.56 eV) and narrow bandgap (1.30 eV) because of chlorination and fused backbone. The pristine NFA18 also

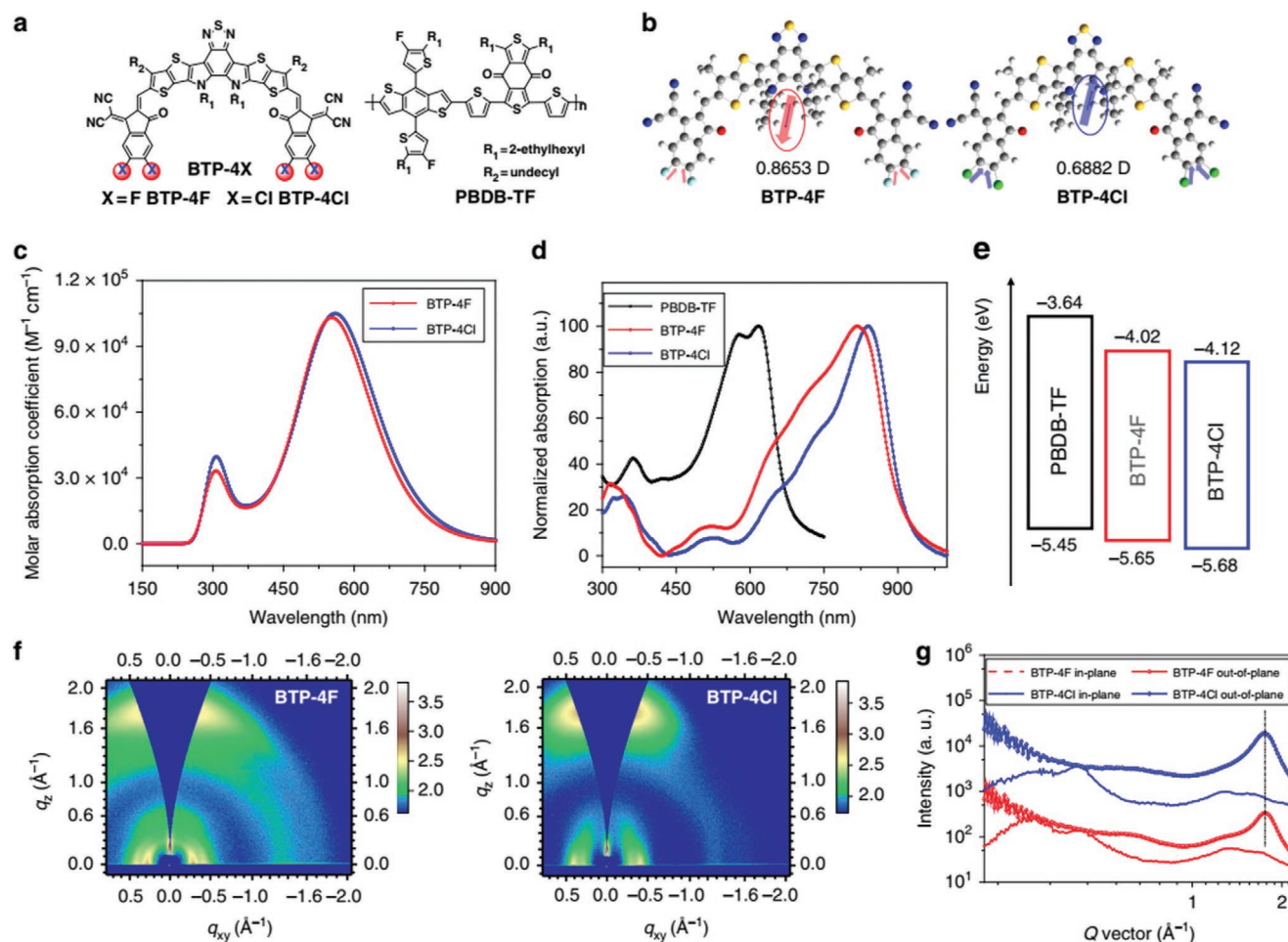


Figure 10. a) Chemical structures of BTP-4X (BTP-4F and BTP-4Cl [NFA17-1]) acceptors and the polymer donor PBDB-TF; b) molecular dipoles in the optimized molecular models for the BTP-4Cl acceptors; c) calculated UV-vis absorption spectra of BTP-4X; d) normalized UV-vis absorption spectra of the materials measured by the square-wave voltammetry method; e) schematic energy level alignment of the materials measured by the square-wave voltammetry method; f) 2D-GIWAXS patterns of the neat BTP-4X films; and g) extracted 1D profiles along the in-plane and out-of-plane directions. a–g) Reproduced with permission.^[2b] Copyright 2019, Springer Nature.

featured a compact π - π stacking distance of 3.54 Å with “face-on” molecular orientation as revealed by the GIWAXS study. Hence, conventional OSC with PM6:NFA18 realized remarkable PCE of 14.13% with high J_{sc} of 23.79 mA cm⁻² due to broad photoresponse range, higher charge mobilities and optimal BHJ morphology.

Other than the insertion of 2Cl-DCI units, Luo et al. introduced the new chlorinated thiophene-fused CPTCN-Cl as an end-capping “A” core into the ITIC design to produce the new acceptor core ITC-2Cl (NFA19, Scheme 5).^[78] Because of the insertion of CPTCN-Cl unit, NFA19 showed broader absorption (E_g^{opt} of 1.58 eV) and a higher absorption coefficient (2.28×10^5 M⁻¹ cm⁻¹ at 709 nm) compared to the non-chlorinated counterpart ITCPTC.^[90] Moreover, GIWAXS and AFM measurements emphasized that the optimized PM6:NFA19 blend favored a “face-on” molecular orientation with a stronger crystallization tendency and a superior nanofibrillar morphology compared to PM6:ITCPTC blend. These factors resulted in higher and more balanced charge mobilities and a superior PCE of 13.6% for PM6:NFA19-based OSC

devices versus 12.3% for PM6:ITCPTC. Furthermore, the authors also evaluated the potential of the new CPTCN-Cl end group by comparison with the well-known efficient IT-4F and NFA3 NFAs having the same central core. Notably, here also NFA19 outperformed both IT-4F and NFA3 acceptors mainly by demonstrating higher V_{OC} , which is originating from the reduced radiative and non-radiative recombination loss, as revealed by an FTPS and EL study (E_{loss} of NFA19, IT-4F and NFA3 was found to be 0.67, 0.73, and 0.76 eV, respectively).

Zhang et al. reported a new Cl-NFA unit, that is, C8-ITCC-Cl (NFA20, Scheme 5), by grafting the new TIC-Cl building block as terminal “A” units into the central indacenodithieno[3,2-b]thiophene (IDTT) core having n-octyl chains.^[79] Benefiting from the higher electron-withdrawing ability and stronger ICT effect of the Cl atom, TIC-Cl demonstrated lower energy levels and redshifted absorption compared to its non-chlorinated counterpart TIC. Moreover, OSCs on PBDB-TF:NFA20 blend also exhibited favorable molecular orientation and optimal phase-separated morphology, leading to a higher μ_e of 6.6×10^{-4} cm² V⁻¹ s⁻¹ and an excellent FF of 73%. As a result,

devices based on PBDB-TF:NFA20 blend films achieved the best PCE of 12.7%.

Wan et al. also introduced TIC-Cl or 2Cl-DCI end groups into the benzo[1,2-*b*:4,5-*b'*]diselenophene-type central “D” core to form two new NFAs, BDSeThCl (NFA21-1) and BDSePhCl (NFA21-2), respectively (Scheme 5).^[80] Compared to NFA21-1, NFA21-2 demonstrated redshifted absorption and deeper HOMO energy levels, resulting in a more complementary absorption and energy level matching with the PM7 donor. Moreover, optimized PM7:NFA21-2 blend also showed predominant “face-on” molecular orientation, well-resolved fibrillar morphology and higher and balanced charge mobilities, thereby enabling superior photovoltaic parameters and a higher PCE of 13.68%. Further to this, these devices had the lowest E_{loss} of 0.49 V, which is rarely reported to date for NF-OSCs with Cl-NFAs (PCE and E_{loss} of NFA21-1 were 11.91% and 0.58 V, respectively).

Cui et al. introduced an 3-((2-ethylhexyl)oxy)thiophene π -spacer between the central indacenodithiophene (IDT)^[64,91] and terminal 2Cl-DCI “A” units to tailor the photophysical properties of new NFA unit, IEICO-4Cl (NFA22, Scheme 5).^[18b] Because of the strong ICT effects of 2Cl-DCI units and non-covalent S–O interactions between the alkoxy group and proximity S atom of IDT, NFA22 exhibits high coplanarity and an ultralow bandgap ($E_{\text{g}}^{\text{opt}} = 1.23$ eV), which is useful for light-harvesting in higher wavelength. As a result, NFA22 based OSCs showed PCEs of $\approx 10.0\%$ with a low $E_{\text{loss}} \approx 0.5$ V for both wide-bandgap polymers J52 or PBDB-T and low bandgap PTB7-Th.

Following the same concept, Chen and co-workers also presented a new NIR-absorbing Cl-NFA named IDTC-4Cl (NFA23, Scheme 5). NFA23 comprised a central IDT core, and terminal 2Cl-DCI cores connected by two cyclopentadithiophene (CPT) rings.^[81] Because of the superior features of NFA23, such as a co-planar backbone, NIR absorption with a low bandgap of 1.35 eV, and a high μ_e of 2.84×10^{-4} cm² V⁻¹ s⁻¹, corresponding OSCs with the PBDB-T donor showed PCEs as high as 9.5% with a favorable BHJ morphology.

Hong et al. replaced alkoxy thiophene π -spacer in NFA22 by 2-ethylhexyl-thiophene and synthesized three new NFAs IEIC, IE-4F, and IE-4Cl (NFA24, Scheme 5) by end-capping with DCI, 2F-DCI, and 2Cl-DCI “A” units, respectively.^[82] Ascribed from the strong electronegativity and ICT effect of halogens, both IE-4F and NFA24 showed lower energy levels and broader absorption than IEIC. In OSCs, optimized blend films with different ED and EA combination demonstrated identical morphologies and charge carrier properties because of their analogous molecular structure. On the other hand, they also showed marked differences in their E_{loss} values (ranging between 0.52 to 0.65 eV) because of their varied energy level alignments. Consequently, PBDB-T:NFA24-based devices produced the highest PCE of 11.1% resulting from efficient charge transfer and excellent charge generation efficiencies with an E_{loss} of 0.64 eV than other blends.

In addition to the variation of central “D” or terminal “A” units, alkyl chain modulation in the A–D–A-type NFAs was also found advantageous to tune the properties and morphology of the NFAs in OSCs.^[2f] With this strategy, Gao et al. synthesized a new NIR-absorbing Cl-NFAs, that is, 3TT-CIC (NFA25-1, main/side chain = without/2-ethyl hexyl alkyl chain)

and 3TT-OCIC (NFA25-2, main/side chain = octyl/ hexyl alkyl chain) (Scheme 5).^[83] Due to the redshifted absorption ($E_{\text{g}}^{\text{opt}} = 1.29$ eV) and an up-shifted LUMO of NFA25-2, its blend film with PCE 10 donor renders simultaneous enhancement of J_{SC} and V_{OC} in the corresponding OSCs. Further, by delicately optimizing the PC10:NFA25-2 blend film morphology, authors achieved an impressive PCE of 12.43% with higher charge mobility, thereby outclassing PC10:NFA25-1 blend (11.96%).

4.3. A–D’–D–D’–A Type or Non-Fused Chlorinated NFAs

To overcome the SC exhibited by the synthesis of FREAs, a few groups synthesized Cl-NFAs with a non-fused architecture, as shown in Scheme 5. In 2018, Zhan et al. first reported a non-fused Cl-NFA, HC-PCIC (NFA26), by end-capping 2Cl-DCI groups to the central pseudo-9-membered fused “D” unit, which comprised two CPT moieties linked to a 2,5-difluorobenzene unit.^[84] Similar to its non-chlorinated predecessor HF-PCIC,^[92] NFA26 also displayed a near-planar conformation, attributed to the F···H noncovalent interactions between the CPT moieties and the 2,5-difluorobenzene core (Scheme 5). Moreover, resulting from stronger ICT interactions in the film state, NFA26 also demonstrated a higher absorption coefficient of 2.19×10^5 m⁻¹ cm⁻¹ and a broader absorption ranging from 600 to 850 nm. Thus, OSCs were fabricated by mixing NFA26 with the PBDB-TF donor showed impressive PCEs as high as 11.48% with a high J_{SC} (17.54 mA cm⁻²) and an FF (72.69%).

Next, Chen and co-workers recently reported two new NFAs, namely, BDTS-4Cl (NFA27-1) and BDTC-4Cl (NFA27-2) (Scheme 5 and Figure 11).^[85] NFA27-2 has a structure similar to that of NFA26, except that the central 2,5-difluorobenzene unit was replaced with a 2D-BDT core. Whereas, NFA27-1 has a 2D-BDT central “D” core and terminal 2Cl-DCI “A” groups connected by two alkyl-substituted dithienosilole (DTS) units (Figure 11a). Ascribed from the electron-donating ability of CPT than DTS, NFA27-2 displayed upshifting of the FMOs and a narrow $E_{\text{g}}^{\text{opt}}$ of 1.42 eV. Additionally, PBDB-T:NFA27-2 blend films also showed more complementary absorption resulting in broader photo-response with EQEs values over 60% ranging from 550 to 800 nm, favorable molecular orientation, and optimal morphology relative to PBDB-T:NFA27-1 blend. As a result, optimized PBDB-T:NFA27-2 blend afforded efficient charge transfer and PCEs of up to 9.54% in OSCs, which is ≈ 2.5 -fold higher than that for PBDB-T:NFA27-1 (PCE of 3.73%).

Overall, unlike traditional methods such as an appropriate selection of the central donor core, π -bridge or end groups used for accomplishing excellent compatibility with the specific ED, insertion of Cl substituents on NFAs provides the versatile opportunity to enhance the absorption and to lower energy levels simultaneously. Furthermore, molecular orientation and crystallinity to afford optimal phase separation with donor materials can also be easily manipulated by controlling the number of Cl substituents on the NFAs. Consequently, impressive PCEs ranging from 12% to 17% were achieved in single-junction OSCs using the ultralow-bandgap Cl-NFAs with complementary absorbing wide-bandgap polymer donor,

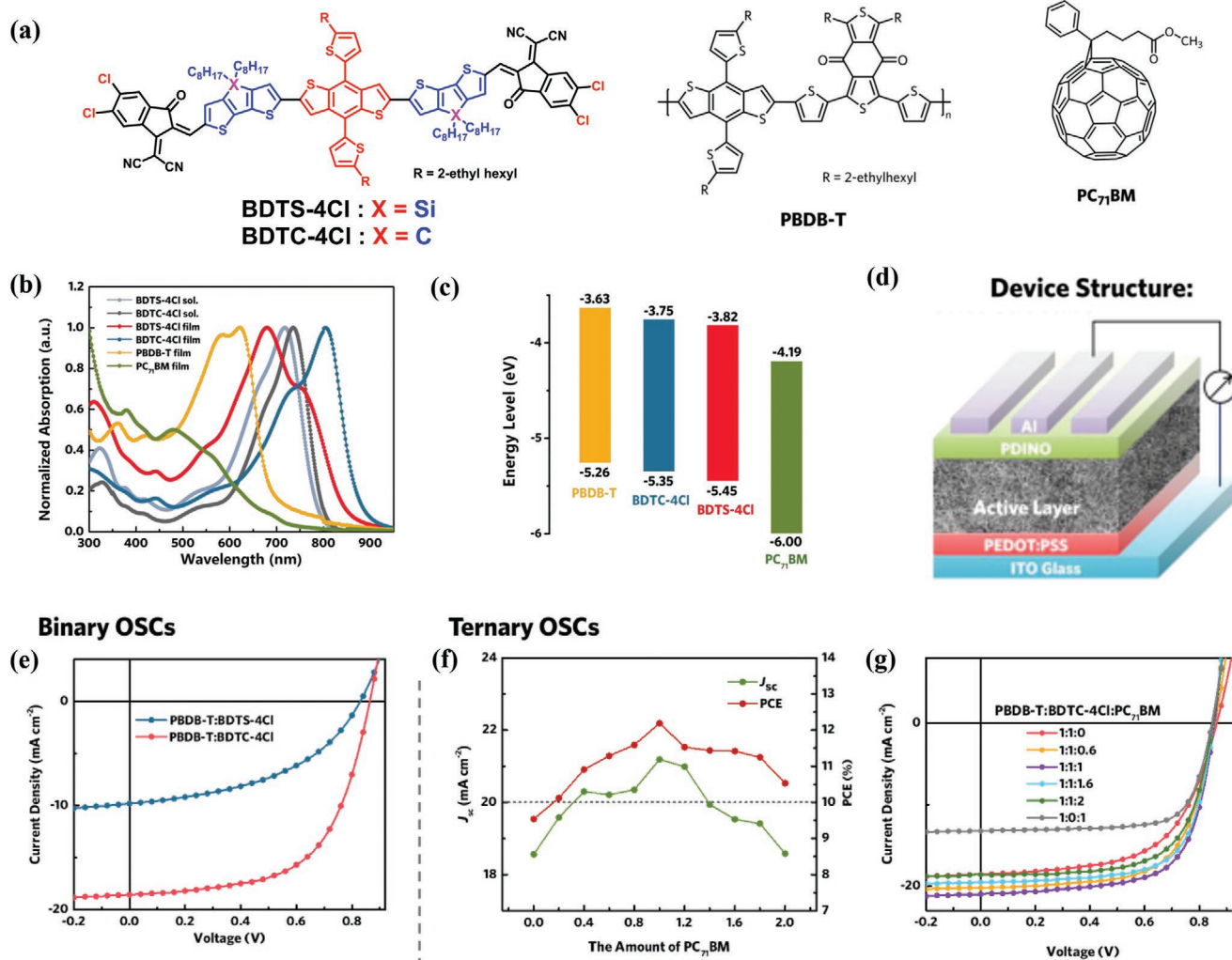


Figure 11. BDTS-4Cl, BDTC-4Cl (NFA27-1 and NFA27-2, respectively), PBDB-T, and PC₇₁BM: a) chemical structures; b) normalized absorption spectra and c) energy levels; d) diagram of a conventional device structure; e) *J*-*V* curves for binary OSCs based on PBDB-T:BDTS-4Cl/BDTC-4Cl; f) *J*_{sc} and PCE versus the amount of PC₇₁BM for ternary OSCs based on PBDB-T:BDTC-4Cl:PC₇₁BM; and g) corresponding *J*-*V* curves for ternary OSCs. a–g) Reproduced with permission.^[85] Copyright 2019, American Chemical Society.

resulting in effective light-harvesting along the broad area of the solar spectrum. Nevertheless, there is a lot of room for enhancing efficiencies of Cl-NFAs. Notably, all these previously reported Cl-NFAs are designed by the addition of chlorinated “A” units on the lateral sides of central fused “D” ring. Thus, research efforts in the innovation of the material designs such as exploring the new chlorinated “A” units, insertion of Cl-substituents in the “D” or “ π -spacer” units, designing NFAs based on “D–A–D”-type structure^[59b] and developing easily scalable material designs involving non-covalent confirmation locks^[93] must be extensively tested in the near future.

5. Long-Term Stability of Cl-PVMs

Since the last decade, huge endeavors have been devoted to optimizing the OSCs material development to meet the need for practical application. Distinctive from the controlled

environment in the labs, various other factors such as photostability of PVMs, metastable BHJ morphology, diffusion of oxygen and water, and radiation and mechanical starching, will confine the stability of OSCs in the real world.^[81,94] Inherent molecular structure of given PVM is likely one of the foremost critical factors, which significantly influences the stability of the photoactive layer.^[94] Thus, to improve the stability of PVMs approaches such as design and development of photo-oxidation stable units, regulating crystallinity polymers and incorporating antioxidant groups have been previously reported.^[1f] Thus, in this section, we focus on the current challenges and role of chlorination in realizing the efficient OSCs with high stability for industrial manufacturing.

He and co-workers investigated oxidation stability of newly synthesized chlorinated polymer P23:PC₇₁BM-based devices by comparing with PffBT4T-2OD:PC₇₁BM (without Cl analog) (Figure 12a).^[15f] The optimal devices were not encapsulated and stored under the glove box. A marked change in the

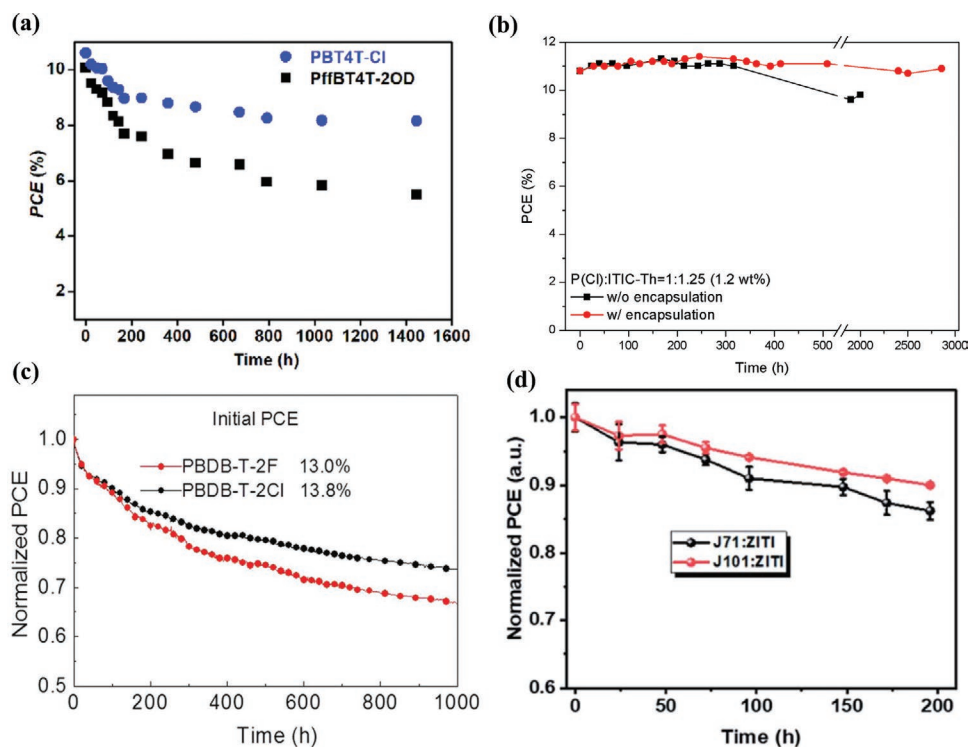


Figure 12. a) Long-lifetime stability results of the PBT4T-Cl (**P23**):PC₇₁BM and PffBT4T-2OD:PC₇₁BM-based unencapsulated devices stored in a glovebox. Reproduced with permission.^[15f] Copyright 2018, Elsevier Inc. b) Long-lifetime stability results obtained using the ISOS-D-1 (shelf) protocol for the optimized P(Cl):ITIC-Th-based inverted OSCs. Reproduced with permission.^[51] Copyright 2019, Wiley-VCH. c) 1000 h lifetime results of the OSCs based on PBDB-T-2F:IT-4F and PBDB-T-2Cl (**P10**):IT-4F with continuous testing under maximum output conditions without controlling the temperature of the devices. Reproduced with permission.^[14b] Copyright 2018, Wiley-VCH. d) Time dependence of normalized photovoltaic performance of the J101 (**P9**):ZITI- and J71:ZITI-based PSCs. Reproduced with permission.^[12] Copyright 2019, The Royal Society of Chemistry.

oxidation stability of these blends was observed. The OSCs of **P23**-based devices retained $\approx 80\%$ of its initial PCEs (8.16% vs $\approx 11\%$ for initial devices) stored for 50 days, whereas PCEs of the PffBT4T-based devices were drastically declined from 10.07% to 5.36% ($\approx 50\%$ PCE drop). Furthermore, a comparison of the time-dependent absorption spectra of both these blends revealed that the poor stability of PffBT4T-based devices attributed to the drastic change in their absorption profile immediately after 48 h. In comparison, **P23**:PC₇₁BM blend displayed a more stable absorption profile, thereby resulting in the higher stabilities of corresponding OSCs. Therefore, these results suggest that the incorporation of Cl substituent in molecular design has a critical role in stabilizing the PCEs.

Recently, our group also evaluated the oxidation stability of low-cost and facile chlorinated **P27**:ITIC-Th-based OSCs in-depth by testing stability both in without and with encapsulation under air-conditioned atmosphere for over 2000 h (Figure 12b).^[51] Surprisingly, both these cells demonstrated excellent oxidation stability, with retention of 91% and 101% of their initial values even after storing these devices over 2000 h. It was speculated that the higher PCEs of these devices were originated from the inclusion of the Cl atom in the molecular structure, which greatly enhanced inter-/intramolecular packing in OSCs. Furthermore, we also tested the photostability of both these devices by storing OSCs under AM 1.5 G xenon lamp.

Both these without and with encapsulation devices showed a $\approx 10\text{--}12\%$ drop in their initial PCEs after 40 h.

To elucidate the effect of chlorination versus fluorination on the long-term photostability of OSCs, Hou and co-workers compared the photostability of **P10** and BDT-T-2F-based (chlorinated and fluorinated analogs, respectively) devices having PCEs of 14.4% and 13.2% with IT-4F as NFAs.^[14b] They stored encapsulated devices in air under the continuous light soaking for 1000 h. As shown in Figure 12c, **P10**:IT-4F-based OSCs demonstrated remarkable stability and retained nearly 75% of its initial PCE, which is comparatively better than that of BDT-T-2F:IT-4F-based devices (68% of initial PCEs was retained). Similarly, in another case study, Wang et al. evaluated the thermal stability of **P9**:ZITI by thermal treatment of devices at 80 °C for 196 h (Figure 12d).^[12] Indeed, in this case also, chlorinated **P9**:ZITI-based OSCs showed slightly superior stability than fluorinated analog J71:ZITI (PCE dropped observed for **P9**:ZITI and J71:ZITI devices were $\approx 9\%$ and 14%, respectively). Therefore, the chlorination approach is a good alternative to fluorination, in terms of enhancing oxidative and thermal stability.

To sum up, these discoveries clearly emphasize that the incorporation of Cl atom in the molecular structure is a valuable strategy to enhance the stability of OSCs compared to non-chlorinated and fluorinated analogs. However, despite the availability of a large number of Cl-PVMs, the stability study of the handful of Cl-PVMs has not been reported to date. In particular,

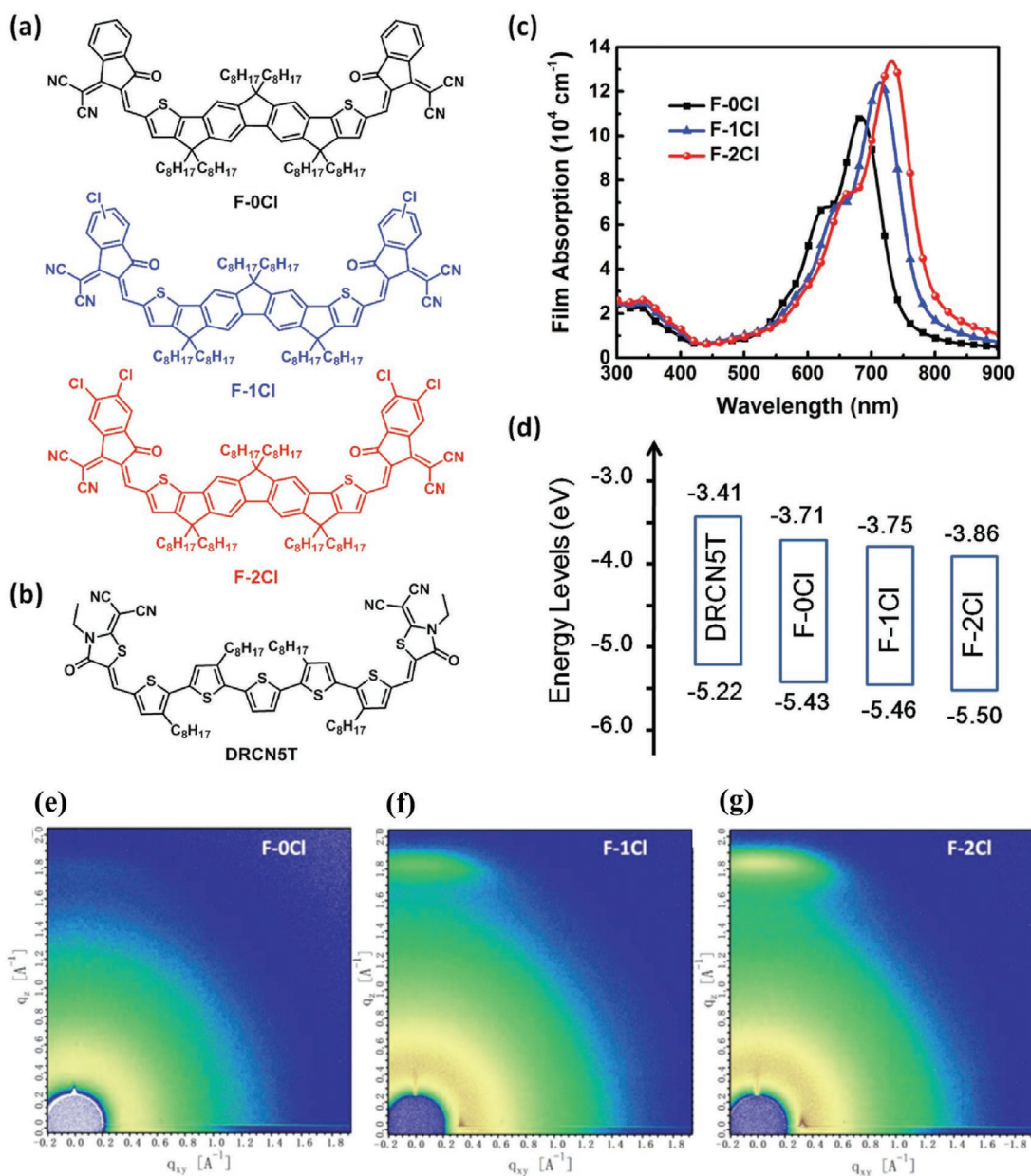


Figure 13. a,b) Chemical structures of: a) acceptors F-0Cl, F-1Cl, and F-2Cl (NFA9 and NFA10) and b) donor DRCN5T; c) absorption of the three acceptors in the solid film state; d) energy level diagrams of the donor and acceptor materials. e–g) GIWAXS patterns of the pure films of: e) F-0Cl, f) F-1Cl, and g) F-2Cl. a–g) Reproduced with permission.^[86] Copyright 2018, Wiley-VCH.

the stability of OSCs based on Cl-NFAs largely remains unexplored. As a result, thorough investigations on different chlorinated blend system is required to get more clarity on the stability of Cl-PVMs to utilize them in large-area photovoltaics.

6. Other Dimensions of Chlorinated Conjugated Materials

6.1. ASMOSCs

Considering the promising advantages of SMs, such as high purity, a well-defined structure, and less batch-to-batch

variation of their photovoltaic performance relative to polymer donors,^[95] ASMOSCs,^[96] which were composed of both SM donor and SM acceptor blended in a BHJ have recently gained significant attention. The reports indicate that further enhancement of the efficiency of ASMOSCs could be realized only by overcoming critical phase separation and unbalanced charge mobility issues.

Wang et al. synthesized two new Cl-NFAs, F-1Cl (NFA9) and F-2Cl (NFA10), to evaluate how the crystallinity of these Cl-NFAs affects the photovoltaic performance with SM donors by comparing them with the unchlorinated analog, F-0Cl (Figure 13).^[86] From GIWAXS measurements of pristine SMs, the authors observed that an increase in the Cl-content from

F-0Cl to **NFA10** led to the enhancement of crystalline network with a more compact π - π stacking and higher coherence length. These factors resulted in a higher absorption coefficient, redshifted absorption, excellent μ_e , and nanoscale phase separation in the blend films of DRCN5T:**NFA9** or **NFA10**. Consequently, the PCE was enhanced with increasing Cl content, and devices based on **NFA9** and **NFA10** yielded PCEs of 8.12% and 9.89%, respectively. Furthermore, a higher PCE of 10.76% was achieved employing DRTB-T:**NFA10** blend. The more complementary absorption, well-aligned energy levels, and superior morphology were the reasons behind this PCE enhancement.

Possibly because of the non-availability of well-matched chlorinated SM donor and acceptor combination, ASMOSCs based on Cl-PVMs are not much explored at present. Since a large number of Cl-NFAs with tunable bandgap (1.23–1.67 eV) have been already reported, precise design of small-molecule donors having well compatible opto-electrochemical properties, crystallinity, and optimal morphology to form efficient ASMOSCs could be an attractive research topic in the forthcoming days.

6.2. STOSCs

Considering the modern urban infrastructure consisting of large surface areas of windows and facades, the development of STOSCs for utilization in building-integrated photovoltaics (BIPVs) has attracted considerable attention in recent years.^[18a,66,97] In addition to efficiency, the future of these STOSC materials is mainly reliant on their transparency in the visible region ranging from 400 to 650 nm. Over the years, most of these STOSCs comprised a polymer donor and fullerene acceptors and thus showed low PCEs (\approx 8%) due to the weak absorbing nature of the fullerene acceptor.^[98] However, the recent rapid advances in various low bandgap FREAs, including NIR-absorbing Cl-NFAs, has provided vast opportunities for the development of efficient STOSCs by combining with the suitable polymer donors (Table 4).

The first example of Cl-NFA-based STOSCs was reported by Forrest and co-workers, who blended their newly synthesized

NIR-absorbing **NFA5** with the low bandgap polymer PTB7-Th to achieve a clear transparency window between 400 and 650 nm.^[18a] A high $J_{SC} = 18.0 \text{ mA cm}^{-2}$, $V_{OC} = 0.68 \text{ V}$, good FF = 67.5%, and a record high PCE of 8.2% with an average visible transmittance (AVT) of 26% were achieved when using 20 nm thick Ag as the cathode (Figure 14a–c). Efficient exploitation of the solar spectral response in the NIR region, coupled with the low sheet resistance of Ag, led to superior efficiency in the STOSCs. Also, this study was the first to show that Cl-NFAs are useful for semitransparent BIPV applications. By blending low bandgap **NFA8** with PM-6 donor, Li et al. achieved STOSCs with the best PCE of 6.99% (active area 4 mm²) when using 15 nm Au as the back electrode.^[71] Besides, they also fabricated 1 cm² large-area devices, where they achieved a PCE of 1.1% with an AVT of 44%.

Because the absorption band of **NFA22** lies in the 700–1000 nm region (which is outside the visible range), Hou and co-workers employed **NFA22** for the fabrication of STOSCs (Figure 14d–g).^[18b] One more unique feature of this study was that the authors tested the compatibility of **NFA22** with different donor polymers (J52, PBDB-T and PTB7-Th), thereby enabling easy color tuning of blend films from purple to blue to cyan. The STOSCs based on these three blends showed PCEs of 6.37%, 6.24%, and 6.97%, respectively, with AVTs ranging between 33% to 36%. Moreover, by optimizing the thickness of Au from 15 nm to 30 nm, the authors achieved the best PCE of 8.38% for the PTB7-Th:**NFA22** blend system, with a slightly lower AVT of 25.6%.

In another instance, Li and co-workers also fabricated STOSCs by using the newly synthesized chlorinated polymer **P17** and IT-4F as an ED and an EA, respectively.^[44] The authors achieved an impressive PCE of 8.18% along with a high AVT of 31.7%, despite the moderate transparency window visible region, which is a unique feature of their study. Recently, the same group achieved a remarkable PCE of 9.1% in STOSCs using the PBFTT:**NFA3** system, which is one of the highest PCE reported to date for STOSCs without any extra treatment and with an AVT over 25% (Figure 14h–j).^[66] The complementary absorption in the NIR region and high EQE values between 600 to 830 nm for the PBFTT:**NFA3** blend films were the reasons behind the enhanced PCEs.

Motivated by the impressive photovoltaic performances and semitransparent window in the visible region, Min and co-workers utilized **P9**:ZITI blend system for fabricating STOSCs.^[12] Remarkably, optimized devices with 15 nm thick Ag electrode yielded a high J_{SC} of 19.06 mA cm⁻², a high $V_{OC} = 0.898 \text{ V}$, and FF = 64.51%, thereby resulting in a new record PCF of 11.04% with an AVT of 21.69% for STOSCs using polymer donor and NFA combination.

Overall, these results clearly show that Cl-PVMs have promising potentials in the STOSCs. In order to utilize these materials for flexible STOSCs, not only there is need of novel donors having complementary NIR absorption and suitable energy level matching with low bandgap NFAs, but also future research should direct toward the development of flexible transparent electrode having low sheet resistance and low-temperature processable interface materials having high conductivity.^[1g]

Table 4. Photovoltaic parameters of STOSCs based on chlorinated donor or acceptor units.

Blend	V_{OC} [V]	J_{SC} [mA cm ²]	FF [%]	PCE [%]	AVT [%] ^{a)}	Ref.
PCE-10:BT-CIC (NFA5)	0.68	18.0	67.5	8.2	26	[18a]
PM6:ID-4Cl (NFA8)	0.748	13.77	67.90	6.99		[71]
J52:IEICO-4Cl (NFA22)	0.673	17.2	55.1	6.37	35.1	[18b]
PBDB-T:IEICO-4Cl (NFA22)	0.724	15.4	56.0	6.24	35.7	[18b]
PTB7-Th:IEICO-4Cl (NFA22)	0.725	19.6	59.0	8.38	25.6	[18b]
PBT-CI (P17):IT-4F	0.749	18.52	58.9	8.18	31.7	[44]
PBFTT:IT-4Cl (NFA3)	0.74	17.6	70.1	9.1	27.6	[66]
J101 (P9):ZITI	0.89	19.06	64.51	11.04	21.69	[12]

^{a)}AVT (average visible transmittance).

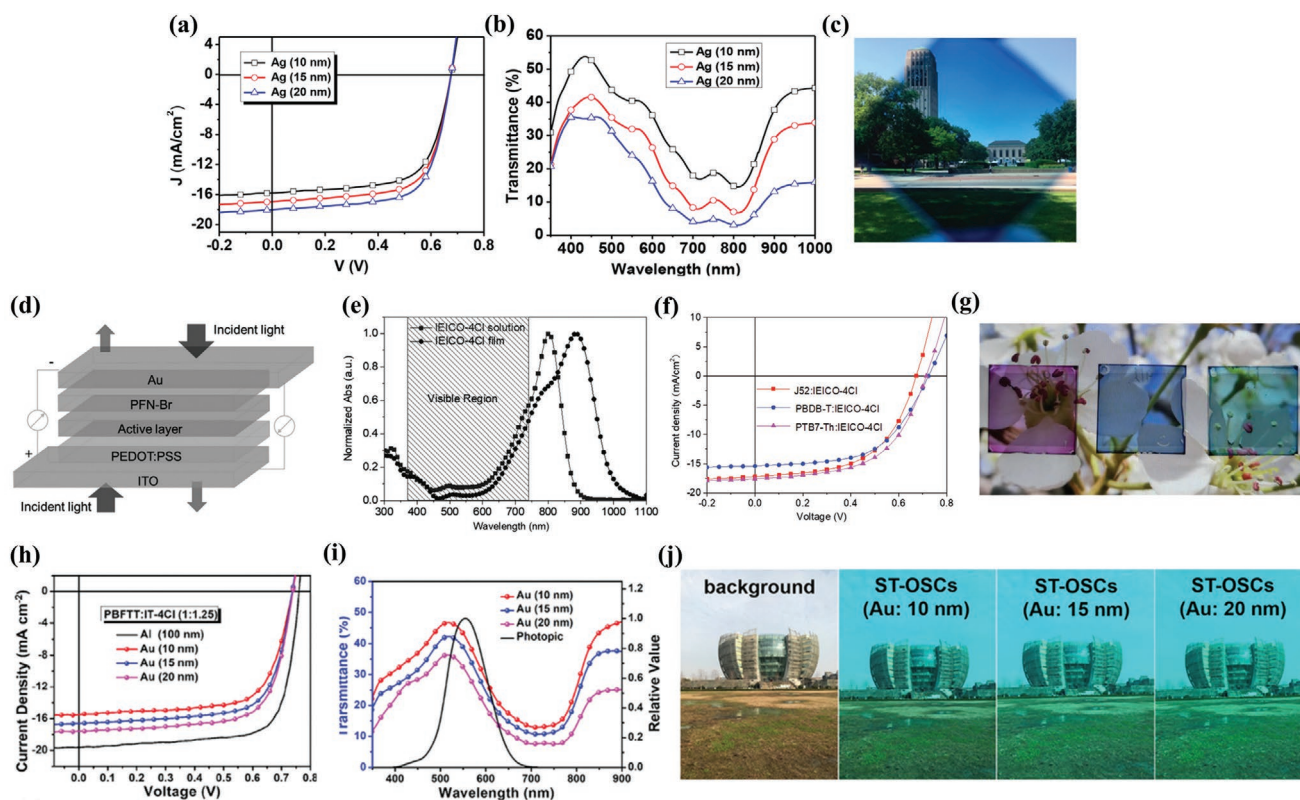


Figure 14. a) J - V characteristics of STOSCs based on PCE-10:BT-CIC (NFA5) (1:1.5, w/w) with different Ag cathode thicknesses; b) corresponding transmission spectra of the STOPVs; and c) outdoor image through the STOPV incorporating a 10 nm thick Ag layer. a-c) Reproduced with permission.^[18a] Copyright 2017, American Chemical Society. d) Device architecture of STOSCs based on IEICO-4Cl (NFA22); e) normalized absorption spectra of IEICO-4Cl; f) J - V curves; and g) photograph of three STOSCs (from left to right: J52:IEICO-4Cl, PBDB-T:IEICO-4Cl, and PTB7-Th:IEICO-4Cl, respectively). d-g) Reproduced with permission.^[18b] Copyright 2017, Wiley-VCH. h) J - V curves of STOSCs based on PBFTT:IT-4Cl (NFA3) with different thickness Au layers; i) corresponding transmission spectra (the embedded red curve is the standard human eye sensitivity spectrum); and j) photographs of the without/STOSCs with different thickness Au layers. h-j) Reproduced with permission.^[66] Copyright 2019, Owner Societies.

6.3. Tandem OSCs

Tandem OSCs, which consist of two or more single cells with compatible and/or complementary absorption wavelength ranges stacked in series, were designed mainly to enhance the light-harvesting capabilities and reduce the thermalization of hot carriers observed in single-junction OSCs.^[99] Owing to the rapid progress in Cl-PVMs with tunable bandgaps, large bandgap chlorinated polymers can be used for front sub-cells, whereas low bandgap chlorinated NFAs are suitable for rear sub-cells.

Recently, Forrest and co-workers reported optimized tandem OSCs comprising of DTDCPB:PC₇₀BM (processed using the vacuum thermal method) and PTB7-Th:NFA5 (spin coating processing) blends as front and rear sub-cells, respectively. They recorded an exceptional PCE of 15.0% when using an antireflection coating.^[20c] Later, by modifying the rear sub-cell with the ternary blend of PTB7-Th:NFA5:TT-FIC (having PCE of 12.6%), the PCE of ternary tandem cell was further improved to 15.4%.^[20d]

Considering that NFA25-2 has NIR absorption with a bandgap of 1.29 eV, Gao et al. fabricated tandem solar cells using ternary PCE10:NFA25-2:PC₇₁BM as the rear sub-cell and PBDB-T:F-M as the front sub-cell (Figure 15).^[83] By optimizing the thickness of the front and rear cells to 150 and

122 nm, respectively, a record PCE for any tandem solar cell using chlorinated photoactive materials of 15.72% was achieved along with a high V_{OC} of 1.64 V, a high FF of 69%, and a J_{SC} of 13.89 mA cm⁻².

Recently, efficiencies of tandem OSCs have been reached over 17% due to rapid advancement in the efficient PVMs, interfacial layers, and device engineering.^[2e] However, utilizing this technique in the production of the large-scale module is still very challenging because of its high cost and complex device fabrication processes. Thus, only limited studies have been reported using these Cl-PVMs.

6.4. Ternary OSCs

The higher light-harvesting capabilities of tandem cells can also be realized by directly combining multiple photoactive materials with complementary absorption into one active layer in a conventional device structure, called a ternary OSC.^[100] In addition to improving light absorption, ternary OSCs can also enhance the charge separation and transport resulting from the cascade energy level alignments, realizing superior performance compared to their binary counterparts.^[100a-f,101] Recently, many groups have synthesized ternary solar cells employing

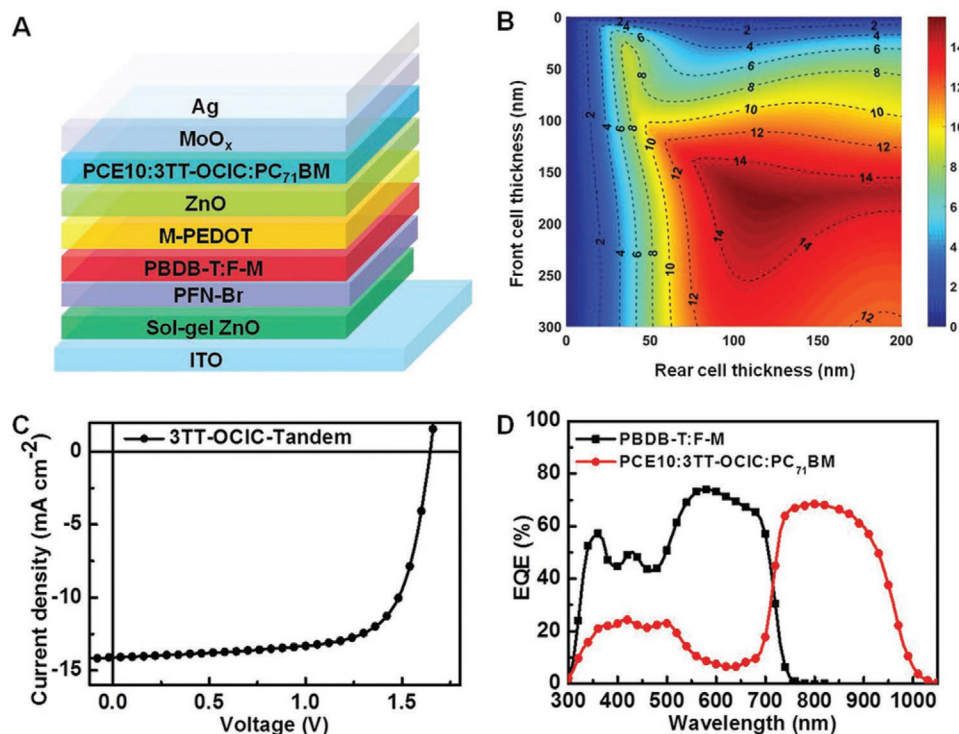


Figure 15. a) Tandem device structure based on 3TT-OCIC (NFA25-2); b) simulated J_{SC} as a function of thickness of the front and rear cells; c) J - V and d) corresponding EQE curves of the optimized tandem devices. a–d) Reproduced with permission.^[83] Copyright 2019, Wiley-VCH.

chlorinated donor polymers or acceptor units, demonstrating impressive performances (Table 5).

For example, He and co-workers enhanced the efficiency of PTB7-Th:NDP-V-C7 blend films from 8.27% to 9.03% by fabricating ternary all-polymer solar cells using P11 (15%) as the third component.^[102] In addition to the increased V_{OC} ascribed to the low-lying HOMO energy levels of P11, it also helped to improve the miscibility by decreasing the excess crystallization of the binary blend films. Thus, P11 eased improving the nanoscale morphology, overall charge transfer and efficiency.

To further improve the V_{OC} in the PBDB-T-2F:NFA3 binary system having a PCE of 13.45%, Hou and co-workers also incorporated NFA2 having higher LUMO than NFA3 at various weight ratios to form ternary blends (Figure 9d,e).^[15d] The optimized ternary OSC with 20% NFA2 in PBDB-T-2F:NFA3

produced a record high PCE of 14.18%, with an improvement in the overall V_{OC} of 0.84 V, a J_{SC} of 22.03 mA cm^{-2} , and an FF of 76.4%. Because of their similar structures, both acceptors exhibit excellent compatibility with each other by forming a cascade energy level alignment, thus favoring nano-scale phase separation, charge transport, and higher PCEs in ternary OSCs.

As indicated in previous studies,^[28,95b,104] Tang and co-workers took advantage of adding PC₇₁BM into ternary OSCs to improve the efficient phase separation and electron transport in the PBDB-T:NFA11 blend.^[73] A remarkable PCE of 14.3%, with an exceptional J_{SC} of 23.3 mA cm^{-2} and a good FF of 74.6% for ternary OSCs, was realized. This high PCE arises from several factors, such as the improved absorption range, higher EQE values, more efficient charge carrier mobility, and superior morphology shown by the ternary blend system compared to

Table 5. Photovoltaic parameters of ternary OSCs based on chlorinated donor or acceptor units.

Blend	Ratio of D:A	V_{oc} [V]	J_{sc} [mA cm^{-2}]	FF [%]	PCE [%]	Ref.
PTB7-Th:PBCIT (P11):NDP-V-C7	0.85:0.15:1.0	0.78	16.77	68.07	9.03	[102]
PBDB-T-2F:IT-2Cl (NFA2):IT-4Cl (NFA3)	1.0:0.2:0.8	0.842	22.03	76.4	14.18	[15d]
PBDB-T:IPIC-4Cl (NFA11):PC ₇₁ BM	1.0:1.0:0.3	0.822	23.3	74.6	14.3	[73]
PBDB-T:IDTC-4Cl (NFA23):PC ₇₁ BM	1.0:0.8:0.2	0.829	19.14	65.6	10.41	[81]
PBDB-TF:HC-PCIC (NFA26):PC ₇₁ BM	1.0:0.85:0.15	0.89	19.29	70.18	12.36	[84]
PBDB-TF:BDTC-4Cl (NFA27-2):PC ₇₁ BM	1.0:1.0:1.0	0.856	21.19	67.2	12.19	[85]
PDBT(E)BTz-p (P21-1):PBDB-T-SF:IT-4F	0.05:1:1.05	0.86	19.90	72.5	12.3	[48]
PDBT(E)BTz-d (P21-2):PBDB-T-SF:IT-4F	0.05:1:1.05	0.86	20.59	74.9	13.1	[48]
PM7 (P10):ITC-2Cl (NFA19):IXIC-4Cl (NFA13)	1.0:0.5:0.5	0.857	23.99	74.7	15.37	[103]

their parent binary counterpart. Likewise, ternary OSCs with PBDB-T:NFA23:PC₇₁BM blends also achieved a promising PCE of 10.41% due to the formation of a cascade energy level alignment and optimal morphology with a suitable domain size formed by adding PC₇₁BM.^[81]

Zhan et al. also employed PC₇₁BM as a third component along with PBDB-TF and NFA26.^[84] Due to the advantageous effects of PC₇₁BM, such as cascade energy level alignment, enhanced absorption in the lower wavelength region, morphology improvement, and lower charge recombination, the overall charge transport mechanism in the ternary OSCs was significantly improved. These factors led to an approximately 10% enhancement in the quantum efficiency in the regions ranging from 600 to 750 nm in the ternary system, thus improving J_{SC} and PCE to 12.36%. Moreover, the authors also tested the thermal stability of these ternary blends at 130 °C for 12 h, where they retained ~80% of the initial PCEs.

The Chen research group also adopted a similar approach to boost the performance of PBDB-T:NFA27-2 by 28%, namely, a PCE of 12.19%, by adding PC₇₁BM as a third component.^[85] As mentioned in the other cases, the addition of PC₇₁BM resulted in improved EQE, higher and balanced charge carrier mobilities in ternary devices, thereby improving the overall photovoltaic parameters and performance (Figure 11f,g). Additionally, these ternary OSCs were fabricated with a significant weight ratio of PC₇₁BM (the optimized PBDB-T:NFA27-2:PC₇₁BM blend ratio was 1:1:1 wt%); such a large scale of the third component had never been used in ternary OSCs before.

Li and co-workers further tested P21-1 and P21-2 as the third component in the PBDB-T-SF:IT-4F system because of their cascade energy level alignment and complementary absorption.^[48] Interestingly, P21-1 and P21-2 were found to be more effective in ternary OSCs, where the PCE of the PBDB-T-SF:IT-4F blend system (PCE = 12.1%) was enhanced up to 12.5% and 13.4% by using 5 wt% of P21-1 or P21-2, respectively. This enhancement in the PCE mainly originated from the higher EQE and J_{SC} in the ternary device, resulting from the enhanced light absorption and Forster resonance energy transfer (FRET) between PBDB-T-SF and P21-1 or P21-2 blends.

Recently, Yan and co-workers fabricated all-chlorinated ternary OSCs by adding NFA13 acceptor having an ultralow bandgap (E_g^{opt} of 1.25 eV) as the third component in the P10:NFA19 host system (Figure 16).^[103] The optimized ternary solar cells (blend ratio of P10:NFA19:NFA13 were 1:0.5:0.5 wt%) completely outperformed their respective binary analogs, yielding an outstanding PCE of 15.37% with a high EQE region covering 400–950 nm (PCE of P10:NFA19 and P10:NFA19 was 13.72% and 12.01%, respectively). Notably, this is the highest efficiency for ternary solar cells reported to date. The higher PCEs were mainly originating from the addition of the NFA13, which enhanced μ_e , absorption profile, favored charge dissociation, and collection efficiencies by improving the morphology and suppressing charge recombination; thereby boosting J_{SC} from 20.27 to 23.99 mA cm⁻².

In brief, combining the advantages of binary and tandem OSCs, ternary OSCs have emerged as an attractive strategy

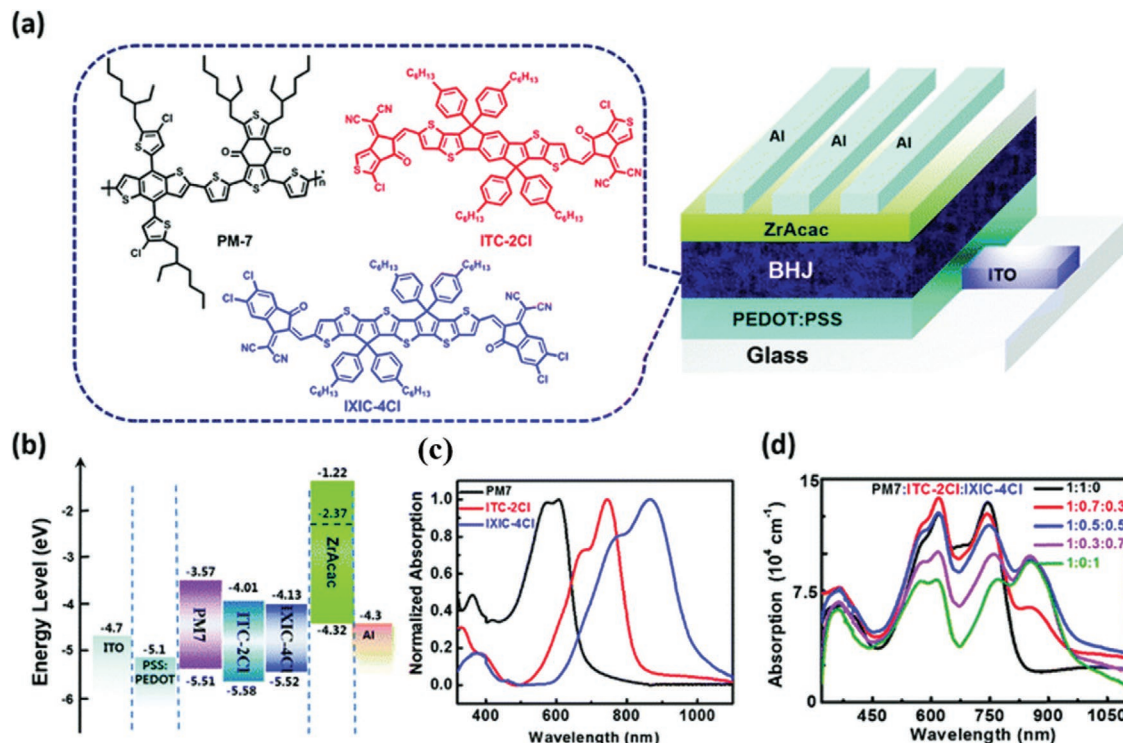


Figure 16. a) Chemical structures of PM7, ITC-2Cl, and IXIC-4Cl (P10, NFA19, and NFA13, respectively) and a schematic diagram of the conventional device structure; b) energy diagrams of all materials used in ternary solar cells; c) normalized UV-vis absorption spectra of neat PM7, ITC-2Cl, and IXIC-4Cl films, and d) absorption spectra of the blend films of PM7:ITC-2Cl:IXIC-4Cl with different ITC-2Cl:IXIC-4Cl weight ratios. a–d) Reproduced with permission.^[103] Copyright 2019, The Royal Society of Chemistry.

to enhance the performance along with benefits such as easy fabrication, lightweight, and flexibility. As summarized above, Cl-PVMs materials with tunable optoelectronic properties proved to be an excellent choice for fabrication of ternary OSCs covering the broad area of the solar spectrum. However, achieving the uniform morphology using the three components in a large-area with suitable thickness tolerance is still crucial for commercialization. Thus, prospects of ternary OSCs are dependent upon resolving these critical challenges.

6.5. SCOSCs

As fine-control of a typical BHJ morphology is one of the crucial factors which hindering the stability of solar cells, SCOSCs comprising a single conjugated material as the active layer have been introduced.^[105] Though these materials have advantages such as a simple fabrication process, excellent stability, and efficient charge separation due to the presence of a single active layer component, their PCEs are still lagging behind binary OSCs.

Recently, Feng et al. synthesized a novel double-cable chlorinated polymer named PBDBPBI-Cl, formed by combining crystalline **P10** as a conjugate backbone (which acts as donor) and perylene bisimide (PBI) as the side-chains (which acts as acceptor) (Figure 17a–c).^[105d] Remarkably, thermal annealing of PBDBPBI-Cl films at 230 °C favored simultaneous crystallization of both the components of the polymers, thereby delivering highly ordered nanostructures compared to as-cast counterparts. Moreover, these films also showed efficient charge transport by suppressing the charge recombination. Consequently, optimized SCOSCs displayed record PCE of 6.32% with a high EQE, FF, and excellent photostability with the retention of

over 90% of its initial PCEs after 300 h of continuous one sun illumination.

Though SCOSCs are considered as the most simplified stage of OSCs, their progress is largely lagging behind all the other kinds of OSCs due to their intrinsic drawbacks. Previous advances in SCOSCs materials emphasize that further improvement in the efficiency of SCOSCs is highly challenging as it involves considerable difficulty.^[105f] Therefore, other than the conventional methods, some new revolutionary design strategies must be explored for the effective take-off of SCOSCs.

6.6. Indoor OSCs

Although the main objective of the OSCs were to provide the infinite power generating source by utilizing the outdoor sunlight, but recent rapid advances in the electronics of the internet of things (IOT) such as low-power consuming electronics goods, sensors, batteries, and data storage devices, will further provide a unique opportunity to utilize OSCs in low light intensity or indoor environment.^[106,107] In recent times, impressive progress has been realized in indoor solar cell research by using various OSCs active layer materials.^[106,7b,c,8]

By replacing the DCI “A” units of ITIC with 5,6-dichloro-1H-indene-1,3(2H)-dione (2Cl-I) groups, Hou and co-workers first reported the synthesis of a novel Cl-NFA abbreviated as IO-4Cl, specifically for use in indoor OSCs (Figure 17d–g).^[106] Due to the use of weaker electronegativity 2Cl-I end groups over DCI units, IO-4Cl exhibited 90 nm blueshifted absorption than ITIC ($E_g^{opt} = 1.80$ eV), thereby ensuring good matching of the absorption with the indoor light spectrum. By blending with PBDB-TF, traditional OSCs showed a PCE of 9.80% with high

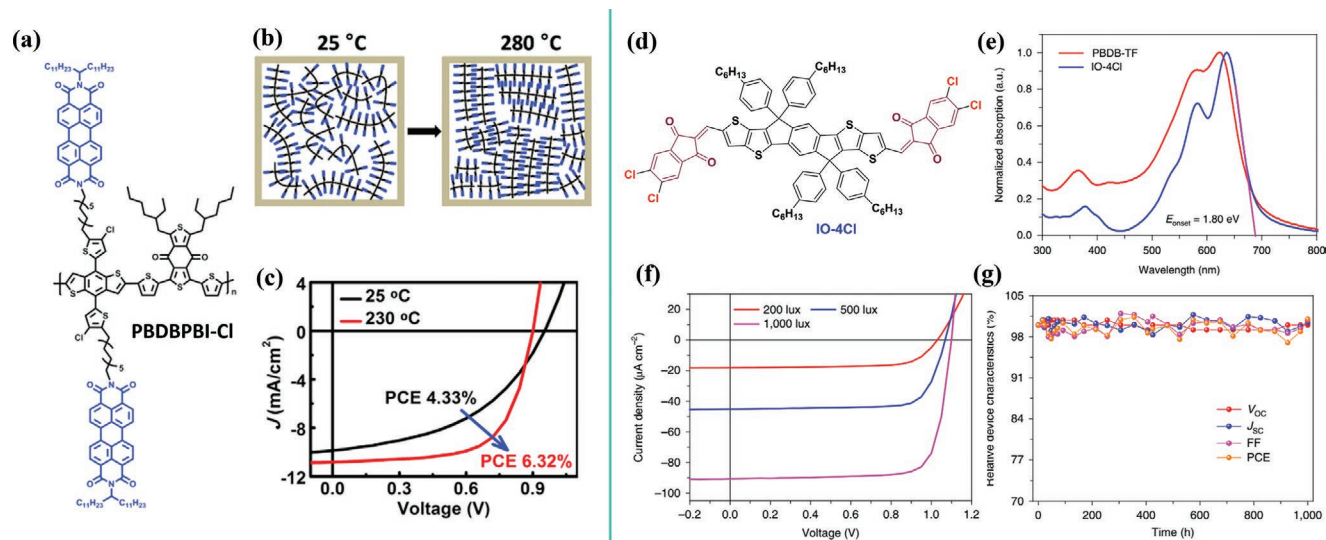


Figure 17. a) The chemical structures of new double-cable polymer, PBDBPBI-Cl; b) proposed illustration of morphology evolution under thermal annealing from 25 to 280 °C (left image indicates that PBDBPBI-Cl thin film without thermal annealing performs disordered structures, while right images display conjugated backbones and PBI side units in PBDBPBI-Cl thin films form lamellar structures after annealed at 280 °C) and c) J - V curves of optimized SCOSCs. a–c) Reproduced with permission.^[105d] Copyright 2019, Elsevier Inc. d) Chemical structure of IO-4Cl acceptor; e) normalized UV-visible absorption spectra of PBDB-TF and IO-4Cl in a thin film state; f) J - V curves of the PBDB-TF:IO-4Cl-based optimal cell under different indoor light intensities, and g) the curves of the photovoltaic characteristics versus time. The curves are normalized to their initial values at the start of the lifetime test. The device was encapsulated, and the testing was carried out at a temperature of 25–30 °C and relative humidity of 40–60%. d–g) Reproduced with permission.^[106] Copyright 2019, Springer Nature.

V_{OC} (1.24 V) and moderate J_{SC} (11.5 mA cm⁻²). Whereas, under indoor LED illumination of 1000 lux (2700 K), they demonstrated remarkable PCE of 26.1% with high a J_{SC} of 90.6 μ A cm⁻², a high V_{OC} of 1.1 V, high FF of 79.1%, and excellent stability (preserving its initial PCE after 1000 h continuous illumination). More importantly, they also tested large area compatibility by fabricating large-area devices using a blade-coating method, where devices based on PBDB-TF:IO-4Cl displayed over 23% PCE for an active area 4 cm⁻².

Owing to the higher power generation capacity of OSCs over silicon-based solar cells in the indoor light conditions,^[107c] indoor OSCs have been gaining popularity among the solar cell research communities. In addition to the development of efficient PVMs having overlapped photo-response spectrum with the indoor light sources, reducing trap-assisted charge recombination and E_{loss} will also play a critical role in enhancing the efficiency of indoor solar cells.^[106]

7. Outlook and Conclusion

We have reviewed the plethora of design approaches that utilize chlorination as an effective tool to modulate the optoelectronic and morphological properties in π -conjugated photovoltaic materials (Cl-PVMs, viz., polymers, SMs, or NFA), thereby enhancing the PCEs of OSCs. Though neglected over the years, these Cl-PVMs enjoy several unique advantages over their fluorinated counterparts, especially further lowering the energy levels, enhancement of the absorption, good control over the crystallinity and morphology, based on their grafting positions. Moreover, the synthesis of these Cl-PVMs is significantly less expensive and less complex compared with fluorinated analogs, which will further diversify the versatility of these materials for large-scale industrialization. Consequently, astonishing advancements have been observed since 2017 by incorporating these Cl-PVMs, with remarkable PCEs up to 17% achieved using single-junction configurations. Based on the carefully studied various examples, we propose a few recommendations for future designing Cl-PVMs for OSCs:

1. Chlorination design strategy: Unlike fluorination, the effects of chlorination on the planarity and crystallinity are directly dependent on the Cl substitution position due to the large size of Cl.
 - a) Chlorination in the main backbone: Usually, Cl incorporation in the polymer backbone often results in blueshifted absorption, decreased planarity, and crystallinity due to the steric hindrance caused by the large size of Cl atoms. Therefore, this strategy can mostly be employed for improving the solubility and BHJ morphology of polymers having high aggregation tendencies.
 - b) Chlorination in the side-chains/terminal positions: In contrast to backbone chlorination, Cl insertion in the side-chains of the donor/acceptor units of the D–A copolymers or at the terminal position of A–D–A-type NFAs remains the preferred way to increase the efficiency by simultaneously augmenting both J_{SC} and V_{OC} through light absorption enhancement and energy level lowering. Currently, this approach has been employed for most of
2. The chlorination method has proven to be highly effective, especially when the fluorinated counterpart has demonstrated excellent performance. Therefore, applying chlorination to efficient fluorinated designs with superior performance is always worth attempting.
3. Most of the recent Cl-NFAs were mainly synthesized by grafting very few chlorinated terminal units, such as Cl-DCI, 2Cl-DCI, and CPTCN, as terminal “A” units. Therefore, the effects of Cl insertion on various other “A” cores can be an exciting research topic.
4. Similarly, a wide scope exists for further exploration of A–D–A-type Cl-NFAs, either by Cl insertion in the central donor/linker/side-chains or by adopting revolutionary design strategies, such as designing asymmetric NFAs^[109] having a large dipole moment, synthesizing D–A–D-type NFAs or easily scalable non-fused molecule involving non-covalent molecular interactions. Thus, these methods need to be further explored.
5. As the performance of OSCs chiefly depends on the nano-scale BHJ morphology, PCE enhancement of existing efficient Cl-PVMs can be further attempted by refining the molecular orientation of EDs/EAs in the active layer by varying the device fabrication conditions, such as by using different solvents or additive combinations or annealing methods (thermal or solvent vapor). Additionally, structural optimization of Cl-PVMs with varying numbers of Cl substituents and side-chain engineering can also be used to further enhance the efficiencies.
6. In addition to the fullerene OSCs and NF-OSCs, all-polymer solar cells (all-PSCs) composed of polymer donors and polymer acceptors have recently gained tremendous attention.^[101b,110] In addition to quickly rising PCEs, these systems also demonstrated several superior features relative to fullerene OSCs and/or NF-OSCs, such as higher thermal and mechanical stabilities and the outstanding film-forming ability for large-area roll-to-roll processing. Interestingly, chlorinated polymer donor or acceptor materials have seldom been explored in all-PSCs. We strongly believe that chlorinated polymers with easily tunable properties can be explored further for all-PSC applications.
7. Although the synthesis cost of Cl-PVMs is lower than that of the corresponding fluorinated counterpart, the SC index of most of the efficient Cl-PVMs reported to date is still very high, making them unviable for industrialization. Therefore, simple structure molecular design strategies with low SC must be focused.
8. For the commercialization of OSCs, photoactive materials must exhibit several features, such as high efficiency, thickness tolerance, green solvent processing, air insensitivity, compatibility with the large-area roll-to-roll processing technique, and excellent stability.^[5c,111] Most of the efficient Cl-PVMs reported until now have demonstrated only one or two properties mentioned above. Moreover, most of these OSCs commonly processed from high boiling chlorinated solvents using spin coating, which is not ideal for reaching the final

goal of large-scale industrialization. Therefore, researchers must focus on designing photoactive materials with high PCE for relatively thick films (>200 nm) processed from green solvents using large-area compatible printing methods, such as roll-to-roll coating.

In conclusion, tailoring the optoelectronic and morphological properties of ED and EA materials via chlorination provides a unique opportunity for enhancing the PCEs of OSCs, and this approach will continue to attract the attention of researchers in the future. Although current OSCs employing Cl-PVMs have delivered a record efficiency of 17% (which is considered one of the prime prerequisites for commercialization), further screening of efficient candidates with low SC, stability/degradation mechanism studies, and long-term lifetime measurements of efficient materials in various environmental conditions are major areas of focus for realizing practical OSCs. We anticipate that more new chlorinated photoactive materials will be designed in the future based on continuous material innovation/synthesis and a better understanding of device physics and interfacial engineering, which will help the successful commercialization of flexible OSCs by surpassing the threshold PCE of 20%.

Acknowledgements

This research was supported by the New & Renewable Energy Core Technology Programs (No. 20153010140030 and No. 20193091010110) of the Korea Institute of Energy Technology Evaluation and Planning (KETEP) grant funded by the Ministry of Trade, Industry & Energy, Republic of Korea. This research was also supported by the 2019 KU Brain Pool of Konkuk University.

Conflict of Interest

The authors declare no conflict of interest.

Keywords

chlorine effect, halogenated polymers, nonfullerene acceptors, organic solar cells, ternary organic solar cells

Received: September 20, 2019

Revised: December 27, 2019

Published online:

- [1] a) F. C. Krebs, N. Espinosa, M. Hösel, R. R. Søndergaard, M. Jørgensen, *Adv. Mater.* **2014**, *26*, 29; b) A. J. Heeger, *Adv. Mater.* **2014**, *26*, 10; c) L. Lu, T. Zheng, Q. Wu, A. M. Schneider, D. Zhao, L. Yu, *Chem. Rev.* **2015**, *115*, 12666; d) Y. Lin, Y. Jin, S. Dong, W. Zheng, J. Yang, A. Liu, F. Liu, Y. Jiang, T. P. Russell, F. Zhang, F. Huang, L. Hou, *Adv. Energy Mater.* **2018**, *8*, 1701942; e) R. R. Søndergaard, N. Espinosa, M. Jørgensen, F. C. Krebs, *Energy Environ. Sci.* **2014**, *7*, 1006; f) R. Xue, J. Zhang, Y. Li, Y. Li, *Small* **2018**, *14*, 1801793; g) Y. Li, G. Xu, C. Cui, Y. Li, *Adv. Energy Mater.* **2018**, *8*, 1701791; h) Q. Xue, R. Xia, C. J. Brabec, H.-L. Yip, *Energy Environ. Sci.* **2018**, *11*, 1688; i) R. Sun, J. Guo,

- C. Sun, T. Wang, Z. Luo, Z. Zhang, X. Jiao, W. Tang, C. Yang, Y. Li, J. Min, *Energy Environ. Sci.* **2019**, *12*, 384; j) T. Yan, W. Song, J. Huang, R. Peng, L. Huang, Z. Ge, *Adv. Mater.* **2019**, *31*, 1902210; k) J. Lee, Y.-H. Seo, S.-N. Kwon, D.-H. Kim, S. Jang, H. Jung, Y. Lee, H. Weerasinghe, T. Kim, J. Y. Kim, D. Vak, S.-I. Na, *Adv. Energy Mater.* **2019**, *9*, 1901805.
- [2] a) J. Yuan, Y. Zhang, L. Zhou, G. Zhang, H.-L. Yip, T.-K. Lau, X. Lu, C. Zhu, H. Peng, P. A. Johnson, M. Leclerc, Y. Cao, J. Ulanski, Y. Li, Y. Zou, *Joule* **2019**, *3*, 1140; b) Y. Cui, H. Yao, J. Zhang, T. Zhang, Y. Wang, L. Hong, K. Xian, B. Xu, S. Zhang, J. Peng, Z. Wei, F. Gao, J. Hou, *Nat. Commun.* **2019**, *10*, 2515; c) R. Yu, H. Yao, Y. Cui, L. Hong, C. He, J. Hou, *Adv. Mater.* **2019**, *31*, 1902302; d) X. Xu, K. Feng, Z. Bi, W. Ma, G. Zhang, Q. Peng, *Adv. Mater.* **2019**, *31*, 1901872; e) L. Hong, H. Yao, Z. Wu, Y. Cui, T. Zhang, Y. Xu, R. Yu, Q. Liao, B. Gao, K. Xian, H. Y. Woo, Z. Ge, J. Hou, *Adv. Mater.* **2019**, *31*, 1903441; f) B. Fan, D. Zhang, M. Li, W. Zhong, Z. Zeng, L. Ying, F. Huang, Y. Cao, *Sci. China Chem.* **2019**, *62*, 746; g) L. Meng, Y. Zhang, X. Wan, C. Li, X. Zhang, Y. Wang, X. Ke, Z. Xiao, L. Ding, R. Xia, H.-L. Yip, Y. Cao, Y. Chen, *Science* **2018**, *361*, 1094; h) Y. Cui, H. Yao, L. Hong, T. Zhang, Y. Tang, B. Lin, K. Xian, B. Gao, C. An, P. Bi, W. Ma, J. Hou, *Natl. Sci. Rev.* **2019**, <https://doi.org/10.1093/nsr/nwz200>.
- [3] a) S. Holliday, Y. Li, C. K. Luscombe, *Prog. Polym. Sci.* **2017**, *70*, 34; b) F. Zhao, C. Wang, X. Zhan, *Adv. Energy Mater.* **2018**, *8*, 1703147.
- [4] a) Y. Ma, Z. Kang, Q. Zheng, *J. Mater. Chem. A* **2017**, *5*, 1860; b) T. Xu, L. Yu, *Mater. Today* **2014**, *17*, 11; c) D. He, F. Zhao, L. Jiang, C. Wang, *J. Mater. Chem. A* **2018**, *6*, 8839.
- [5] a) H. Fu, Z. Wang, Y. Sun, *Angew. Chem. Int. Ed.* **2019**, *58*, 4442; b) S. Dey, *Small* **2019**, *15*, 1900134; c) G. Wang, M. A. Adil, J. Zhang, Z. Wei, *Adv. Mater.* **2019**, *31*, 1805089.
- [6] a) Y. Liu, J. Zhao, Z. Li, C. Mu, W. Ma, H. Hu, K. Jiang, H. Lin, H. Ade, H. Yan, *Nat. Commun.* **2014**, *5*, 5293; b) L. Ye, S. Zhang, L. Huo, M. Zhang, J. Hou, *Acc. Chem. Res.* **2014**, *47*, 1595; c) Y. Cui, H. Yao, L. Hong, T. Zhang, Y. Xu, K. Xian, B. Gao, J. Qin, J. Zhang, Z. Wei, J. Hou, *Adv. Mater.* **2019**, *31*, 1808356; d) Y. Lin, F. Zhao, Y. Wu, K. Chen, Y. Xia, G. Li, S. K. K. Prasad, J. Zhu, L. Huo, H. Bin, Z.-G. Zhang, X. Guo, M. Zhang, Y. Sun, F. Gao, Z. Wei, W. Ma, C. Wang, J. Hodgkiss, Z. Bo, O. Inganäs, Y. Li, X. Zhan, *Adv. Mater.* **2017**, *29*, 1604155; e) D. He, F. Zhao, J. Xin, J. J. Rech, Z. Wei, W. Ma, W. You, B. Li, L. Jiang, Y. Li, C. Wang, *Adv. Energy Mater.* **2018**, *8*, 1802050; f) M. An, F. Xie, X. Geng, J. Zhang, J. Jiang, Z. Lei, D. He, Z. Xiao, L. Ding, *Adv. Energy Mater.* **2017**, *7*, 1602509; g) D. He, L. Qian, L. Ding, *Polym. Chem.* **2016**, *7*, 2329; h) H. Li, D. He, P. Mao, Y. Wei, L. Ding, J. Wang, *Adv. Energy Mater.* **2017**, *7*, 1602663; i) Y. Lin, F. Zhao, Q. He, L. Huo, Y. Wu, T. C. Parker, W. Ma, Y. Sun, C. Wang, D. Zhu, A. J. Heeger, S. R. Marder, X. Zhan, *J. Am. Chem. Soc.* **2016**, *138*, 4955; j) F. Xie, D. He, H. Pan, J. Jiang, L. Ding, *Macromol. Rapid Commun.* **2017**, *38*, 1700074; k) X. Xu, G. Zhang, Y. Li, Q. Peng, *Chin. Chem. Lett.* **2019**, *30*, 809.
- [7] a) J. Mei, Z. Bao, *Chem. Mater.* **2014**, *26*, 604; b) J. Zhao, Y. Li, G. Yang, K. Jiang, H. Lin, H. Ade, W. Ma, H. Yan, *Nat. Energy* **2016**, *1*, 15027; c) G. P. Kini, S. K. Lee, W. S. Shin, S.-J. Moon, C. E. Song, J.-C. Lee, *J. Mater. Chem. A* **2016**, *4*, 18585; d) Z. Liao, Y. Xie, L. Chen, Y. Tan, S. Huang, Y. An, H. S. Ryu, X. Meng, X. Liao, B. Huang, Q. Xie, H. Y. Woo, Y. Sun, Y. Chen, *Adv. Funct. Mater.* **2019**, *29*, 1808828; e) W. Su, G. Li, Q. Fan, Q. Zhu, X. Guo, J. Chen, J. Wu, W. Ma, M. Zhang, Y. Li, *J. Mater. Chem. A* **2019**, *7*, 2351; f) C. E. Song, Y. J. Kim, S. R. Suranagi, G. P. Kini, S. Park, S. K. Lee, W. S. Shin, S.-J. Moon, I.-N. Kang, C. E. Park, J.-C. Lee, *ACS Appl. Mater. Interfaces* **2016**, *8*, 12940; g) T. Liu, W. Gao, Y. Wang, T. Yang, R. Ma, G. Zhang, C. Zhong, W. Ma, H. Yan, C. Yang, *Adv. Funct. Mater.* **2019**, *29*, 1902155; h) Y. Wu, H. Yang, Y. Zou, Y. Dong, J. Yuan, C. Cui, Y. Li, *Energy Environ. Sci.* **2019**, *12*, 675; i) G. P. Kini, Q. V. Hoang, C. E. Song, S. K. Lee, W. S. Shin,

- W.-W. So, M. A. Uddin, H. Y. Woo, J.-C. Lee, *Polym. Chem.* **2017**, *8*, 3622; j) S. J. Jeon, J. E. Yu, Y. W. Han, I. S. Suh, D. K. Moon, *J. Ind. Eng. Chem.* **2019**, *71*, 137; k) S. Pang, R. Zhang, C. Duan, S. Zhang, X. Gu, X. Liu, F. Huang, Y. Cao, *Adv. Energy Mater.* **2019**, *9*, 1901740; l) F. Zhao, D. He, J. Xin, S. Dai, H. Xue, L. Jiang, Z. Wei, W. Ma, X. Zhan, Y. Li, C. Wang, *Sci. China Chem.* **2019**, *62*, 790; m) Y. Yang, Z. Liu, G. Zhang, X. Zhang, D. Zhang, *Adv. Mater.* **2019**, *31*, 1903104.
- [8] a) Q. Zhang, M. A. Kelly, N. Bauer, W. You, *Acc. Chem. Res.* **2017**, *50*, 2401; b) X.-P. Xu, Y. Li, M.-M. Luo, Q. Peng, *Chin. Chem. Lett.* **2016**, *27*, 1241; c) A. Casey, S. D. Dimitrov, P. Shakya-Tuladhar, Z. Fei, M. Nguyen, Y. Han, T. D. Anthopoulos, J. R. Durrant, M. Heeney, *Chem. Mater.* **2016**, *28*, 5110; d) P. Chao, N. Johnner, X. Zhong, H. Meng, F. He, *J. Energy Chem.* **2019**, *39*, 208; e) G. E. Park, S. Choi, S. Y. Park, D. H. Lee, M. J. Cho, D. H. Choi, *Adv. Energy Mater.* **2017**, *7*, 1700566; f) Y. Liu, W. Zhao, Y. Wu, J. Zhang, G. Li, W. Li, W. Ma, J. Hou, Z. Bo, *J. Mater. Chem. A* **2016**, *4*, 8097; g) Y. Qin, M. A. Uddin, Y. Chen, B. Jang, K. Zhao, Z. Zheng, R. Yu, T. J. Shin, H. Y. Woo, J. Hou, *Adv. Mater.* **2016**, *28*, 9416; h) X. Zhong, H. Chen, M. Wang, S. Gan, Q. He, W. Chen, F. He, *Macromolecules* **2019**, *52*, 2393; i) X. Xu, T. Yu, Z. Bi, W. Ma, Y. Li, Q. Peng, *Adv. Mater.* **2018**, *30*, 1703973; j) G. P. Kini, J. Y. Choi, S. J. Jeon, I. S. Suh, D. K. Moon, *Polym. Chem.* **2019**, *10*, 4459; k) G. P. Kini, J. Y. Choi, S. J. Jeon, I. S. Suh, D. K. Moon, *Dyes Pigment.* **2019**, *164*, 62; l) S. Rasool, V. V. Doan, H. K. Lee, S. K. Lee, J. C. Lee, S. J. Moon, W. W. So, C. E. Song, W. S. Shin, *Thin Solid Films* **2019**, *669*, 42.
- [9] a) G. P. Kini, S. Oh, Z. Abbas, S. Rasool, M. Jahandar, C. E. Song, S. K. Lee, W. S. Shin, W.-W. So, J.-C. Lee, *ACS Appl. Mater. Interfaces* **2017**, *9*, 12617; b) Y. Jin, Z. Chen, S. Dong, N. Zheng, L. Ying, X.-F. Jiang, F. Liu, F. Huang, Y. Cao, *Adv. Mater.* **2016**, *28*, 9811; c) Y. Jin, Z. Chen, M. Xiao, J. Peng, B. Fan, L. Ying, G. Zhang, X.-F. Jiang, Q. Yin, Z. Liang, F. Huang, Y. Cao, *Adv. Energy Mater.* **2017**, *7*, 1700944; d) S. J. Jeon, Y. W. Han, D. K. Moon, *ACS Appl. Mater. Interfaces* **2019**, *11*, 9239.
- [10] a) W. Zhao, S. Li, H. Yao, S. Zhang, Y. Zhang, B. Yang, J. Hou, *J. Am. Chem. Soc.* **2017**, *139*, 7148; b) H. Yao, Y. Cui, R. Yu, B. Gao, H. Zhang, J. Hou, *Angew. Chem. Int. Ed.* **2017**, *56*, 3045; c) S. J. Xu, Z. Zhou, W. Liu, Z. Zhang, F. Liu, H. Yan, X. Zhu, *Adv. Mater.* **2017**, *29*; d) J. E. Yu, S. J. Jeon, J. Y. Choi, Y. W. Han, E. J. Ko, D. K. Moon, *Small* **2019**, *15*, 1805321; e) F. Zhao, S. Dai, Y. Wu, Q. Zhang, J. Wang, L. Jiang, Q. Ling, Z. Wei, W. Ma, W. You, C. Wang, X. Zhan, *Adv. Mater.* **2017**, *29*, 1700144.
- [11] M. L. Tang, J. H. Oh, A. D. Reichardt, Z. Bao, *J. Am. Chem. Soc.* **2009**, *131*, 3733.
- [12] T. Wang, R. Sun, S. Xu, J. Guo, W. Wang, J. Guo, X. Jiao, J. Wang, S. Jia, X. Zhu, Y. Li, J. Min, *J. Mater. Chem. A* **2019**, *7*, 14070.
- [13] a) G. P. Kini, J. Y. Choi, S. J. Jeon, I. S. Suh, D. K. Moon, *Polymer* **2018**, *148*, 330; b) T. L. Nguyen, H. Choi, S. J. Ko, M. A. Uddin, B. Walker, S. Yum, J. E. Jeong, M. H. Yun, T. J. Shin, S. Hwang, J. Y. Kim, H. Y. Woo, *Energy Environ. Sci.* **2014**, *7*, 3040.
- [14] a) Q. Zhang, L. Yan, X. Jiao, Z. Peng, S. Liu, J. J. Rech, E. Klump, H. Ade, F. So, W. You, *Chem. Mater.* **2017**, *29*, 5990; b) S. Zhang, Y. Qin, J. Zhu, J. Hou, *Adv. Mater.* **2018**, *30*, 1800868.
- [15] a) D. Mo, H. Wang, H. Chen, S. Qu, P. Chao, Z. Yang, L. Tian, Y.-A. Su, Y. Gao, B. Yang, W. Chen, F. He, *Chem. Mater.* **2017**, *29*, 2819; b) Q. Fan, Q. Zhu, Z. Xu, W. Su, J. Chen, J. Wu, X. Guo, W. Ma, M. Zhang, Y. Li, *Nano Energy* **2018**, *48*, 413; c) P. Chao, L. Liu, J. Zhou, J. Qu, D. Mo, H. Meng, Z. Xie, F. He, Y. Ma, *ACS Appl. Energy Mater.* **2018**, *1*, 6549; d) H. Zhang, H. Yao, J. Hou, J. Zhu, J. Zhang, W. Li, R. Yu, B. Gao, S. Zhang, J. Hou, *Adv. Mater.* **2018**, *30*, 1800613; e) J.-L. Wang, K.-K. Liu, L. Hong, G.-Y. Ge, C. Zhang, J. Hou, *ACS Energy Lett.* **2018**, *3*, 2967; f) H. Chen, Z. Hu, H. Wang, L. Liu, P. Chao, J. Qu, W. Chen, A. Liu, F. He, *Joule* **2018**, *2*, 1623.
- [16] Y. Zhang, H. Yao, S. Zhang, Y. Qin, J. Zhang, L. Yang, W. Li, Z. Wei, F. Gao, J. Hou, *Sci. China Chem.* **2018**, *61*, 1328.
- [17] M. L. Tang, Z. Bao, *Chem. Mater.* **2011**, *23*, 446.
- [18] a) Y. Li, J. D. Lin, X. Che, Y. Qu, F. Liu, L. S. Liao, S. R. Forrest, *J. Am. Chem. Soc.* **2017**, *139*, 17114; b) Y. Cui, C. Yang, H. Yao, J. Zhu, Y. Wang, G. Jia, F. Gao, J. Hou, *Adv. Mater.* **2017**, *29*, 1703080.
- [19] F. Yang, C. Li, W. Lai, A. Zhang, H. Huang, W. Li, *Mater. Chem. Front.* **2017**, *1*, 1389.
- [20] a) Z. Liu, Y. Gao, J. Dong, M. Yang, M. Liu, Y. Zhang, J. Wen, H. Ma, X. Gao, W. Chen, M. Shao, *J. Phys. Chem. Lett.* **2018**, *9*, 6955; b) Y. Wu, C. An, L. Shi, L. Yang, Y. Qin, N. Liang, C. He, Z. Wang, J. Hou, *Angew. Chem. Int. Ed.* **2018**, *57*, 12911; c) X. Che, Y. Li, Y. Qu, S. R. Forrest, *Nat. Energy* **2018**, *3*, 422; d) Y. Li, J. D. Lin, X. Liu, Y. Qu, F. P. Wu, F. Liu, Z. Q. Jiang, S. R. Forrest, *Adv. Mater.* **2018**, *30*, 1804416.
- [21] a) S. Qu, H. Wang, D. Mo, P. Chao, Z. Yang, L. Li, L. Tian, W. Chen, F. He, *Macromolecules* **2017**, *50*, 4962; b) P. Chao, H. Wang, D. Mo, H. Meng, W. Chen, F. He, *J. Mater. Chem. A* **2018**, *6*, 2942; c) Z. Hu, H. Chen, J. Qu, X. Zhong, P. Chao, M. Xie, W. Lu, A. Liu, L. Tian, Y.-A. Su, W. Chen, F. He, *ACS Energy Lett.* **2017**, *2*, 753; d) P. Chao, Z. Mu, H. Wang, D. Mo, H. Chen, H. Meng, W. Chen, F. He, *ACS Appl. Energy Mater.* **2018**, *1*, 2365.
- [22] Y. Li, Y. Fu, H. Tong, Z. Xie, L. Wang, *J. Polym. Sci. A* **2013**, *51*, 2910.
- [23] Y. Li, B. Meng, H. Tong, Z. Xie, L. Wang, *Polym. Chem.* **2014**, *5*, 1848.
- [24] T. Lei, J.-H. Dou, Z.-J. Ma, C.-J. Liu, J.-Y. Wang, J. Pei, *Chem. Sci.* **2013**, *4*, 2447.
- [25] Y.-Q. Zheng, Z. Wang, J.-H. Dou, S.-D. Zhang, X.-Y. Luo, Z.-F. Yao, J.-Y. Wang, J. Pei, *Macromolecules* **2015**, *48*, 5570.
- [26] a) D. Zhu, X. Bao, Q. Zhu, C. Gu, M. Qiu, S. Wen, J. Wang, B. Shahid, R. Yang, *Energy Environ. Sci.* **2017**, *10*, 614; b) C. Zhang, X. Zhu, *Acc. Chem. Res.* **2017**, *50*, 1342.
- [27] C. Cui, W.-Y. Wong, Y. Li, *Energy Environ. Sci.* **2014**, *7*, 2276.
- [28] H. Wang, P. Chao, H. Chen, Z. Mu, W. Chen, F. He, *ACS Energy Lett.* **2017**, *2*, 1971.
- [29] P. Chao, H. Wang, S. Qu, D. Mo, H. Meng, W. Chen, F. He, *Macromolecules* **2017**, *50*, 9617.
- [30] Z. Yang, H. Chen, H. Wang, D. Mo, L. Liu, P. Chao, Y. Zhu, C. Liu, W. Chen, F. He, *Polym. Chem.* **2018**, *9*, 940.
- [31] Y. Zhang, F. Ren, Q. Li, Z. Zhang, X. He, Z. Chen, J. Shi, G. Tu, *J. Mater. Chem. C* **2018**, *6*, 4658.
- [32] Y. Wang, T. Michinobu, *J. Mater. Chem. C* **2016**, *4*, 6200.
- [33] J. Lee, M. Jang, S. M. Lee, D. Yoo, T. J. Shin, J. H. Oh, C. Yang, *ACS Appl. Mater. Interfaces* **2014**, *6*, 20390.
- [34] a) J. H. Kim, C. E. Song, N. Shin, H. Kang, S. Wood, I. N. Kang, B. J. Kim, B. Kim, J. S. Kim, W. S. Shin, D. H. Hwang, *ACS Appl. Mater. Interfaces* **2013**, *5*, 12820; b) Y. Gao, Z. Wang, J. Zhang, H. Zhang, K. Lu, F. Guo, Z. Wei, Y. Yang, L. Zhao, Y. Zhang, *Macromolecules* **2018**, *51*, 2498; c) H. Bin, L. Gao, Z.-G. Zhang, Y. Yang, Y. Zhang, C. Zhang, S. Chen, L. Xue, C. Yang, M. Xiao, Y. Li, *Nat. Commun.* **2016**, *7*, 13651; d) H. Bin, Y. Yang, Z. Peng, L. Ye, J. Yao, L. Zhong, C. Sun, L. Gao, H. Huang, X. Li, B. Qiu, L. Xue, Z.-G. Zhang, H. Ade, Y. Li, *Adv. Energy Mater.* **2018**, *8*, 1702324; e) L. Gao, Z.-G. Zhang, H. Bin, L. Xue, Y. Yang, C. Wang, F. Liu, T. P. Russell, Y. Li, *Adv. Mater.* **2016**, *28*, 8288; f) Y. Chen, Q. Zhang, M. Du, G. Li, Z. Li, H. Huang, Y. Geng, X. Zhang, E. Zhou, *ACS Appl. Polym. Mater.* **2019**, *1*, 906.
- [35] a) Q. Fan, H. Jiang, Y. Liu, W. Su, H. Tan, Y. Wang, R. Yang, W. Zhu, *J. Mater. Chem. C* **2016**, *4*, 2606; b) S. Xu, L. Feng, J. Yuan,

- Z.-G. Zhang, Y. Li, H. Peng, Y. Zou, *ACS Appl. Mater. Interfaces* **2017**, *9*, 18816.
- [36] H. Yao, L. Ye, H. Zhang, S. Li, S. Zhang, J. Hou, *Chem. Rev.* **2016**, *116*, 7397.
- [37] a) L. Huo, S. Zhang, X. Guo, F. Xu, Y. Li, J. Hou, *Angew. Chem. Int. Ed.* **2011**, *123*, 9871; b) G. P. Kini, S. R. Suranagi, M. Kumar, R. Singh, *Dyes Pigm.* **2019**, <https://doi.org/10.1016/j.dyepig.2019.108083>.
- [38] Z. Ji, X. Xu, G. Zhang, Y. Li, Q. Peng, *Nano Energy* **2017**, *40*, 214.
- [39] a) H. Chen, J. Qu, L. Liu, W. Chen, F. He, *J. Phys. Chem. Lett.* **2019**, *10*, 936; b) R. Yu, H. Yao, Z. Chen, J. Xin, L. Hong, Y. Xu, Y. Zu, W. Ma, J. Hou, *Adv. Mater.* **2019**, *31*, 1900477.
- [40] Q. Fan, T. Liu, W. Gao, Y. Xiao, J. Wu, W. Su, X. Guo, X. Lu, C. Yang, H. Yan, M. Zhang, Y. Li, *J. Mater. Chem. A* **2019**, *7*, 15404.
- [41] A. Tang, W. Song, B. Xiao, J. Guo, J. Min, Z. Ge, J. Zhang, Z. Wei, E. Zhou, *Chem. Mater.* **2019**, *31*, 3941.
- [42] A. Tang, Q. Zhang, M. Du, G. Li, Y. Geng, J. Zhang, Z. Wei, X. Sun, E. Zhou, *Macromolecules* **2019**, *52*, 6227.
- [43] P. Chao, L. Liu, J. Qu, Q. He, S. Gan, H. Meng, W. Chen, F. He, *Dyes Pigm.* **2019**, *162*, 746.
- [44] Y. Dong, H. Yang, Y. Wu, Y. Zou, J. Yuan, C. Cui, Y. Li, *J. Mater. Chem. A* **2019**, *7*, 2261.
- [45] S. Huang, X. Huang, L. Chen, Z. Liao, S. Ding, Z. Yuan, Y. Chen, *Org. Electron.* **2019**, *70*, 86.
- [46] X. Yuan, Q. Wang, D. Zhu, B. Shahid, R. Yang, *Macromol. Rapid Commun.* **2019**, *40*, 1900035.
- [47] B. Qiu, S. Chen, H. Li, Z. Luo, J. Yao, C. Sun, X. Li, L. Xue, Z.-G. Zhang, C. Yang, Y. Li, *Chem. Mater.* **2019**, *31*, 6558.
- [48] D. Liu, Y. Zhang, L. Zhan, T.-K. Lau, H. Yin, P. W. K. Fong, S. K. So, S. Zhang, X. Lu, J. Hou, H. Chen, W.-Y. Wong, G. Li, *J. Mater. Chem. A* **2019**, *7*, 14153.
- [49] J. Huang, L. Xie, L. Hong, L. Wu, Y. Han, T. Yan, J. Zhang, L. Zhu, Z. Wei, Z. Ge, *Mater. Chem. Front.* **2019**, *3*, 1244.
- [50] Q. Wang, M. Li, X. Zhang, Y. Qin, J. Wang, J. Zhang, J. Hou, R. A. J. Janssen, Y. Geng, *Macromolecules* **2019**, *52*, 4464.
- [51] S. J. Jeon, Y. W. Han, D. K. Moon, *Sol. RRL3*, 1900094.
- [52] S. J. Jeon, Y. W. Han, D. K. Moon, *Small* **2019**, *15*, 1902598.
- [53] a) H. A. Saadeh, L. Lu, F. He, J. E. Bullock, W. Wang, B. Carsten, L. Yu, *ACS Macro Lett.* **2012**, *1*, 361; b) T. Dong, L. Lv, L. Feng, Y. Xia, W. Deng, P. Ye, B. Yang, S. Ding, A. Facchetti, H. Dong, H. Huang, *Adv. Mater.* **2017**, *29*, 1606025; c) L. Dou, W.-H. Chang, J. Gao, C.-C. Chen, J. You, Y. Yang, *Adv. Mater.* **2013**, *25*, 825; d) F.-Y. Cao, C.-C. Tseng, F.-Y. Lin, Y. Chen, H. Yan, Y.-J. Cheng, *Chem. Mater.* **2017**, *29*, 10045.
- [54] a) J. Wolf, F. Cruciani, A. El Labban, P. M. Beaujuge, *Chem. Mater.* **2015**, *27*, 4184; b) Z. Fei, M. Shahid, N. Yaacobi-Gross, S. Rossbauer, H. Zhong, S. E. Watkins, T. D. Anthopoulos, M. Heeney, *Chem. Commun.* **2012**, *48*, 11130; c) E. Collado-Fregoso, P. Boufflet, Z. Fei, E. Gann, S. Ashraf, Z. Li, C. R. McNeill, J. R. Durrant, M. Heeney, *Chem. Mater.* **2015**, *27*, 7934; d) Z. Li, D. Tang, Z. Ji, W. Zhang, X. Xu, K. Feng, Y. Li, Q. Peng, *J. Mater. Chem. C* **2018**, *6*, 9119; e) J. J. Rech, L. Yan, Z. Peng, S. Dai, X. Zhan, H. Ade, W. You, *Macromolecules* **2019**, *52*, 6523.
- [55] a) R. Po, J. Roncali, *J. Mater. Chem. C* **2016**, *4*, 3677; b) R. Po, G. Bianchi, C. Carbonera, A. Pellegrino, *Macromolecules* **2015**, *48*, 453.
- [56] a) W. Li, G. Li, H. Guo, X. Guo, B. Guo, Q. Zhu, Q. Fan, W. Ma, M. Zhang, Y. Li, *J. Mater. Chem. A* **2019**, *7*, 1307; b) B. Fan, X. Du, F. Liu, W. Zhong, L. Ying, R. Xie, X. Tang, K. An, J. Xin, N. Li, W. Ma, C. J. Brabec, F. Huang, Y. Cao, *Nat. Energy* **2018**, *3*, 1051; c) D. Ding, J. Wang, Z. Du, F. Li, W. Chen, F. Liu, H. Li, M. Sun, R. Yang, *J. Mater. Chem. A* **2017**, *5*, 10430.
- [57] a) Y. He, Y. Li, *Phys. Chem. Chem. Phys.* **2011**, *13*, 1970; b) Y. He, H.-Y. Chen, J. Hou, Y. Li, *J. Am. Chem. Soc.* **2010**, *132*, 1377.
- [58] G. Zhang, J. Zhao, P. C. Y. Chow, K. Jiang, J. Zhang, Z. Zhu, J. Zhang, F. Huang, H. Yan, *Chem. Rev.* **2018**, *118*, 3447.
- [59] a) Z. Zhang, J. Yuan, Q. Wei, Y. Zou, *Front. Chem.* **2018**, *6*, 414; b) S. A. Lopez, B. Sanchez-Lengeling, J. de Goes Soares, A. Aspuru-Guzik, *Joule* **2017**, *1*, 857; c) Z.-Q. Jiang, T.-T. Wang, F.-P. Wu, J.-D. Lin, L.-S. Liao, *J. Mater. Chem. A* **2018**, *6*, 17256.
- [60] a) K. Cnops, B. P. Rand, D. Cheyns, B. Verreert, M. A. Empl, P. Heremans, *Nat. Commun.* **2014**, *5*, 3406; b) B. Ebenhoch, N. B. A. Prasetya, V. M. Rotello, G. Cooke, I. D. W. Samuel, *J. Mater. Chem. A* **2015**, *3*, 7345.
- [61] K. Cnops, G. Zango, J. Genoe, P. Heremans, M. V. Martinez-Diaz, T. Torres, D. Cheyns, *J. Am. Chem. Soc.* **2015**, *137*, 8991.
- [62] a) K. Jiang, Q. Wei, J. Y. L. Lai, Z. Peng, H. K. Kim, J. Yuan, L. Ye, H. Ade, Y. Zou, H. Yan, *Joule* **2019**, *3*, 3020; b) J. Yuan, Y. Zhang, L. Zhou, C. Zhang, T.-K. Lau, G. Zhang, X. Lu, H.-L. Yip, S. K. So, S. Beaupré, M. Mainville, P. A. Johnson, M. Leclerc, H. Chen, H. Peng, Y. Li, Y. Zou, *Adv. Mater.* **2019**, *31*, 1807577.
- [63] Y. Lin, J. Wang, Z.-G. Zhang, H. Bai, Y. Li, D. Zhu, X. Zhan, *Adv. Mater.* **2015**, *27*, 1170.
- [64] H. Bai, Y. Wang, P. Cheng, J. Wang, Y. Wu, J. Hou, X. Zhan, *J. Mater. Chem. A* **2015**, *3*, 1910.
- [65] A. Laventure, G. C. Welch, *J. Mater. Chem. C* **2018**, *6*, 9060.
- [66] W. Su, Q. Fan, X. Guo, J. Wu, M. Zhang, Y. Li, *Phys. Chem. Chem. Phys.* **2019**, *21*, 10660.
- [67] Y. Li, L. Zhong, B. Gautam, H.-J. Bin, J.-D. Lin, F.-P. Wu, Z. Zhang, Z.-Q. Jiang, Z.-G. Zhang, K. Gundogdu, Y. Li, L.-S. Liao, *Energy Environ. Sci.* **2017**, *10*, 1610.
- [68] B. Kan, H. Feng, H. Yao, M. Chang, X. Wan, C. Li, J. Hou, Y. Chen, *Sci. China Chem.* **2018**, *61*, 1307.
- [69] Y.-C. Lin, Y.-J. Lu, C.-S. Tsao, A. Saeki, J.-X. Li, C.-H. Chen, H.-C. Wang, H.-C. Chen, D. Meng, K.-H. Wu, Y. Yang, K.-H. Wei, *J. Mater. Chem. A* **2019**, *7*, 3072.
- [70] a) B. Guo, W. Li, X. Guo, X. Meng, W. Ma, M. Zhang, Y. Li, *Adv. Mater.* **2017**, *29*, 1702291; b) Q. Fan, Y. Wang, M. Zhang, B. Wu, X. Guo, Y. Jiang, W. Li, B. Guo, C. Ye, W. Su, J. Fang, X. Ou, F. Liu, Z. Wei, T. C. Sum, T. P. Russell, Y. Li, *Adv. Mater.* **2018**, *30*, 1704546.
- [71] X. Li, H. Meng, F. Shen, D. Su, S. Huo, J. Shan, J. Huang, C. Zhan, *Dyes Pigm.* **2019**, *166*, 196.
- [72] Y. Wang, Y. Zhang, N. Qiu, H. Feng, H. Gao, B. Kan, Y. Ma, C. Li, X. Wan, Y. Chen, *Adv. Energy Mater.* **2018**, *8*, 1702870.
- [73] R. Geng, X. Song, H. Feng, J. Yu, M. Zhang, N. Gasparini, Z. Zhang, F. Liu, D. Baran, W. Tang, *ACS Energy Lett.* **2019**, *4*, 763.
- [74] Y. Chen, T. Liu, H. Hu, T. Ma, J. Y. L. Lai, J. Zhang, H. Ade, H. Yan, *Adv. Energy Mater.* **2018**, *8*, 1801203.
- [75] H. Feng, Y. Q. Q. Yi, X. Ke, J. Yan, Y. Zhang, X. Wan, C. Li, N. Zheng, Z. Xie, Y. Chen, *Adv. Energy Mater.* **2019**, *9*, 1803541.
- [76] J. Qu, Q. Zhao, J. Zhou, H. Lai, T. Liu, D. Li, W. Chen, Z. Xie, F. He, *Chem. Mater.* **2019**, *31*, 1664.
- [77] M. Luo, C. Zhu, J. Yuan, L. Zhou, M. L. Keshtov, D. Y. Godovsky, Y. Zou, *Chin. Chem. Lett.* **2019**, *30*, 2343.
- [78] Z. Luo, T. Liu, Y. Wang, G. Zhang, R. Sun, Z. Chen, C. Zhong, J. Wu, Y. Chen, M. Zhang, Y. Zou, W. Ma, H. Yan, J. Min, Y. Li, C. Yang, *Adv. Energy Mater.* **2019**, *9*, 1900041.
- [79] J. Zhang, Y. Li, H. Hu, G. Zhang, H. Ade, H. Yan, *Chem. Mater.* **2019**, *31*, 6672.
- [80] S.-S. Wan, X. Xu, J.-L. Wang, G.-Z. Yuan, Z. Jiang, G.-Y. Ge, H.-R. Bai, Z. Li, Q. Peng, *J. Mater. Chem. A* **2019**, *7*, 11802.
- [81] Y.-Q.-Q. Yi, H. Feng, X. Ke, J. Yan, M. Chang, X. Wan, C. Li, Y. Chen, *J. Mater. Chem. C* **2019**, *7*, 4013.
- [82] L. Hong, H. Yao, R. Yu, Y. Xu, B. Gao, Z. Ge, J. Hou, *ACS Appl. Mater. Interfaces* **2019**, *11*, 29124.
- [83] H. H. Gao, Y. Sun, Y. Cai, X. Wan, L. Meng, X. Ke, S. Li, Y. Zhang, R. Xia, N. Zheng, Z. Xie, C. Li, M. Zhang, H. L. Yip, Y. Cao, Y. Chen, *Adv. Energy Mater.* **2019**, *9*, 1901024.

- [84] L. Zhan, S. Li, S. Zhang, X. Chen, T. K. Lau, X. Lu, M. Shi, C. Z. Li, H. Chen, *ACS Appl. Mater. Interfaces* **2018**, *10*, 42444.
- [85] Y.-Q.-Q. Yi, H. Feng, N. Zheng, X. Ke, B. Kan, M. Chang, Z. Xie, X. Wan, C. Li, Y. Chen, *Chem. Mater.* **2019**, *31*, 904.
- [86] Y. Wang, Y. Wang, B. Kan, X. Ke, X. Wan, C. Li, Y. Chen, *Adv. Energy Mater.* **2018**, *8*, 1802021.
- [87] N. Qiu, H. Zhang, X. Wan, C. Li, X. Ke, H. Feng, B. Kan, H. Zhang, Q. Zhang, Y. Lu, Y. Chen, *Adv. Mater.* **2017**, *29*, 1604964.
- [88] a) J. Sun, X. Ma, Z. Zhang, J. Yu, J. Zhou, X. Yin, L. Yang, R. Geng, R. Zhu, F. Zhang, W. Tang, *Adv. Mater.* **2018**, *30*, 1707150; b) X. Ma, W. Gao, J. Yu, Q. An, M. Zhang, Z. Hu, J. Wang, W. Tang, C. Yang, F. Zhang, *Energy Environ. Sci.* **2018**, *11*, 2134; c) W. Li, M. Chen, Z. Zhang, J. Cai, H. Zhang, R. S. Gurney, D. Liu, J. Yu, W. Tang, T. Wang, *Adv. Funct. Mater.* **2019**, *29*, 1807662.
- [89] a) T. Li, S. Dai, Z. Ke, L. Yang, J. Wang, C. Yan, W. Ma, X. Zhan, *Adv. Mater.* **2018**, *30*, 1705969; b) X. Shi, J. Chen, K. Gao, L. Zuo, Z. Yao, F. Liu, J. Tang, A. K.-Y. Jen, *Adv. Energy Mater.* **2018**, *8*, 1702831; c) S. Dai, T. Li, W. Wang, Y. Xiao, T.-K. Lau, Z. Li, K. Liu, X. Lu, X. Zhan, *Adv. Mater.* **2018**, *30*, 1706571.
- [90] D. Xie, T. Liu, W. Gao, C. Zhong, L. Huo, Z. Luo, K. Wu, W. Xiong, F. Liu, Y. Sun, C. Yang, *Sol. RRL* **2017**, *1*, 1700044.
- [91] a) Y. Lin, Q. He, F. Zhao, L. Huo, J. Mai, X. Lu, C.-J. Su, T. Li, J. Wang, J. Zhu, Y. Sun, C. Wang, X. Zhan, *J. Am. Chem. Soc.* **2016**, *138*, 2973; b) P. Cheng, H. Bai, N. K. Zawacka, T. R. Andersen, W. Liu, E. Bundgaard, M. Jørgensen, H. Chen, F. C. Krebs, X. Zhan, *Adv. Sci.* **2015**, *2*, 1500096.
- [92] a) L. Zhan, S. Li, H. Zhang, F. Gao, T.-K. Lau, X. Lu, D. Sun, P. Wang, M. Shi, C.-Z. Li, H. Chen, *Adv. Sci.* **2018**, *5*, 1800755; b) S. Li, L. Zhan, F. Liu, J. Ren, M. Shi, C.-Z. Li, T. P. Russell, H. Chen, *Adv. Mater.* **2018**, *30*, 1705208; c) S. Li, L. Zhan, W. Zhao, S. Zhang, B. Ali, Z. Fu, T.-K. Lau, X. Lu, M. Shi, C.-Z. Li, J. Hou, H. Chen, *J. Mater. Chem. A* **2018**, *6*, 12132.
- [93] Z.-P. Yu, Z.-X. Liu, F.-X. Chen, R. Qin, T.-K. Lau, J.-L. Yin, X. Kong, X. Lu, M. Shi, C.-Z. Li, H. Chen, *Nat. Commun.* **2019**, *10*, 2152.
- [94] P. Cheng, X. Zhan, *Chem. Soc. Rev.* **2016**, *45*, 2544.
- [95] a) Y. Lin, X. Zhan, *Acc. Chem. Res.* **2016**, *49*, 175; b) Z. Zhou, S. Xu, J. Song, Y. Jin, Q. Yue, Y. Qian, F. Liu, F. Zhang, X. Zhu, *Nat. Energy* **2018**, *3*, 952.
- [96] a) B. Qiu, L. Xue, Y. Yang, H. Bin, Y. Zhang, C. Zhang, M. Xiao, K. Park, W. Morrison, Z.-G. Zhang, Y. Li, *Chem. Mater.* **2017**, *29*, 7543; b) L. Yang, S. Zhang, C. He, J. Zhang, H. Yao, Y. Yang, Y. Zhang, W. Zhao, J. Hou, *J. Am. Chem. Soc.* **2017**, *139*, 1958; c) H. Bin, Y. Yang, Z. G. Zhang, L. Ye, M. Ghasemi, S. Chen, Y. Zhang, C. Zhang, C. Sun, L. Xue, C. Yang, H. Ade, Y. Li, *J. Am. Chem. Soc.* **2017**, *139*, 5085; d) J. Shi, A. Isakova, A. Abudulimu, M. van den Berg, O. K. Kwon, A. J. Meixner, S. Y. Park, D. Zhang, J. Gierschner, L. Lüer, *Energy Environ. Sci.* **2018**, *11*, 211.
- [97] a) J. Min, C. Bronnbauer, Z.-G. Zhang, C. Cui, Y. N. Luponosov, I. Ata, P. Schweizer, T. Przybilla, F. Guo, T. Ameri, K. Forberich, E. Spiecker, P. Bäuerle, S. A. Ponomarenko, Y. Li, C. J. Brabec, *Adv. Funct. Mater.* **2016**, *26*, 4543; b) J. Zhang, G. Xu, F. Tao, G. Zeng, M. Zhang, Y. Yang, Y. Li, Y. Li, *Adv. Mater.* **2019**, *31*, 1807159.
- [98] a) A. R. B. M. Yusoff, S. J. Lee, F. K. Shneider, W. J. da Silva, J. Jang, *Adv. Energy Mater.* **2014**, *4*, 1301989; b) G. Xu, L. Shen, C. Cui, S. Wen, R. Xue, W. Chen, H. Chen, J. Zhang, H. Li, Y. Li, Y. Li, *Adv. Funct. Mater.* **2017**, *27*, 1605908.
- [99] a) T. Ameri, N. Li, C. J. Brabec, *Energy Environ. Sci.* **2013**, *6*, 2390; b) J. You, L. Dou, Z. Hong, G. Li, Y. Yang, *Prog. Polym. Sci.* **2013**, *38*, 1909.
- [100] a) L. Yang, L. Yan, W. You, *J. Phys. Chem. Lett.* **2013**, *4*, 1802; b) T. Ameri, P. Khoram, J. Min, C. J. Brabec, *Adv. Mater.* **2013**, *25*, 4245; c) P. Bi, X. Hao, *Sol. RRL* **2019**, *3*, 1800263; d) Q. An, J. Zhang, W. Gao, F. Qi, M. Zhang, X. Ma, C. Yang, L. Huo, F. Zhang, *Small* **2018**, *14*, 1802983; e) N. Gasparini, A. Salleo, I. McCulloch, D. Baran, *Nat. Rev. Mater.* **2019**, *4*, 229; f) H. Huang, L. Yang, B. Sharma, *J. Mater. Chem. A* **2017**, *5*, 11501; g) H. B. Naveed, W. Ma, *Joule* **2018**, *2*, 621.
- [101] a) K. Li, Y. Wu, Y. Tang, M.-A. Pan, W. Ma, H. Fu, C. Zhan, J. Yao, *Adv. Energy Mater.* **2019**, *9*, 1901728; b) M. Nam, J. h. Kang, J. Shin, J. Na, Y. Park, J. Cho, B. Kim, H. H. Lee, R. Chang, D. H. Ko, *Adv. Energy Mater.* **2019**, *9*, 1901856.
- [102] H. Chen, Y. Guo, P. Chao, L. Liu, W. Chen, D. Zhao, F. He, *Sci. China Chem.* **2018**, *62*, 238.
- [103] T. Liu, Z. Luo, Y. Chen, T. Yang, Y. Xiao, G. Zhang, R. Ma, X. Lu, C. Zhan, M. Zhang, C. Yang, Y. Li, J. Yao, H. Yan, *Energy Environ. Sci.* **2019**, *12*, 2529.
- [104] W. Huang, P. Cheng, Y. Yang, G. Li, Y. Yang, *Adv. Mater.* **2018**, *30*, 1705706.
- [105] a) T. L. Nguyen, T. H. Lee, B. Gautam, S. Y. Park, K. Gundogdu, J. Y. Kim, H. Y. Woo, *Adv. Funct. Mater.* **2017**, *27*, 1702474; b) G. Feng, J. Li, F. J. M. Colberts, M. Li, J. Zhang, F. Yang, Y. Jin, F. Zhang, R. A. J. Janssen, C. Li, W. Li, *J. Am. Chem. Soc.* **2017**, *139*, 18647; c) J. H. Lee, C. G. Park, A. Kim, H. J. Kim, Y. Kim, S. Park, M. J. Cho, D. H. Choi, *ACS Appl. Mater. Interfaces* **2018**, *10*, 18974; d) G. Feng, J. Li, Y. He, W. Zheng, J. Wang, C. Li, Z. Tang, A. Osvet, N. Li, C. J. Brabec, Y. Yi, H. Yan, W. Li, *Joule* **2019**, *3*, 1765; e) W. Wang, R. Sun, J. Guo, J. Guo, J. Min, *Angew. Chem. Int. Ed.* **2019**, *58*, 14556; f) J. Roncali, I. Grosu, *Adv. Sci.* **2019**, *6*, 1801026.
- [106] Y. Cui, Y. Wang, J. Bergqvist, H. Yao, Y. Xu, B. Gao, C. Yang, S. Zhang, O. Inganäs, F. Gao, J. Hou, *Nat. Energy* **2019**, *4*, 768.
- [107] a) R. Steim, T. Ameri, P. Schilinsky, C. Waldauf, G. Dennler, M. Scharber, C. J. Brabec, *Sol. Energy Mater. Sol. Cells* **2011**, *95*, 3256; b) H. K. H. Lee, J. Wu, J. Barbé, S. M. Jain, S. Wood, E. M. Speller, Z. Li, F. A. Castro, J. R. Durrant, W. C. Tsoi, *J. Mater. Chem. A* **2018**, *6*, 5618; c) S. Kim, M. Jahandar, J. H. Jeong, D. C. Lim, *Curr. Altern. Energy* **2019**, *3*, 3.
- [108] a) Y.-J. You, C. E. Song, Q. V. Hoang, Y. Kang, J. S. Goo, D.-H. Ko, J.-J. Lee, W. S. Shin, J. W. Shim, *Adv. Funct. Mater.* **2019**, *29*, 1901171; b) Y. Cui, H. Yao, T. Zhang, L. Hong, B. Gao, K. Xian, J. Qin, J. Hou, *Adv. Mater.* **2019**, *31*, 1904512.
- [109] C. Li, H. Fu, T. Xia, Y. Sun, *Adv. Energy Mater.* **2019**, *9*, 1900999.
- [110] Z. Genene, W. Mammo, E. Wang, M. R. Andersson, *Adv. Mater.* **2019**, *31*, 1807275.
- [111] a) Y. W. Han, S. J. Jeon, H. S. Lee, H. Park, K. S. Kim, H.-W. Lee, D. K. Moon, *Adv. Energy Mater.* **2019**, *9*, 1902065; b) S. Rasool, D. V. Vu, C. E. Song, H. K. Lee, S. K. Lee, J.-C. Lee, S.-J. Moon, W. S. Shin, *Adv. Energy Mater.* **2019**, *9*, 1900168.